Relative Performances of Laminated Composite Hyperbolic and Elliptical Paraboloidal Shells with Cutouts Under Free Vibration

M.Tech Thesis

By

RAVINDRA SOLANKI

DEPARTMENT OF CIVIL ENGINEERING

INDIAN INSTITUTE OF TECHNOLOGY INDORE

MAY 2025

Relative Performances of Laminated Composite Hyperbolic and Elliptical Paraboloidal Shells with Cutouts Under Free Vibration

A THESIS

Submitted in partial fulfillment of the
requirements for the award of the degree
of
Master of Technology
by

RAVINDRA SOLANKI

DEPARTMENT OF CIVIL ENGINEERING
INDIAN INSTITUTE OF TECHNOLOGY INDORE
MAY 2025

INDIAN INSTITUTE OF TECHNOLOGY INDORE

CANDIDATE'S DECLARATION

I hereby certify that the work which is being presented in the thesis entitled **Relative Performances of Laminated Composite Hyperbolic and Elliptical Paraboloidal Shells with Cutouts Under Free Vibration** in the partial fulfillment of the requirements for the award of the degree of **MASTER OF TECHNOLOGY** and submitted in the **Department of Civil Engineering, Indian Institute of Technology Indore**, is an authentic record of my own work carried out during the time period from July 2024 to May 2025 under the supervision of Dr. Kaustav Bakshi, Assistant professor, Department of civil engineering, IIT INDORE

The matter presented in this thesis has not been submitted by me for the award of any other degree of this or any other institute.

Signature of the student
(RAVINDRA SOLANKI)

This is to certify that the above statement made by the candidate is correct to the best of my/our knowledge.

Signature of the Supervisor of
M.Tech. thesis
Dr. KAUSTAV BAKSHI

RAVINDRA SOLANKI has successfully given his M.Tech. Oral Examination held on **9th May 2025.**

Signature of Supervisor of M.Tech. thesis
Date: 23 May 2025

Convener, DPGC
Date: May 27, 2025

ACKNOWLEDGEMENTS

The author owes his most sincere thanks and profound gratitude to his supervisor,Dr. Kaustav Bakshi, for the indispensable advice and inspiration rendered at each phase of the research work. His valuable suggestions, constructive criticism and critical evaluation throughout the research work are thankfully acknowledged. The author is grateful to the Civil Engineering Department for their cooperation. The author also expresses his gratitude to the library of Indian Institute of Technology Indore. The excellent cooperation and support of the co-researchers are thankfully acknowledged. It would not have been possible for the author to pursue the research work without the constant effort, sacrifices and encouragement of his parents from the very first day of his student life till date. The author is thankful to all those whose efforts either directly or indirectly have contributed substantially during this thesis work.

Date: 23 MAY 2025

Place: IIT Indore

Signature of the Candidate: **RAVINDRA SOLANKI**

DEDICATION

To Dr. Kaustav Bakshi,

Thank you for your guidance, wisdom, and inspiration throughout this journey. Your mentorship and clarity made all the difference.

I also want to thank all my PhD seniors and friends for their support, guidance and motivating me throughout this journey.

Abstract

Laminated composite materials have gained widespread acceptance in civil engineering due to their outstanding mechanical properties, such as high strength-to-weight and stiffness-to-weight ratios, excellent durability, and resistance to environmental degradation. Among various structural forms, hyperbolic and elliptical paraboloidal shells, which possess a smooth double-curved geometry, offer superior stiffness and aesthetic qualities. These characteristics make them well-suited for long-span roofing systems and architecturally significant structures. The integration of laminated composites further enhances their efficiency, making them increasingly popular in modern engineering applications.

However, practical implementations often require cutouts in shell surfaces for functional necessities such as air-conditioning ducts, skylights, or maintenance access, which may significantly affect their dynamic behaviour. Despite the growing use of hyperbolic and elliptical paraboloidal shells, studies addressing the impact of cutouts on their free vibration characteristics remain limited. Moreover, variations in lamination schemes and support conditions further influence their dynamic response and demand systematic evaluation.

The present study aims to fill this research gap by investigating the free vibration behaviour of laminated composite hyperbolic and elliptical paraboloidal shells with cutouts under various boundary conditions and laminate stacking sequences. The influence of cutout geometry, location, and laminate configuration on the fundamental natural frequencies and mode shapes is assessed through detailed finite element modelling. The findings from this research are expected to provide valuable insights for optimizing the design of such advanced shell structures in civil engineering practice.

LIST OF PUBLICATIONS

Conference Paper

Madhu Trivedi, Natvar Singh, Ravindra Solanki and Kaustav Bakshi, “Relative Performances of Skewed Hyperbolic Paraboloidal Stiffened Shells- A Geometrically Nonlinear Approach”, ICMAMS-2024 held at Ramaiah Institute of Technology Bangalore, Karnataka from December 11to13 2024

TABLE OF CONTENTS

Chapter	Title of the chapter	Page number
	List of figures	*x*
	List of tables	*xii*
	Nomenclature	*xiv*
Chapter 1	**INTRODUCTION**	1 - 6
	1.1 Background and motivation	1
	1.2 Classification of shell	2
	1.3 Use of shells in last century	3
	1.4 Introduction to laminated composite	4
	1.5 Methods of analysis	5
	1.6 Present study – its importance in research	6
Chapter 2	**LITERATURE REVIEW**	7 - 11
	2.1 General	7
	2.2 Historical review	7
Chapter 3	**SCOPE OF THE PRESENT STUDY**	12 - 13
	3.1 General overview	12
	3.2 Present scope	12
Chapter 4	**MATHEMATICAL FORMULATION**	14 - 41
	4.1 General	14
	4.2 Finite element method:	15
	4.3 Element selection and geometric representation	15
	4.4 Discretization of the shell surface	16
	4.5 Selection of shape functions	17
	4.6 Selection of generalized displacement fields	18
	4.7 Strain-displacement relationship	19
	4.8 Force-strain relationship of the composite material	24
	4.9 Generalized inertia matrix	33
	4.10 General dynamic problem	34

	4.11 Imposition of boundary conditions and solution procedure	40
	4.12 Formulating free vibration problem	41
Chapter 5	**VIBRATION CHARACTERISTICS OF ELLIPTICAL PARABOLOIDAL SHELL WITH CUTOUT**	42 -68
	5.1 General	42
	5.2 Numerical Problems on Elliptical Paraboloidal Panels	42
	5.3 Results and Discussion	48
	5.4 Conclusions	67
Chapter 6	**VIBRATION CHARACTERISTICS OF HYPERBOLIC PARABOLOIDAL SHELL WITH CUTOUT**	69 - 81
	6.1 General	69
	6.2 Numerical Problems on Hyperbolic Paraboloidal panels	69
	6.3 Results and Discussion	77
	6.4 Conclusions	81
Chapter 7	**FUTURE SCOPE**	82
Chapter 8	**REFERENCES**	83 -88

LIST OF FIGURES

Figure No.	Title of the Figure	Page Number
4.1	Laminated elliptic paraboloidal panel with composite stiffeners and concentric cutout.	14
4.2	Laminated hyperbolic paraboloidal panel with composite stiffeners and concentric cutout.	15
4.3	The shell element in isoparametric coordinates.	16
5.1	Elliptic paraboloidal panel with central stiffeners.	46
5.2	Centrally stiffened elliptical paraboloidal shell with cutout.	47
5.3	Nondimensional fundamental frequencies $\left[\varpi = \omega a^2 \left(\frac{\rho}{E_{22}h^2}\right)^{\frac{1}{2}}\right]$ of elliptical paraboloid with cutout for simply supported boundary condition with graphite epoxy composite.	50
5.4	Nondimensional fundamental frequencies of elliptical paraboloid with cutout for clamped boundary condition with graphite epoxy composite.	51
5.5	Nondimensional fundamental frequencies of elliptical paraboloid with cutout for simply supported boundary condition with bamboo epoxy composite.	55
5.6	Nondimensional fundamental frequencies of elliptical paraboloid with cutout for clamped supported boundary condition with bamboo epoxy composite.	56
5.7	Nondimensional fundamental frequencies of elliptical paraboloid with cutout for simply supported and clamped boundary conditions.	61
5.8	Cases of elliptical paraboloidal shell with cutout locations.	62
5.9	Nondimensional fundamental frequencies of elliptical paraboloid with cutout for 45^0/-45^0/45^0, R_{yy}/R_{xx} =1.0, and 9×9 stiffeners.	64

5.10	Mode shapes of simply supported elliptical paraboloidal shell for varying positions of cutouts.	65
5.11	Mode shapes of clamped elliptical paraboloidal shell for varying position of cutouts.	67
6.1	Centrally stiffened hyperbolic paraboloidal shell with cutout in plan.	69
6.2	Hyperbolic paraboloidal panel with central stiffeners.	76

LIST OF TABLES

Table No.	Title of the Table	Page Number
5.1	Nondimensional fundamental frequencies [$\varpi = \omega a^2(\rho/E_{22}h^2)^{0.5}$] of simply supported composite spherical shell.	42
5.2	Nondimensional frequency of 0°/90°/0°/90° composite skew elliptic paraboloid.	43
5.3	Nonlinear fundamental frequencies of simply supported $[0^0/0^0/\pm30^0]_2$ spherical shell.	43
5.4	Frequencies (rad/sec) of biaxially stiffened $90^0/0^0/0^0/90^0$ spherical shell.	44
5.5	Natural frequencies (Hz) of orthogonally stiffened cylindrical panel.	44
5.6	Laminations for elliptical panels.	45
5.7	Engineering properties of the elliptical composite panels.	45
5.8	Dimensions of the elliptical paraboloidal panels.	46
5.9	Nondimensional fundamental frequencies of simply supported and clamped elliptical paraboloid shell with cutout and graphite epoxy composite.	48
5.10	Nondimensional fundamental frequencies of simply supported and clamped elliptical paraboloid shell with cutout and bamboo epoxy composite.	53
5.11	Nondimensional fundamental frequencies of biaxially stiffened simply supported and clamped elliptical paraboloids with varying locations of cutouts along.	58
5.12	Nondimensional fundamental frequencies of simply supported and clamped elliptical paraboloid with cutout.	59
5.13	Nondimensional fundamental frequencies of elliptical paraboloid with cutout for $45^0/-45^0/45^0$, R_{yy}/R_{xx} =1.0, and 9×9 stiffeners.	63
6.1	Non-dimensional fundamental frequencies of clamped and simply supported hyperbolic paraboloidal panels. ω = frequency in rad/sec, ρ = mass density.	70

6.2	Non-dimensional fundamental frequencies of CFFF and CFFC hyperbolic paraboloidal panels. ω = frequency in rad/sec, ρ = mass density.	71
6.3	Non-dimensional fundamental frequencies of skewed hypar panels. ω = frequency in rad/sec, ρ = mass density.	72
6.4	Non-dimensional fundamental frequencies of simply supported skewed stiffened hypar panels. ω = frequency in rad/sec, ρ = mass density.	73
6.5	Nonlinear fundamental frequencies [$\varpi = \omega a^2(\rho/E_{22}h^2)^{0.5}$] of simply supported $[0^0/0^0/30^0/\text{-}30^0]_2$ hyperbolic paraboloid shell.	73
6.6	Fundamental frequencies (Hz) of centrally stiffened clamped square plate	74
6.7	Laminations for skewed hypar panels.	74
6.8	Engineering properties of the hypar composites.	75
6.9	Dimensions of the hypar shell with Cutout.	75
6.10	Non-dimensional fundamental frequencies of CSCS and SCSC laminated composite hyperbolic-paraboloidal shell with varying (a_1/a) ratio and lamination.	77
6.11	Non-dimensional fundamental frequencies of CSCS and SCSC laminated composite hyperbolic-paraboloidal shell $45^0/\text{-}45^0/\text{-}45^0/45^0$ and a_1/a =0.1.	78
6.12	Non-dimensional fundamental frequencies of simple supported composite hyperbolic-paraboloidal shell.	79
6.13	Non-dimensional fundamental frequency of panels for a_1/a = 0.125, 0°/90°/90°/0° composite, ϕ = 35° and n_x=0, n_y=1 stiffeners.	81

NOMENCLATURE

Variables	Representations
A_0-A_7	Constant terms of displacement polynomial.
a', b'	Length and width of shell in plan.
D	Flexural rigidity matrix.
$\{\delta\}$	element displacement vector
$\{d\}$	Global displacement vector.
$\dot{d}$	Global acceleration vector.
E_1, E_2, E_3	Modulus of elasticity along the directions 1, 2 and 3.
1,2 and 3	Local co-ordinates of a lamina.
h	Shell thickness.
M_x, M_y	Moment resultants per unit length of doubly curved shell.
M_{xy}	Torsion resultant per unit length of doubly curved shell.
N_1 to N_8	Shape functions for first to eight nodes of an element respectively.
N_x, N_y	In-plane normal force resultants per unit length in X and Y directions.
N_{xy}	In-plane shear force resultant per unit length of shell.
n	Number of plies in a laminate.
Q_x , Q_y	Transverse shear resultants per unit length of shell.
R_{xy}	Radius of cross curvature of shell.
R_{yy}	Principle radius of curvature of doubly curved shell along Y axis.

R_{xx}	Principle radius of curvature of doubly curved shell along X axis.
ϕ	Skew angle.
θ	Lamination.

Chapter 1

INTRODUCTION

1.1 Background and Motivation

Many human innovations have been inspired by nature, and shell structures are a prime example of this phenomenon. A shell can be defined as an arbitrarily curved structural surface that resists externally applied loads through a combination of in-plane forces and bending moments. This coupling of membrane and flexural actions imparts high strength and stiffness to shell forms. In nature, examples such as the human skull, eggshells, coconuts, and animal shells demonstrate how curved geometries provide superior resistance against transverse loading. For instance, applying a significant force to a coconut or human skull is more likely to harm the hand exerting the force than to damage the shell itself, owing to their geometric efficiency.

The curvature of shell structures allows them to effectively utilize both bending and axial stiffness, enabling civil engineers to cover large column-free spans using minimal material thickness without compromising structural integrity. This makes shell structures highly efficient and aesthetically appealing, which is why they are widely used in architectural and structural applications such as stadiums, auditoriums, and exhibition halls. Their ability to reduce material usage while achieving both functional and visual goals has made shell structures popular in construction. Historical examples like the Pantheon in Rome (AD 125) and the Hagia Sophia in Istanbul (AD 537) highlight the early use and importance of shell structures in architecture.

Over time, the applications of shell structures have expanded far beyond roofing. Their unique geometry and mechanical behavior have found relevance across various fields of engineering:

- *Architecture and Building:* The evolution of masonry domes and vaults during the Middle Ages enabled the construction of more spacious and impressive buildings.
- *Power and Chemical Engineering:* The industrial revolution saw the development of steam power, where the use of shell-like geometries in boilers was essential.
- *Structural Engineering:* Shell forms such as tubular sections were instrumental in solving buckling problems in compression members during the early stages of steel construction.
- *Shipping Industry:* Ship hulls designed as shell structures helped displace more water relative to their weight, improving buoyancy and stability.

- *Miscellaneous Applications:* Shell concepts have also influenced a wide array of inventions, including the prototype submarine (1620), pressure cooker (1688), balloon (as a thin-walled pressure vessel in the 18th century), and pneumatic tyre (1845).

With the expansion of shell structures into domains involving complex geometries and loading conditions—such as internal pressure in balloons and pressure cookers or external water pressure in submarines—the stress distributions on the shell surface have become more intricate. This necessitates detailed and area-specific research to better understand the behavior of these forms under diverse loading scenarios.

In this context, the present study focuses on laminated composite hyperbolic and elliptical paraboloidal shells with cutouts, a configuration that adds complexity due to both material anisotropy and geometric discontinuities. Understanding their free vibration behavior is crucial for ensuring the structural performance and dynamic stability of such systems, especially in advanced engineering applications. The use of composite materials further enhances the potential of shell structures by offering high strength-to-weight ratios, but also requires sophisticated analytical approaches due to their layered nature. Hence, a systematic investigation using numerical methods is essential to evaluate their vibrational characteristics and relative performances under various parameters.

1.2 Classification of shell

Shell structures can broadly be classified into two major categories based on their curvature: singly curved surfaces and doubly curved surfaces. Singly curved shells, such as cylindrical shells, are widely used in practice due to their ease of construction. Being singly ruled surfaces, they can be formed using straight-line generators, which simplifies the shuttering process requiring formwork only along the curved boundaries of opposite edges.

On the other hand, doubly curved shell surfaces exhibit curvature in two directions, providing enhanced structural strength and aesthetic appeal. Examples of such geometries include hyperbolic paraboloids, elliptic paraboloids, and conoids. These surfaces distribute loads more efficiently and offer greater resistance to deformation under external forces.

Among the various doubly curved shells, conoidal shells are often preferred in architectural applications due to their visual elegance, the ability to admit natural daylight, and relatively simpler construction, as they are also singly ruled despite having double curvature.

In the context of the present study, hyperbolic and elliptical paraboloidal shells a type of doubly curved surface are of particular interest. Their geometry allows for efficient load transfer and favourable dynamic performance, especially when constructed using laminated composite materials. However, the introduction of cutouts in such shell forms adds complexity to their vibrational behaviour, necessitating detailed investigation. The classification and understanding of these shell types form the foundation for analysing their structural response under free vibration conditions.

1.3 Use of shells in last century

Shell structures have found widespread applications across numerous branches of engineering throughout the last century, owing to their ability to efficiently carry loads while minimizing material usage. Their curved geometries offer superior mechanical performance under various loading conditions, making them suitable for both static and dynamic environments. The following are some prominent examples of shell structure applications in modern engineering:

i. Aircraft fuselages and wings.
ii. Ship hulls.
iii. Roofs of buildings, auditoriums, and stadiums.
iv. Storage tanks for liquids and gases.
v. Long-span pipelines.
vi. Submarine pressure hulls.
vii. Nuclear reactor containment vessels.
viii. Refinery components and biomedical equipment housings.
ix. Elevated and underground water tanks.
x. Natural draft cooling towers.
xi. Protective military structures like bunkers and silos.

The continued evolution of these applications has been significantly influenced by the introduction of composite materials and cutout features, which improve functionality but also bring new challenges in terms of structural behaviour especially under free vibration conditions. This highlights the importance of the present investigation into the dynamic performance of laminated composite hyperbolic and elliptical paraboloidal shells with cutouts.

1.4 Introduction to laminated composite

The advent of modern materials like laminated composites has brought a significant transformation in the construction industry, particularly in the development of shell structures. Their application has gained momentum due to the unique combination of high strength, stiffness, and reduced weight. The use of composites in engineering began during World War II, driven by the shortage of bauxite and the subsequent limited availability of aluminium alloys. In response, Britain developed a material named 'Gordon Aerolite', a fiber-reinforced plastic made from untwisted flax fibers embedded in phenolic resin. This was the first known composite material to be used in a major structural component, specifically for aircraft fuselages, and marked the beginning of composite usage in modern engineering.

From an engineering perspective, a composite material is a combination of two or more distinct materials that remain chemically inactive with respect to each other but work together to achieve superior mechanical properties. Composites are broadly classified into particulate composites and fibrous composites. Particulate composites involve particles dispersed in a continuous matrix phase, while fibrous composites consist of long, strong, and stiff fibers—either continuous or chopped—embedded in a binding matrix. These fibers may be inorganic (such as glass, carbon, or boron) or organic (like aramid or Kevlar), and matrices can be metallic (e.g., aluminium) or non-metallic (e.g., epoxy, polyester, phenolic resin, or ceramics).

A lamina is formed by embedding aligned fibers in a resin, which is then hardened. When multiple such laminae or plies are stacked together at different orientations and bonded, they form a laminate. At the macroscopic level, each lamina is homogeneous and anisotropic, while the laminate behaves as orthotropic. These laminates are widely used in a variety of structural elements including beams, plates, stiffened plates, shells, and stiffened shells, owing to their high strength-to-weight and stiffness-to-weight ratios, low cost of fabrication, ease of repair, excellent fatigue resistance, and damage tolerance.

The advantages of laminated composites have led to their increasing use in curved shell structures, particularly in aerospace, marine, civil, and mechanical engineering domains. As a result, from the latter half of the 20th century onwards, researchers have extensively investigated their behaviour under different loading conditions, including free vibration. In the present study, the focus is on laminated composite hyperbolic and elliptical paraboloidal shells with cutouts,

where the impact of such cutouts on the free vibration characteristics is analysed to provide deeper insights into their structural performance.

1.5 Methods of analysis

Shells may be analyzed either by linear elastic analysis based on theory of elasticity, but it is rarely performed due to its tedious and difficult computational procedures for evaluation of deflection and stress.

There are several numerical methods through which the shell analysis can be performed.

i. Finite Difference Method.
ii. Energy Methods such as Rayleigh's Method, Rayleigh-Ritz Method, and Galerkin Method.
iii. Dynamic Relaxation Method.
iv. Finite Element Method (FEM).

A thorough review of the literature indicates that researchers across the globe have predominantly relied on the finite element method for analysing composite shells, owing to its versatility and robustness. FEM proves to be particularly effective in scenarios involving:

i. Complex boundary or support conditions.
ii. Irregular surface geometries.
iii. Highly variable or localized loading.
iv. Material non-homogeneity.
v. Dynamic or time-dependent loads, and.
vi. Shell structures containing cutouts or openings large enough to disturb the global stress distribution.

In the present study, the hyperbolic and elliptical paraboloidal shell made of laminated composite material and having cutouts is investigated under free vibration conditions. The structure is subjected to non-conventional boundary conditions relevant to real-world industrial applications, where two opposite edges are clamped while the remaining are simply supported, in addition to the classical fully clamped or simply supported cases. Considering the complexity introduced by cutouts, non-uniform boundary constraints, and free vibration analysis, the finite element method is adopted as the most suitable and efficient analytical approach for the current research.

1.6 Present Study – Its Importance in Research

A close examination of the evolution of shell structures in both industrial applications and academic research highlights that several critical aspects, particularly involving complex geometries and material combinations, remain insufficiently explored. Among these, the dynamic behaviour of laminated composite hyperbolic and elliptical paraboloidal shells with cutouts under free vibration has received limited attention, despite its growing relevance in modern structural systems. Recognizing this gap, the present study aims to systematically review the existing literature to identify key areas demanding detailed investigation. Within this broader context, a focused scope has been defined for the thesis, which involves the use of the finite element method to analyse the free vibration characteristics of laminated composite hyperbolic and elliptical paraboloidal shells incorporating cutouts. This shape is of particular interest due to its complex double curvature and potential for lightweight yet strong construction. The study involves a detailed numerical investigation and comparison of shell performance under various boundary conditions and cutout configurations. The complete analysis undertaken in this research is presented systematically in the following chapters.

Chapter 2

LITERATURE REVIEW

2.1 General

Shell structures have a long and rich history of use across various engineering applications, and the accumulated research in this domain is extensive. Among their diverse functions, the use of shell forms as roofing units remains a topic of significant current interest due to their strength, efficiency, and aesthetic appeal. This chapter begins with a historical overview in Section 2.2, tracing the evolution of shell research that started as early as 1833. A significant milestone in the development of shell structures was the introduction of laminated composites during the second half of the twentieth century, particularly in weight-sensitive engineering sectors. These advanced materials, known for their high strength-to-weight and stiffness-to-weight ratios, brought a revolutionary change and began to be used in constructing shell roofs, among other structural applications. The present review places special emphasis on laminated composite shells, especially those with complex doubly curved geometries like hyperbolic and elliptical paraboloidal shells with cutouts, which are relevant to the current research. However, some references to isotropic shell behaviour are also included where necessary for completeness. Wherever possible, the reviewed literature is presented chronologically to provide a coherent understanding of the progress made in this field.

2.2 Historical Review

2.2.1 *Linear and Nonlinear study of shells*

The somewhat thin elliptic paraboloidal panels are capable of displaying considerable vibration amplitudes. For accurate predictions, the researchers, therefore, used nonlinear strains. Sathyamoorthy (1995) investigated the linear and nonlinear frequencies of moderately thick orthotropic spherical shells for different amplitude ratios using the numerical Runge-Kutta integration approach. Przekop et al. (2004) examined the free vibration of spherical panels while considering the impacts of numerous modes. Amabili (2005) examined the two distinct nonlinear strain–displacement equations from Donnell's and Novozhilov's shell theories, which are utilized to compute the elastic strain energy in spherical shells with various geometric flaws. Using delaminated shells, Nanda et al. (2010) investigated nonlinear forced vibration in a hygrothermal setting. Later, when researching the nonlinear vibrations of composite laminated panels, Nanda

(2010) took piezoelectric effects into account. Nanda and Pradyumna (2011) used FSDT to report the impact of defects and hygrothermal changes on the fundamental frequencies of spherical shells. To describe the frequencies of spherical shells for different hygrothermal exposures, Naidu and Sinha (2007) used Green-Lagrange nonlinear stresses, taking into account geometric nonlinearity, transverse shear deformation, and radius of curvature. Fazzolari (2014) reported frequencies for the lowest five modes of vibrations using Wittrick-William's algorithm and higher-order shear deformations. Singh and Panda (2014) used Hamilton's concept to obtain nonlinear fundamental frequencies by varying the panel thicknesses. In a hygrothermal setting, Mahapatra and Panda (2016) and Karimiasl et al. (2019) investigated the nonlinear vibration of composite panels. Karimiasl et al. (2019) used the Halpin–Tsai model, while Mahapatra and Panda (2016) used a micromechanics technique. Hirwani et al. (2021) investigated the steady-state response of weakly bonded composite shell structures under hygro-thermo-mechanical stress. In contrast, Sayyad and Ghugal (2019) used generalized HSDT to assess static and free vibration behaviour on sandwiched panels.

2.2.2 Cutout in shells

Roof structures typically have cutouts to let light in, improve ventilation, make other building areas more accessible, and occasionally change the resonance frequency. A thorough understanding of these forms' behaviour under vibration is necessary to capture and effectively use them. In civil engineering, laminated composite is the material of choice for fabricating plates and shells due to its high strength/stiffness-to-weight ratio, cheap fabrication cost, and superior durability. Laminated composites, as opposed to isotropic ones, lower the mass-induced seismic forces and foundation expenses when used in shell production. Past studies on stiffened shells with linearly shaped cutouts include those by Hota and Chakravorty (2007), Sahoo (2014), Chaudhuri et al. (2018,2022), and Hangyu et al. (2024), who examined the buckling limitations and the free vibration behaviour, respectively. Hota and Chakravorty (2007) examined the stiffened conoidal shell, and they found that for various edge restrictions of complete and truncated conoids, the cutout sizes and locations concerning the shell center changed. For a range of edge limitations, Sahoo (2014) examined shallow spherical shell panels with varying concentric and eccentric cutout sizes and locations concerning the shell center. Based on FSDT, Chaudhuri et al. (2018) examined a hyper shell stiffened along the edge of cutouts with different boundary and antisymmetric angle ply lamination conditions. Chaudhuri et al. (2022) used the Taguchi resilient

design, FSDT, and finite element process to optimize shell parameters (lamination angle, width-to-thickness ratio, and cutout location) to study the fundamental frequencies of hyper shells. The curved grid-honeycomb sandwich constructions with cutouts were proposed by Hangyu et al. (2024), who also optimized the curved grid pattern according to the least mass required under buckling limitations. The studies above only looked at linear analysis, which has less fundamental frequency and offers flexibility compared to nonlinear analysis; cutoff, on the other hand, lessens the rigidity of the structure. Therefore, the nonlinear behaviour of the shell structure must be taken into account. The nonlinear behaviour of the stiffened shell construction with cutout has only been examined by a few scholars. Fazilati and Oyesy (2013) used a developed finite strip method (FSM) and HSDT to explore the dynamic instability of longitudinally stiffened panels with rectangular interior cutouts under parametric in-plane loads Karpov (2018) modelled a shell with cutouts, reinforcement plates, and ribs and created a nonlinear mathematical model of the deformation of shells with stepwise variable thickness. None, however, have examined the free vibration behaviour of shallow elliptical paraboloidal shells with cutouts that are strengthened geometrically nonlinearly.

2.2.3 Stiffened and Unstiffened shells

Composite elliptic paraboloids can perform better with stiffeners. Those authors employed linear formulation, as demonstrated by Goswami and Mukhopadhyay (1995), who examined the frequencies of stiffened and unstiffened panels. Because of its simplicity, the linear formulation was chosen. Prusty and Satsangi (2001) adopted a similar strategy and concluded that applying stiffeners reduces the dynamic displacements of panels. Later, Prusty (2008) developed laminated spherical panels with stiffeners in the shapes of Ts, hats, and rectangles for the investigation of stiffened truncated spherical shells Ansari et al. (2023) and sandwiched porous functionally graded panels Rao and Fu (2024), the comparatively more straightforward linear technique was chosen. Later, Goswami and Mukhopadhyay (1995) used geometric nonlinearity for stiffened laminated composite panels to produce dynamic deflections and stress results of supported panels. Bich et al. also employed the nonlinear approach for functionally graded panels with eccentrically stiffened faults (2013, 2014). Duc (2013) studied the panels on elastic foundations using a nonlinear approach. The nonlinear vibration of defective panels under temperature changes was examined by Ahmadi et al. in 2021.

Stiffened elliptic paraboloidal panels are frequently cast using modular components in real-world applications. Skewed modular panels can be used to cover parallelogram-shaped facilities. The hull panels of ships and the wings of airplanes are two more real-world skewed panels. Numerous researchers have written about how skewness affects laminated composites, but they have only looked at plate structures. The linear formulation was preferred in those investigations. Wang (1997) reported the fundamental frequencies of skew plates using Mindlin theory. A number of skew-clamped plate modes' frequencies were reported by Ashour (2009). Noh and Lee (2014) investigated the instability of skew plates subjected to hygrothermal variations. Kallannavar and associates (2020) looked at sandwiched and hybrid skew plates. The dynamic properties of point-supported graphene platelet-reinforced plates were investigated by Kiani and Żur (2022). For skewed plates, some researchers used geometrically nonlinear formulas. The nonlinear stability of skew plates under biaxial follower forces was examined by Liao and Lee (1993). Malekzadeh and Karami (2006) reported the deflections and stress findings of skew plates using Von-Karman strains. Nonlinear frequencies were discovered on skew plates by Singha and Ganapathi (2004) and Singha and Daripa (2007). Daripa and Singha (2009) and Singha et al. (2006) investigated the nonlinear buckling of skew plates. Higher-order shear deformation on skew plates with cutouts was noted by Lee (2010). Upadhyay and Shukla (2012) computed nonlinear deflections and moment findings of skew plates using the Chebyshev polynomial. Later, they looked into the nonlinear vibration and bending of skew plates made of composites with functional grades. Naghsh and Azhari (2015) worked with point-supported plates using nonlinear strains and the Galerkin approach. CNT-reinforced skew plates were examined by Zhang and Xiao (2017) under dynamic stresses. Skewed functionally graded plates were assessed by Tomar and Talha (2019) at different temperatures. Nonlinear frequencies in porous skew plates were examined by Naveen et al. in 2021. Sengar et al. (2023) used the isogeometric method on sandwiched skew plates. The first description of the free vibration of skewed composite elliptic paraboloids was given by Chaubey et al. (2018). The authors reported fundamental frequencies and mode shapes for cuts of different sizes using both concentrated and distributed mass approaches. However, the authors did not experiment with stiffened panels and instead employed a geometrically linear model.

Surprisingly, few studies have been conducted on stiffened panels, but many have been conducted on circular paraboloidal panels using geometrically nonlinear formulas. This research

gap highlights the pressing need for more study and potential contributions to the field. Important contributions were made by Goswami and Mukhopadhyay (1995) through their study of laminated composite stiffened panels.

Chapter 3

SCOPE OF THE PRESENT STUDY

3.1 General Overview

In the previous chapter, a comprehensive review of existing literature related to shell structures was presented, highlighting key developments in the analysis of laminated composite shells over the past few decades. It became evident from the review that although numerous studies have addressed different shell geometries, the specific investigation of laminated composite elliptical and hyperbolic paraboloidal shells—particularly those with cutouts—remains relatively underexplored. This is despite their growing significance in structural applications due to their excellent stiffness characteristics and architectural appeal.

Considering the increasing need for lightweight and high-performance structural elements in fields such as civil, aerospace, and mechanical engineering, laminated composite shells with advanced geometries have emerged as promising solutions. Among them, elliptical and hyperbolic paraboloidal shells, when integrated with cutouts for functional or aesthetic reasons, present unique challenges in terms of their vibration behaviour. However, there exists a research gap in understanding how these structural modifications influence their free vibration response.

The present study aims to fill this gap by examining the dynamic characteristics—specifically the free vibration response of laminated composite elliptical and hyperbolic paraboloidal shells with various cutout configurations. This investigation considers different lamination sequences and boundary conditions to evaluate their influence on natural frequencies and mode shapes.

Accordingly, the specific scope and objectives of this study are elaborated in the subsequent sections of this chapter, with the intention of contributing meaningful insights to the design and analysis of complex composite shell structures used in modern engineering applications.

3.2 Present Scope

The present study focuses on the free vibration behaviour of graphite-epoxy and bamboo mat reinforced polymer (BMRP) laminated elliptical paraboloidal shell and graphite-epoxy hyperbolic paraboloidal shell structures with cutouts, considering their significance in advanced structural applications. The shell configurations are analysed under various boundary conditions, representing practical support scenarios often encountered in real-world applications.

During the course of this research, it was recognized that comprehensive information on the free vibration response of such shell forms, particularly with cutouts and different lamination schemes, is essential for structural designers. Such data would aid in selecting suitable lamination sequences and support conditions to achieve optimum dynamic performance based on design requirements.

A detailed finite element formulation has been developed, as presented in Chapter 4, using an eight-noded curved quadratic isoparametric shell element. This element is employed to study the free vibration characteristics of laminated elliptical paraboloidal shells with and without cutouts.

To validate the methodology, standard benchmark problems are first solved. Following validation, a range of parametric studies are performed involving variations in:

- Lamination schemes (eight different stacking sequences of graphite-epoxy composite),
- Boundary conditions (four practical support configurations),
- Cutout geometries (size and location).

The influence of these parameters on the fundamental natural frequencies and mode shapes is analysed in detail, and critical observations are highlighted to guide future design practices.

Chapter 4

MATHEMATICAL FORMULATION

4.1 General

This chapter outlines the mathematical framework and computational approach employed to analyse the free vibration behaviour of laminated composite hyperbolic and elliptical paraboloidal shells incorporating cutouts. The formulation is developed using the Finite Element Method, which is well-suited for capturing the complexities introduced by composite layering, curved geometries, and material anisotropy. All notations and variables used throughout the chapter are either defined at their first occurrence or included in the comprehensive 'List of Notations' section at the beginning of this thesis for clarity and consistency. The structural model under consideration is an hyperbolic and elliptical paraboloidal shell (refer to Figure 4.1), composed of laminated composite material with a uniform total thickness h. The geometry is defined by its principal radii of curvature R_{xx} and R_{yy} . The shell comprises multiple thin laminae stacked through the thickness, with each lamina possibly oriented at an arbitrary fiber angle θ relative to the global x-axis. Despite variations in fiber orientation, the overall thickness remains constant.

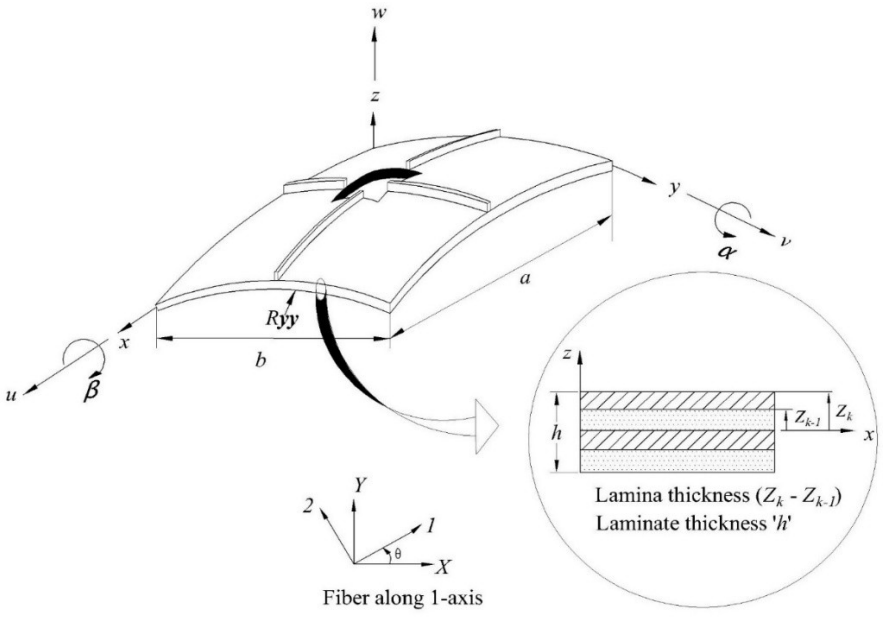

$$z = \frac{x^2}{a^2} + \frac{y^2}{b^2}$$

Figure 4.1: Laminated elliptic paraboloidal panel with composite stiffeners and concentric cutout.

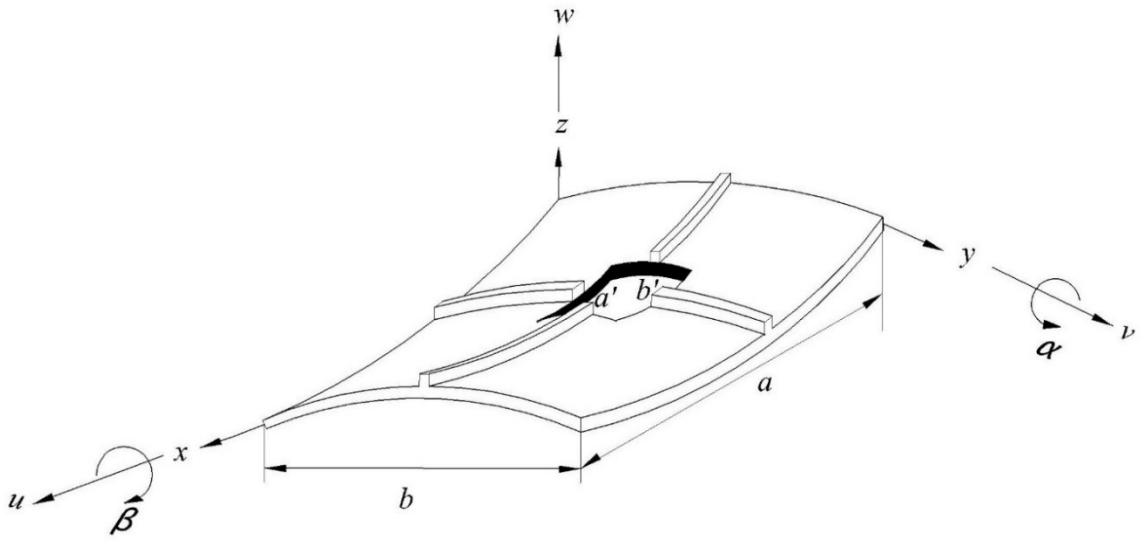

$$\frac{z}{c} = -\frac{x^2}{a^2} + \frac{y^2}{b^2}$$

Figure 4.2: Laminated hyperbolic paraboloidal panel with composite stiffeners and concentric cutout.

4.2 Finite Element Method

In the context of this study, the laminated composite hyperbolic and elliptical paraboloidal shell with cutouts is analysed using the Finite Element Method (FEM). This approach involves dividing the shell surface into a finite number of smaller subregions, known as elements, where the governing equations of motion are numerically approximated. The entire structural domain is discretized into these interconnected elements to simplify the complex geometry and material behaviour into manageable computations. Each element shares boundary information with its neighbouring elements through common connection points known as nodes. This discretization process enables a comprehensive simulation of the shell's vibrational behaviour by systematically assembling the individual element equations to represent the entire shell structure.

4.3 Element Selection and Geometric Representation

For accurate modelling using the Finite Element Method, the selected element must be capable of capturing the geometric configuration of the shell structure both in its undeformed and deformed states. In the present study, a doubly curved eight-noded quadratic element is employed, which accommodates the three principal radii of curvature relevant to hyperbolic and elliptical paraboloidal shell geometry.

This element configuration includes four corner nodes and four mid-side nodes, enabling higher-order interpolation of displacement fields. The formulation is initially defined in the natural coordinate system $(\xi, \eta, \zeta)$and is subsequently mapped to the Cartesian coordinate system using the Jacobian transformation. This allows for an accurate geometric representation and efficient computation over the curved shell surface.

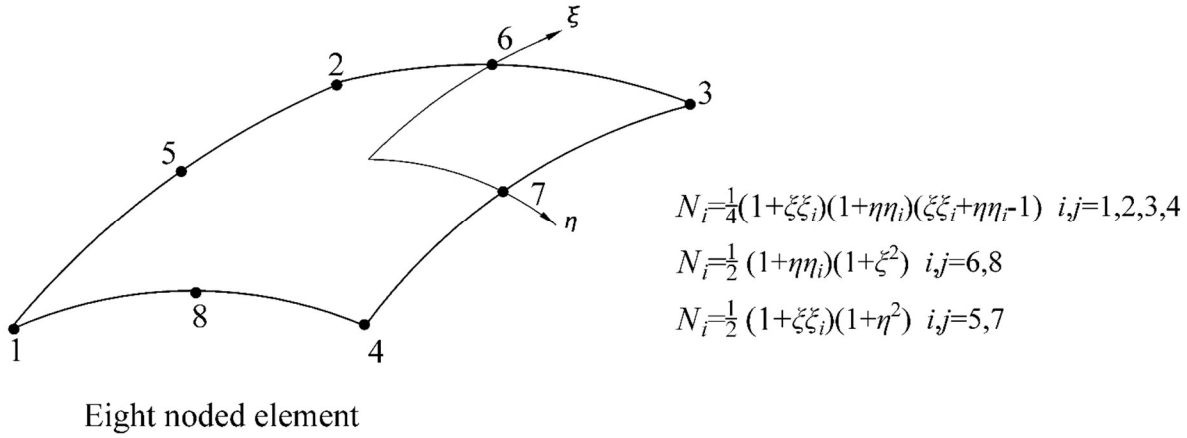

Figure 4.3 (i): The shell element in isoparametric coordinates.

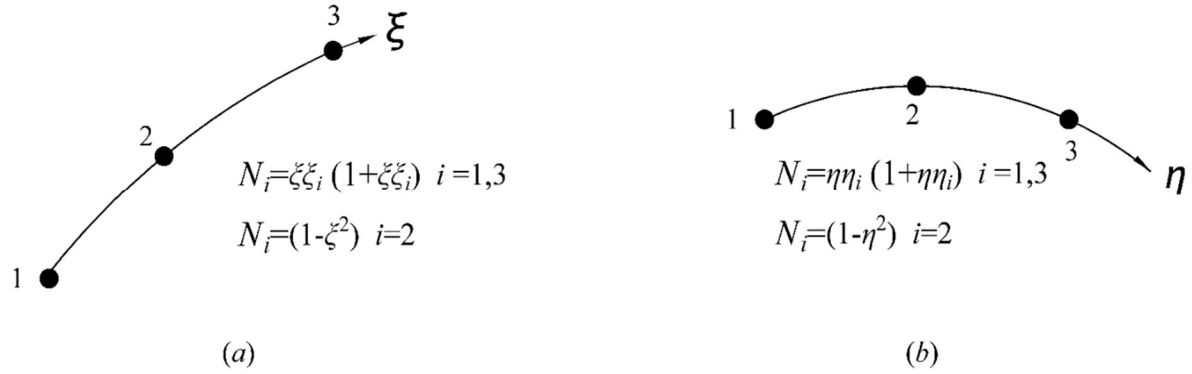

Figure 4.3 (ii): The Elements for (a) x – stiffener and (b) y – stiffener

4.4 Discretization of the Shell Surface

In this study, the hyperbolic and elliptical paraboloidal shell surface is discretized into multiple finite elements to facilitate numerical analysis. The mesh must be generated such that it can effectively capture the variation in the displacement field across the shell geometry. To ensure this, an appropriate number of divisions must be determined. This optimal mesh refinement is identified through a convergence study, the details of which are discussed in the following chapter.

4.5 Selection of Shape Functions

In the finite element formulation adopted for this study, shape functions also referred to as interpolation functions are employed to approximate displacement fields within each element using known nodal displacements. The analysis utilizes isoparametric elements, which allow both geometry and displacement fields to be interpolated using the same set of shape functions. These functions play a critical role in capturing the deformation behavior of the hyperbolic and elliptical paraboloidal shell. Since the shell elements considered here are thin, it is sufficient to define the shape functions as polynomials in terms of the natural coordinates ξ and η, assuming mid-surface nodes only. The displacement field is initially expressed as a general polynomial function, and by applying nodal constraints or boundary conditions, the shape functions specific to each element are determined.

The displacement field within each element is formulated using a polynomial expression constructed based on the structure of Pascal's triangle, which ensures inclusion of all relevant terms for accurate interpolation of displacements over the shell surface.

$$u(\xi,\eta) = A_0 + A_1\xi + A_2\eta + A_3\xi^2 + A_4\xi\eta + A_5\eta^2 + A_6\xi^2\eta + A_7\xi\eta^2 \quad (4.1)$$

By solving it at eight nodal points we can obtain the shape functions,

$$N_i = \frac{1}{4}(1+\xi\xi_i)(1+\eta\eta_i)(\xi\xi_i+\eta\eta_i-1) \quad i = 1,2,3,4$$

$$N_i = \frac{1}{2}(1+\xi\xi_i)(1+\eta^2), \mathrm{i} = 5,7$$

$$N_i = \frac{1}{2}(1+\eta\eta_i)(1+\xi^2), \mathrm{i} = 6,8 \quad (4.2)$$

Shape functions for stiffeners,

For stiffener in *x*-direction

$$\begin{aligned} N_i &= \xi\xi_i(1+\xi\xi_i) && i = 1,3 \\ N_i &= (1-\xi^2) && i = 2 \end{aligned} \quad (4.3)$$

For stiffener in *y*-direction

$$\begin{aligned} N_i &= \eta\eta_i(1+\eta\eta_i) && i = 1,3 \\ N_i &= (1-\eta^2) && i = 2 \end{aligned} \quad (4.4)$$

Where N_i denotes the shapes function at i^{th} node having natural coordinates ξ_i and η_i . The correctness of the shape functions is checked from the relations

$$\sum N_i = 1, \frac{\sum \partial N_i}{\partial \xi} = 0 \text{ and } \frac{\sum \partial N_i}{\partial \eta} = 0 \quad (4.5)$$

Interpolation of geometric co-ordinates can also be performed by using the isoparametric finite element shape functions,

$x = \sum N_i x_i$ and $y = \sum N_i y_i$, i $= 1\ to\ 8$ (4.6)

Where x and y are the geometric co-ordinates of the ith node.

4.6 Selection of Generalized Displacement Fields

Although shell structures are inherently three-dimensional, their representation in finite element modeling can be optimized by using two-dimensional elements due to their relatively small thickness. Incorporating full three-dimensional elements would lead to an increase in the number of nodes and degrees of freedom, which in turn would raise computational costs without significant benefits for thin shell analysis. Therefore, in the present work, a two-dimensional element with five degrees of freedom per node—three translational $(u^{/}, v^{/}, w^{/})$ and two rotational $(\alpha^{/}, \beta^{/})$ is utilized. The formulation assumes mid-surface nodes only, and the normal line through the thickness remains straight after deformation, though it may not remain perpendicular to the mid-surface. The directions of the generalized displacements considered are illustrated in Figure 4.1. The relationships between the nodal degrees of freedom and the displacement at any given position with regard to the coordinates ξ and η are established by the following formulas.

$$u = \sum_{i=1}^{8} N_i u_i \quad v = \sum_{i=1}^{8} N_i v_i \quad w = \sum_{i=1}^{8} N_i w_i \quad \alpha = \sum_{i=1}^{8} N_i \alpha_i \quad \beta = \sum_{i=1}^{8} N_i \beta_i \tag{4.7}$$

The shape functions $[N]$and nodal degrees of freedom $\{\delta_i\}$ can be used to express an element's generalised displacement vector $\{\delta\}$ as follows:

$$\{\delta\} = \sum_{i=1}^{8} [N_i]\{\delta_i\} \tag{4.8}$$

$$\{\delta\} = \begin{Bmatrix} u \\ v \\ w \\ \alpha \\ \beta \end{Bmatrix} = \begin{bmatrix} [N_i] & & & & \\ & [N_i] & & & \\ & & [N_i] & & \\ & & & [N_i] & \\ & & & & [N_i] \end{bmatrix} \begin{bmatrix} u_i \\ v_i \\ w_i \\ \alpha_i \\ \beta_i \end{bmatrix} \tag{4.9}$$

where, $[N_i] = [N_1 \quad N_2 \quad N_3 \quad . \quad . \quad . \quad N_8]$

and, $[u_i] = [u_1 \quad u_2 \quad u_3 \quad . \quad . \quad u_8]$

$[v_i] = [v_1 \quad v_2 \quad v_3 \quad . \quad . \quad . \quad v_8]$

$[w_i] = [w_1 \quad w_2 \quad w_3 \quad . \quad . \quad w_8]$

$$[\alpha_i] = [\alpha_1 \quad \alpha_2 \quad \alpha_3 \quad . \quad . \quad \alpha_8]$$
$$[\beta_i] = [\beta_1 \quad \beta_2 \quad \beta_3 \ldots \quad \beta_8] \qquad (4.10)$$

Degrees of Freedom for Stiffeners

Single-layered composites with longitudinal lamination make up the stiffeners. The stiffener's three noded elements and interpolation functions are shown in Figure 4.3.

The rotations and displacements of stiffeners are as follows:

$\{\delta_{sx}\} = \{u_{sx} \quad w_{sx} \quad \alpha_{sx} \quad \beta_{sx}\}^T$ for x – stiffener.

$\{\delta_{sy}\} = \{v_{sy} \quad w_{sy} \quad \alpha_{sy} \quad \beta_{sy}\}^T$ for y – stiffener.

***x* – stiffener**

The element displacements $\{\delta_{sx}\}$ are given below,

$\{\delta_{sx}\} = \sum_{j=1}^{3}[N_{\xi j}]\{\delta_{sxj}\}$, where $\{\delta_{sxj}\} = \{u_{sxj} \quad w_{sxj} \quad \alpha_{sxj} \quad \beta_{sxj}\}^T$ (4.11)

$[N_{\xi j}]$ and $\{\delta_{sxj}\}$ are interpolation functions and displacements at the j^{th} node of the stiffener.

***y* – stiffener**

The element displacements $\{\delta_{sy}\}$ are given below,

$\{\delta_{sy}\} = \sum_{j=1}^{3}[N_{\eta j}]\{\delta_{syj}\}$, where $\{\delta_{syj}\} = \{v_{syj} \quad w_{syj} \quad \alpha_{syj} \quad \beta_{syj}\}^T$ (4.12)

$[N_{\eta j}]$ and $\{\delta_{syj}\}$ are interpolation functions and displacements at the j^{th} node of the stiffener element.

4.7 Strain-Displacement Relationship

The strain-displacement relationships are formulated based on an enhanced first-order shear deformation theory suitable for thin shell structures. The displacement components are described as follows:

$$u = u_0 + z\alpha, \quad v = v_0 + z\beta, \quad w = w_0$$

where, u_0, v_0, w_0= Mid-plane translations along *x, y* and *z* axis respectively and *z* is the distance of fiber from mid-plane along thickness direction.

The generalized strain vector at any arbitrary depth (z) of the panel can be represented as,

$\{\varepsilon'\} = \{\varepsilon'\}^0 + z\{\kappa\}$ (4.13)

$$\begin{Bmatrix} \varepsilon_x \\ \varepsilon_y \\ \gamma_{xy} \\ \gamma_{xz} \\ \gamma_{yz} \end{Bmatrix} = \begin{Bmatrix} \varepsilon_x^0 \\ \varepsilon_y^0 \\ \gamma_{xy}^0 \\ \gamma_{xz}^0 \\ \gamma_{yz}^0 \end{Bmatrix} + z \begin{Bmatrix} k_x \\ k_y \\ k_{xy} \\ k_{xz} \\ k_{yz} \end{Bmatrix} \qquad (4.14)$$

he first vector on the right-hand side corresponds to the strains at the mid-plane, while the second vector accounts for the changes in the curvatures of the shell surface induced by loading. These vectors are associated with the degrees of freedom as follows:

and $\{\varepsilon^{/}\}^{0}$ is given below,

$$\{\varepsilon^{/}\}^{0} = \{\varepsilon^{/}\}^{L} + \{\varepsilon^{/}\}^{NL} \tag{4.15}$$

$\{\varepsilon^{/}\}^{L}$, $\{\varepsilon^{/}\}^{NL}$ = Linear and nonlinear strain vectors at mid-surface of shell, respectively, which are expressed below,

$$\{\varepsilon^{/}\}^{L} = \begin{Bmatrix} \frac{\partial u_0^{/}}{\partial x^{/}} + \frac{w_0^{/}}{R_{xx}} \\ \frac{\partial v_0^{/}}{\partial y^{/}} + \frac{w_0^{/}}{R_{yy}} \\ \frac{\partial u_0^{/}}{\partial y^{/}} + \frac{\partial v_0^{/}}{\partial x^{/}} + \frac{2w_0^{/}}{R_{xy}} \\ \alpha^{/} + \frac{\partial w_0^{/}}{\partial x^{/}} - \frac{u_0^{/}}{R_{xx}} \\ \beta^{/} + \frac{\partial w_0^{/}}{\partial y^{/}} - \frac{v_0^{/}}{R_{yy}} \end{Bmatrix}, \{\varepsilon^{/}\}^{NL} = \begin{Bmatrix} \frac{1}{2}\left(\frac{\partial w_0^{/}}{\partial x^{/}} - \frac{u_0^{/}}{R_{xx}}\right)^2 \\ \frac{1}{2}\left(\frac{\partial w_0^{/}}{\partial y^{/}} - \frac{v_0^{/}}{R_{yy}}\right)^2 \\ \left(\frac{\partial w_0^{/}}{\partial x^{/}} - \frac{u_0^{/}}{R_{xx}}\right)\left(\frac{\partial w_0^{/}}{\partial y^{/}} - \frac{v_0^{/}}{R_{yy}}\right) \\ 0 \\ 0 \end{Bmatrix}$$

$$\begin{Bmatrix} \varepsilon_x^0 \\ \varepsilon_y^0 \\ \gamma_{xy}^0 \\ \gamma_{xz}^0 \\ \gamma_{yz}^0 \end{Bmatrix} = \begin{Bmatrix} \frac{\partial u_0^{/}}{\partial x^{/}} + \frac{w_0^{/}}{R_{xx}} \\ \frac{\partial v_0^{/}}{\partial y^{/}} + \frac{w_0^{/}}{R_{yy}} \\ \frac{\partial u_0^{/}}{\partial y^{/}} + \frac{\partial v_0^{/}}{\partial x^{/}} + \frac{2w_0^{/}}{R_{xy}} \\ \alpha^{/} + \frac{\partial w_0^{/}}{\partial x^{/}} - \frac{u_0^{/}}{R_{xx}} \\ \beta^{/} + \frac{\partial w_0^{/}}{\partial y^{/}} - \frac{v_0^{/}}{R_{yy}} \end{Bmatrix} + \begin{Bmatrix} \frac{1}{2}\left(\frac{\partial w_0^{/}}{\partial x^{/}} - \frac{u_0^{/}}{R_{xx}}\right)^2 \\ \frac{1}{2}\left(\frac{\partial w_0^{/}}{\partial y^{/}} - \frac{v_0^{/}}{R_{yy}}\right)^2 \\ \left(\frac{\partial w_0^{/}}{\partial x^{/}} - \frac{u_0^{/}}{R_{xx}}\right)\left(\frac{\partial w_0^{/}}{\partial y^{/}} - \frac{v_0^{/}}{R_{yy}}\right) \\ 0 \\ 0 \end{Bmatrix} \tag{4.16}$$

$$\text{and, } \begin{Bmatrix} k_x \\ k_y \\ k_{xy} \\ k_{xz} \\ k_{yz} \end{Bmatrix} = \begin{Bmatrix} \frac{\partial \alpha^{/}}{\partial x^{/}} \\ \frac{\partial \beta^{/}}{\partial y^{/}} \\ \frac{\partial \alpha^{/}}{\partial y^{/}} + \frac{\partial \beta^{/}}{\partial x^{/}} \\ 0 \\ 0 \end{Bmatrix} \tag{4.17}$$

In the above relations R_{xx}, R_{yy} are principal curvature and R_{xy} cross curvature of the element. For the elliptic paraboloidal panel, $R_{xy} = 10^{40}$ is assigned to have the curvature effectively zero. The surface equation of any shell form can be represented by the equation $z = f(x, y)$. For shallow shells where, according to Vlasov (1958), the ratio of the rise to the shorter plan dimension is less than 0.2, the surface curvatures can be approximately represented as,

$$\frac{1}{R_x} = \frac{\partial^2 z}{\partial x^2}, \frac{1}{R_y} = \frac{\partial^2 z}{\partial y^2} \text{ and } \frac{1}{R_{xy}} = \frac{\partial^2 z}{\partial x\, \partial y} \tag{4.18}$$

The strain-displacement equation is furnished below,

$\{\varepsilon\}^0 = [B]\{\delta_i\}$

where, $\{\delta_i\}$ can be expressed with Equation (4.8).

$$[B] = \left([B_L] + \frac{1}{2}[B_{NL}]\right)$$

$$\{\varepsilon'\}^0 = \left([B_L] + \frac{1}{2}[B_{NL}]\right)\{\delta_i\} \tag{4.19}$$

where, $\{\varepsilon'\}^0 = \{\varepsilon^0_{x'} \quad \varepsilon^0_{y'} \quad \gamma^0_{xy'} \quad k_{x'} \quad k_{y'} \quad k_{xy'} \quad \gamma^0_{xz'} \quad \gamma^0_{yz'}\}^T$ (4.20)

$[B]^L$ matrix used here given earlier by Chakravorty et al. (1995). $[B]^{NL}$ is given as follows,

$[B]^{NL} = [A][G]$

$$[A] = \begin{bmatrix} \frac{\partial w_0}{\partial x} - \frac{u_0}{R_{xx}} & 0 \\ 0 & \frac{\partial w_0}{\partial y} - \frac{v_0}{R_{yy}} \\ \frac{\partial w_0}{\partial y} - \frac{v_0}{R_{yy}} & \frac{\partial w_0}{\partial x} - \frac{u_0}{R_{xx}} \end{bmatrix},$$

$$[G] = \begin{bmatrix} -\frac{N_i}{R_{xx}} & 0 & \frac{\partial N_i}{\partial x} & 0 & 0 \\ 0 & -\frac{N_i}{R_{yy}} & \frac{\partial N_i}{\partial y} & 0 & 0 \end{bmatrix} \quad i = 1 \text{ to } 8$$

$$[B]^L = \sum_{i=1}^{8} \begin{bmatrix} \frac{\partial N_i}{\partial x} & 0 & -\frac{N_i}{R_{xx}} & 0 & 0 \\ 0 & \frac{\partial N_i}{\partial y} & -\frac{N_i}{R_{yy}} & 0 & 0 \\ \frac{\partial N_i}{\partial y} & \frac{\partial N_i}{\partial x} & -\frac{2N_i}{R_{xy}} & 0 & 0 \\ 0 & 0 & 0 & \frac{\partial N_i}{\partial x} & 0 \\ 0 & 0 & 0 & 0 & \frac{\partial N}{\partial y} \\ 0 & 0 & 0 & \frac{\partial N_i}{\partial y} & \frac{\partial N_i}{\partial x} \\ 0 & 0 & \frac{\partial N_i}{\partial x} & N_i & 0 \\ 0 & 0 & \frac{\partial N_i}{\partial y} & 0 & N_i \end{bmatrix} \quad (4.21)$$

For $\phi \geq 0^0$, both $[B]^L$ and $[B]^{NL}$ matrices adopt

$R_{xx} = R'_{xx}$ and $R_{yy} = -R'_{yy}\cos\phi$.

The following can be obtained from Equation (4.19),

$$\frac{\partial\{\varepsilon'\}^0}{\partial\{\delta\}} = \left[\overline{B}\right] \qquad \text{and} \qquad [\bar{B}] = [B_L] + [B_{NL}] \quad (4.22)$$

Strain displacement relationship for stiffeners

For stiffener- x' : The mid-surface strains are as follows:

$$\{\varepsilon_{sx'}\} = \begin{Bmatrix} \frac{\partial u'_{sx'}}{\partial x'} - \frac{w'_0}{R'_{xx}} \\ \frac{\partial \alpha'_{sx'}}{\partial x'} \\ \frac{\partial \beta_{sx'}}{\partial x'} \\ \alpha'_{sx'} + \frac{\partial w'_{sy'}}{\partial x'} \end{Bmatrix} + \begin{Bmatrix} \frac{1}{2}\left(\frac{\partial w'_{sx'}}{\partial x'} - \frac{u_{sx'}}{R'_{xx}}\right)^2 \\ 0 \\ 0 \\ 0 \end{Bmatrix} = \{\varepsilon_{sx'}\}^L + \{\varepsilon_{sx'}\}^{NL} \quad (4.23)$$

The strain-displacement equation is,

$$\{\varepsilon_{sx'}\} = \left([B_L]^{sx} + \frac{1}{2}[B_{NL}]^{sx}\right)\{\delta_{sxj}\} \quad (4.24)$$

where $\{\delta_{sxj}\} = \{u_{sxj} \quad w_{sxj} \quad \alpha_{sxj} \quad \beta_{sxj}\}^T$ and $j = 1$ to 3.

Equation (4.24) leads to the following:

$\frac{\partial\{\varepsilon_{sx'}\}}{\partial\{\delta_{sx}\}} = [\bar{B}]_x$ and $[\bar{B}]_x = [B_L]^{sx} + [B_{NL}]^{sx}$

The matrices, $[B_{sx}]^L$ and $[B_{sx}]^{NL}$ are given below,

$$[B_{sx}]^L = \sum_{i=1}^{3} \begin{bmatrix} \frac{\partial N_i^{sx}}{\partial x} & \frac{N_i^{sx}}{R_{xx}} & 0 & 0 \\ 0 & 0 & \frac{\partial N_i^{sx}}{\partial x} & 0 \\ 0 & 0 & 0 & \frac{\partial N_i^{sx}}{\partial x} \\ 0 & \frac{\partial N_i^{sx}}{\partial x} & N_i^{sx} & 0 \end{bmatrix}$$

and $$[B_{sx}]^{NL} = \frac{1}{2}\left[\frac{\partial w_{sx}}{\partial x} - \frac{u_{sx'}}{R_{xx}}\right] \sum_{i=1}^{3} \begin{bmatrix} \frac{N_i^{sx}}{R_{xx}} & \frac{\partial N_i^{sx}}{\partial x} & 0 & 0 \\ 0 & 0 & 0 & 0 \\ 0 & 0 & 0 & 0 \\ 0 & 0 & 0 & 0 \end{bmatrix}$$

For $\phi \geq 0^0$, the above matrices adopt, $R_{xx} = R'_{xx}$

For stiffener- y' : The mid-surface strains are as follows:

$$\{\varepsilon_{sy'}\} = \begin{Bmatrix} \frac{\partial v_{sy'}}{\partial y'} - \frac{w_{sy'}}{R'_{yy}} \\ \frac{\partial \beta_{sy'}}{\partial y'} \\ \frac{\partial \alpha_{sy'}}{\partial y'} \\ \beta_{sy'} + \frac{\partial w_{sy'}}{\partial y'} \end{Bmatrix} + \begin{Bmatrix} \frac{1}{2}\left(\frac{\partial w_{sy'}}{\partial y'} - \frac{v_{sy'}}{R'_{yy}}\right)^2 \\ 0 \\ 0 \\ 0 \end{Bmatrix} = \{\varepsilon_{sy'}\}^L + \{\varepsilon_{sy'}\}^{NL} \qquad (4.25)$$

The strain-displacement equation is,

$$\{\varepsilon_{sy'}\} = \left([B_L]^{sy} + \frac{1}{2}[B_{NL}]^{sy}\right)\{\delta_{syj}\} \qquad (4.26)$$

where $\{\delta_{syj}\} = \{u_{syj} \quad w_{syj} \quad \alpha_{syj} \quad \beta_{syj}\}^T$ j = 1 to 3

Equation (4.26) leads to the following:

$$\frac{\partial\{\varepsilon_{sy'}\}}{\partial\{\delta_{sy}\}} = [\bar{B}]_y \qquad \text{where} \qquad [\bar{B}]_y = [B_L]^{sy} + [B_{NL}]^{sy} \qquad (4.27)$$

$[B_{sy}]^L$ and $[B_{sy}]^{NL}$ are given in Bakshi (2021*a*) considering $R_{yy} = R'_{yy}\cos\phi$.

It can be observed from the strain-displacement matrix $[B]$ that interpolation functions are required to derive with respect to global Cartesian co-ordinates. But the shape functions used to describe the geometry and displacement variation are expressed in natural co-ordinate (ξ, η) system. The relationship between two co-ordinate systems can be computed using chain rule of partial differentiation and it is given below,

$$\begin{bmatrix} \frac{\partial}{\partial \xi} \\ \frac{\partial}{\partial \eta} \end{bmatrix} = \begin{bmatrix} \frac{\partial x}{\partial \xi} & \frac{\partial y}{\partial \xi} \\ \frac{\partial x}{\partial \eta} & \frac{\partial y}{\partial \eta} \end{bmatrix} \begin{bmatrix} \frac{\partial}{\partial x} \\ \frac{\partial}{\partial y} \end{bmatrix} \tag{4.28}$$

$$\begin{Bmatrix} \frac{\partial}{\partial \xi} \\ \frac{\partial}{\partial \eta} \end{Bmatrix} = [J] \begin{Bmatrix} \frac{\partial}{\partial x} \\ \frac{\partial}{\partial y} \end{Bmatrix} \tag{4.29}$$

where $[J]$ is the Jacobian matrix. Hence the derivatives with respect to Cartesian co-ordinate system is,

$$\begin{Bmatrix} \frac{\partial}{\partial x} \\ \frac{\partial}{\partial y} \end{Bmatrix} = [J]^{-1} \begin{Bmatrix} \frac{\partial}{\partial \xi} \\ \frac{\partial}{\partial \eta} \end{Bmatrix} \tag{4.30}$$

Using Equation (4.4) the Jacobian matrix will be,

$$[J] = \begin{bmatrix} \sum_{i=1}^{8} x_i \frac{\partial N_i}{\partial \xi} & \sum_{i=1}^{8} y_i \frac{\partial N_i}{\partial \xi} \\ \sum_{i=1}^{8} x_i \frac{\partial N_i}{\partial \eta} & \sum_{i=1}^{8} y_i \frac{\partial N_i}{\partial \eta} \end{bmatrix} \tag{4.31}$$

Now, by using the Jacobian matrix, the elements of strain-displacement matrix are obtained.

4.8 Force-Strain Relationship of the Composite Material:

Before evaluating the structural behaviour of laminated composite shells, it is essential to understand the derivation of force-strain relationships for composite materials. The microstructure of a fiber-reinforced lamina is inherently complex; therefore, to facilitate micromechanical modelling and analysis, several idealized assumptions are typically adopted:

1. The fiber and matrix constituents are assumed to be individually homogeneous and isotropic in nature.

2. Both constituents and the resulting composite exhibit linear elastic behavior under applied loading.
3. A perfect interfacial bond between the fiber and matrix is assumed, implying no relative motion or slippage at the interface.
4. Fibers are considered to be uniformly distributed, regularly spaced, and perfectly aligned within the matrix.
5. The matrix is assumed to be free from voids or imperfections.
6. The composite lamina is considered to be in an initial stress-free state prior to loading.

4.8.1 Elastic Properties of Unidirectional Lamina

4.8.1.1 Stress- strain relationship

$$\begin{Bmatrix}\sigma_1\\ \sigma_2\\ \sigma_3\\ \sigma_4\\ \sigma_5\\ \sigma_6\end{Bmatrix} = \begin{bmatrix}C_{11} & C_{12} & C_{13} & C_{14} & C_{15} & C_{16}\\ C_{21} & C_{22} & C_{23} & C_{24} & C_{25} & C_{26}\\ C_{31} & C_{32} & C_{33} & C_{34} & C_{35} & C_{36}\\ C_{41} & C_{42} & C_{43} & C_{44} & C_{45} & C_{46}\\ C_{51} & C_{52} & C_{53} & C_{54} & C_{55} & C_{56}\\ C_{61} & C_{62} & C_{63} & C_{64} & C_{65} & C_{66}\end{bmatrix}\begin{Bmatrix}\varepsilon_1\\ \varepsilon_2\\ \varepsilon_3\\ \varepsilon_4\\ \varepsilon_5\\ \varepsilon_6\end{Bmatrix}$$

Or, $\sigma_i = C_{ij}\varepsilon_j$ (4.32)

Where, ε_j =strain components corresponding to σ_i and (i,j=1,2,3,4,5,6)

And, C_{ij}=constitutive relationship matrix. $W = \frac{\sigma_i \varepsilon_i}{2}$ (4.33)

Work done per unit volume of the continuum, $W = \frac{C_{ij}\varepsilon_i\varepsilon_j}{2}$ (4.34)

Substituting σ_i from 4.20 to 4.21, we get, $\sigma_i = \frac{\partial W}{\partial \varepsilon_i} = C_{ij}\varepsilon_j$ (4.35)

Differentiating again with respect to ε_j we get, $\frac{\partial^2 W}{\partial \varepsilon_i \partial \varepsilon_j} = C_{ij}$ (4.36)

Based on the above procedure, if the differentiation is first performed with respect to ε_j, and aw then with respect to ε_i,, we get,

$$C_{ij} = \frac{\partial^2 W}{\partial \varepsilon_j \partial \varepsilon_i} \quad (4.37)$$

So, we can see from Equations (4.24) and (4.25) that $C_{ij} = C_{ji}$ and hence it is also established that the constitutive matrix for an anisotropic material is symmetric.

Now from the theory of elasticity compliance matrix can be written as,

$$\begin{Bmatrix}\varepsilon_1\\ \varepsilon_2\\ \varepsilon_3\\ \varepsilon_4\\ \varepsilon_5\\ \varepsilon_6\end{Bmatrix} = \begin{bmatrix} \frac{1}{E_1} & -\frac{\nu_{21}}{E_2} & \frac{\nu_{31}}{E_3} & 0 & 0 & 0 \\ -\frac{\nu_{12}}{E_1} & \frac{1}{E_2} & -\frac{\nu_{32}}{E_3} & 0 & 0 & 0 \\ -\frac{\nu_{13}}{E_1} & -\frac{\nu_{23}}{E_2} & \frac{1}{E_3} & 0 & 0 & 0 \\ 0 & 0 & 0 & \frac{1}{G_{23}} & 0 & 0 \\ 0 & 0 & 0 & 0 & \frac{1}{G_{31}} & 0 \\ 0 & 0 & 0 & 0 & 0 & \frac{1}{G_{12}} \end{bmatrix} \begin{Bmatrix}\sigma_1\\ \sigma_2\\ \sigma_3\\ \sigma_4\\ \sigma_5\\ \sigma_6\end{Bmatrix} \quad (4.38)$$

By inversing the above compliance matrix, we get the constitutive relationship matrix of the anisotropic material as,

$$\begin{bmatrix}\sigma_1\\ \sigma_2\\ \sigma_3\\ \sigma_4\\ \sigma_5\\ \sigma_6\end{bmatrix} = \begin{bmatrix} C_{11} & C_{12} & C_{13} & 0 & 0 & 0 \\ C_{21} & C_{22} & C_{23} & 0 & 0 & 0 \\ C_{31} & C_{32} & C_{33} & 0 & 0 & 0 \\ 0 & 0 & 0 & C_{44} & 0 & 0 \\ 0 & 0 & 0 & 0 & C_{55} & 0 \\ 0 & 0 & 0 & 0 & 0 & C_{66} \end{bmatrix} \begin{bmatrix}\varepsilon_1\\ \varepsilon_2\\ \varepsilon_3\\ \varepsilon_4\\ \varepsilon_5\\ \varepsilon_6\end{bmatrix} \quad (4.37)$$

Where, $C_{11} = E_1 \frac{1-\nu_{23}\nu_{32}}{\Delta}, C_{12} = E_1 \frac{\nu_{21}+\nu_{31}\nu_{23}}{\Delta} = E_2 \frac{\nu_{12}+\nu_{32}\nu_{13}}{\Delta}$

$C_{13} = E_1 \frac{\nu_{31}+\nu_{21}\nu_{32}}{\Delta} = E_3 \frac{\nu_{13}+\nu_{12}\nu_{23}}{\Delta}, C_{22} = E_2 \frac{1-\nu_{13}\nu_{31}}{\Delta}, C_{33} = E_2 \frac{1-\nu_{12}\nu_{21}}{\Delta},$

$C_{23} = E_2 \frac{\nu_{32}+\nu_{12}\nu_{31}}{\Delta} = E_3 \frac{\nu_{23}+\nu_{21}\nu_{13}}{\Delta}, C_{44} = G_{23}, C_{55} = G_{31}, C_{66} = G_{12}$

$\Delta = 1 - \nu_{12}\nu_{21} - \nu_{23}\nu_{32} - \nu_{13}\nu_{31} - 2\nu_{12}\nu_{23}\nu_{13}$

4.8.1.2 Derivation of Reduced Stiffness Matrix of an Individual Lamina:

Now individual lamina is very thin and any stress component in the transverse direction can be neglected, but in the present study transverse shear deformation is considered. So, for an individual lamina $\sigma_{33} = 0$ Now, we are separating the in plane and out-of-plan stress components and hence Equation (4.37) results into,

$$\begin{Bmatrix}\sigma_1\\ \sigma_2\\ 0\\ \sigma_6\end{Bmatrix} = \begin{bmatrix} C_{11} & C_{12} & C_{13} & 0 \\ C_{21} & C_{22} & C_{23} & 0 \\ C_{31} & C_{32} & C_{33} & 0 \\ 0 & 0 & 0 & C_{66} \end{bmatrix} \begin{Bmatrix}\varepsilon_1\\ \varepsilon_2\\ \varepsilon_3\\ \varepsilon_6\end{Bmatrix} \quad (4.38)$$

And, $\begin{Bmatrix}\sigma_4\\ \sigma_5\end{Bmatrix} = \begin{bmatrix} C_{44} & 0 \\ 0 & C_{55} \end{bmatrix} \begin{Bmatrix}\varepsilon_4\\ \varepsilon_5\end{Bmatrix}$ (4.29)

Solving 4.38, yields

$$\sigma_1 = \left(C_{11} - \frac{C_{13}C_{13}}{C_{33}}\right)\varepsilon_1 + \left(C_{12} - \frac{C_{13}C_{23}}{C_{33}}\right)\varepsilon_2$$

$$= Q_{11}\varepsilon_1 + Q_{12}\varepsilon_2$$

And, $\sigma_2 = \left(C_{12} - \frac{C_{23}C_{13}}{C_{33}}\right)\varepsilon_1 + \left(C_{22} - \frac{C_{23}C_{23}}{C_{33}}\right)\varepsilon_2$

$= Q_{12}\varepsilon_1 + Q_{22}\varepsilon_2$

$\sigma_{66} = C_{66}\varepsilon_{66} = Q_{66}\varepsilon_6$

Writing the above equations in a matrix form, we get

$$\begin{Bmatrix}\sigma_1\\ \sigma_2\\ \sigma_6\end{Bmatrix} = \begin{bmatrix}Q_{11} & Q_{12} & 0\\ Q_{12} & Q_{22} & 0\\ 0 & 0 & Q_{66}\end{bmatrix}\begin{Bmatrix}\varepsilon_1\\ \varepsilon_2\\ \varepsilon_6\end{Bmatrix} \quad (4.39)$$

$$\{\sigma\}_{1,2} = [Q]_{1,2}\{\varepsilon\}_{1,2} \quad (4.40)$$

Where, $Q_{11} = (1 - \nu_{12}\nu_{21})^{-1}E_1; Q_{22} = (1 - \nu_{12}\nu_{21})^{-1}E_2; Q_{12} = (1 - \nu_{12}\nu_{21})^{-1}E_1\nu_{21}$

And $Q_{66} = G_{12}$

The $[Q]$ matrix in Equation (4.40) is termed as the reduced stiffness matrix of an individual lamina in the local co-ordinate system.

4.8.1.3 Derivation of Transformation Matrix:

Performing transformation of in-plane stress components from local co-ordinate system to global co-ordinate system,

$$\begin{Bmatrix}\sigma_x\\ \sigma_y\\ \tau_{xy}\end{Bmatrix} = \begin{bmatrix}m^2 & n^2 & -2mn\\ n^2 & m^2 & 2mn\\ mn & -mn & m^2 - n^2\end{bmatrix}\begin{Bmatrix}\sigma_1\\ \sigma_2\\ \tau_6\end{Bmatrix} \quad (4.41)$$

$$\{\sigma\}_{x,y} = [M]\{\sigma\}_{1,2} \quad (4.42)$$

As transverse shear deformation is considered in the present study, thus performing transformation of out-of-plan stress components from local co-ordinate system to global co-ordinate system,

$$\begin{Bmatrix}\tau_{yz}\\ \tau_{xz}\end{Bmatrix} = \begin{bmatrix}m & -n\\ n & m\end{bmatrix}\begin{Bmatrix}\tau_4\\ \tau_5\end{Bmatrix} \quad (4.43)$$

$$\{\sigma\}_{x,y} = [M]'\{\sigma\}_{1,2} \quad (4.44)$$

And $m = cos\theta\ n = sin\theta$

In Equation (4.42), the matrix, $[M]$ is termed as transformation matrix which is used to transfer in plane stress and strain components from local to global co-ordinate system transfer out-off plane stress and strain components from local to global co-ordinate system

4.8.1.4 Transformation of strain vector from Local to Global Co-Ordinate System:

Transformation matrix derived in Equation (4.42) can also be used to transform in plane strain components from local to global co-ordinate system.

$$\begin{Bmatrix} \varepsilon_x \\ \varepsilon_y \\ \frac{\varepsilon_{xy}}{2} \end{Bmatrix} = \begin{bmatrix} m^2 & n^2 & -2mn \\ n^2 & m^2 & 2mn \\ mn & -mn & m^2 - n^2 \end{bmatrix} \begin{Bmatrix} \varepsilon_1 \\ \varepsilon_2 \\ \frac{\varepsilon_6}{2} \end{Bmatrix} \tag{4.45}$$

$$\{\varepsilon\}_{x,y} = [M]\{\varepsilon\}_{1,2} \tag{4.46}$$

Performing transformation of out-of-plan stress components from local co-ordinate system to global co-ordinate system,

$$\begin{Bmatrix} \varepsilon_{yz} \\ \varepsilon_{xz} \end{Bmatrix} = \begin{bmatrix} m & -n \\ n & m \end{bmatrix} \begin{Bmatrix} \varepsilon_4 \\ \varepsilon_5 \end{Bmatrix} \tag{4.47}$$

$$\{\varepsilon\}_{x,y} = [M]'\{\varepsilon\}_{1,2} \tag{4.48}$$

4.8.1.5 Transformation of stress-strain matrix from Local to Global Co-Ordinate System:

Combining Equations (4.39), (4.41) and (4.45) we get in stress-strain relationship in global co-ordinate system,

$$\begin{Bmatrix} \sigma_x \\ \sigma_y \\ \tau_{xy} \end{Bmatrix} = \begin{bmatrix} m^2 & n^2 & -2mn \\ n^2 & m^2 & 2mn \\ mn & -mn & m^2 - n^2 \end{bmatrix} \begin{bmatrix} Q_{11} & Q_{12} & 0 \\ Q_{12} & Q_{22} & 0 \\ 0 & 0 & Q_{66} \end{bmatrix} \begin{bmatrix} m^2 & n^2 & 2mn \\ n^2 & m^2 & -2mn \\ -mn & mn & m^2 - n^2 \end{bmatrix} \begin{Bmatrix} \varepsilon_x \\ \varepsilon_y \\ \frac{\varepsilon_{xy}}{2} \end{Bmatrix} \tag{4.49}$$

$$\begin{Bmatrix} \sigma_x \\ \sigma_y \\ \tau_{xy} \end{Bmatrix} = \begin{bmatrix} Q_{xx} & Q_{xy} & Q_{xs} \\ Q_{yx} & Q_{yy} & Q_{ys} \\ Q_{sx} & Q_{xy} & Q_{xs} \end{bmatrix} \begin{Bmatrix} \varepsilon_x \\ \varepsilon_y \\ \varepsilon_{xy} \end{Bmatrix} \quad \because \varepsilon_{xy} = 2\gamma_{xy} \tag{4.50}$$

And combining Equations (4.29), (4.43) and (4.47) we get out of plane stress-strain relationships in global co-ordinate system,

$$\begin{Bmatrix} \tau_{yz} \\ \tau_{xz} \end{Bmatrix} = \begin{bmatrix} m & -n \\ n & m \end{bmatrix} \begin{bmatrix} C_{44} & 0 \\ 0 & C_{55} \end{bmatrix} \begin{bmatrix} m & n \\ -n & m \end{bmatrix} \begin{bmatrix} \gamma_{yz} \\ \gamma_{xz} \end{bmatrix} \tag{4.51}$$

$$\begin{Bmatrix} \tau_{yz} \\ \tau_{xz} \end{Bmatrix} = \begin{bmatrix} m^2 G_{23} - n^2 G_{31} & mn(G_{23} - G_{31}) \\ mn(G_{23} - G_{31}) & n^2 G_{23} + m^2 G_{31} \end{bmatrix} \begin{Bmatrix} \gamma_{yz} \\ \gamma_{xz} \end{Bmatrix} \tag{4.52}$$

$$\{\tau\} = (G_{ij})\{\gamma\}$$

$[Q]_{x,y}$ in Equation (4.50) represents the reduced stiffness of an individual lamina in global co-ordinate system. Elements of $[Q]_{x,y}$ has a specific significance. The elements show the coupling

effects of normal and shearing strain on normal stress and in the same way it also represents the coupling of shear strain and normal strain on shear stress. The terms of $[Q]_{x,y}$ are described below,

$$Q_{xx} = m^4Q_{11} + n^4Q_{22} + 2m^2n^2Q_{12} + 4m^2n^2Q_{66}$$
$$Q_{yy} = n^4Q_{11} + m^4Q_{22} + 2m^2n^2Q_{12} + 4m^2n^2Q_{66}$$
$$Q_{xy} = m^2n^2Q_{11} + m^2n^2Q_{22} + (m^4 + n^4)Q_{12} - 4m^2n^2Q_{66}$$
$$Q_{xs} = m^3nQ_{11} - mn^3Q_{22} + (mn^3 - m^3n)Q_{12} + 2(mn^3 - m^3n)Q_{66}$$
$$Q_{ys} = mn^3Q_{11} - m^3nQ_{22} + (m^3n - mn^3)Q_{12} + 2(m^3n - mn^3)Q_{66}$$
$$Q_{ss} = m^2n^2Q_{11} + m^2n^2Q_{22} - 2m^2n^2Q_{12} + (m^2 - n^2)Q_{66}$$

4.8.2 Stress-Strain Relationship for Laminate:

In the present study, the hyperbolic and elliptical paraboloidal shell is modeled as a laminate, which is a structural assembly composed of multiple laminae stacked and bonded together to behave as a single structural unit. Each lamina may possess distinct mechanical properties and orientations, but collectively, they form a unified shell structure suitable for dynamic analysis. To analyze the mechanical behavior of such a laminated composite system, the following assumptions are employed:

4.8.2.1 Assumptions to analyses a laminate:

1. Each individual layer (lamina) within the laminate is assumed to be quasi-homogeneous and anisotropic, meaning its material properties vary with direction but are uniform within each layer.
2. Displacement continuity is maintained across all layers, ensuring a smooth deformation profile through the thickness of the shell.
3. The laminate experiences small deformations, allowing linearization of governing equations.
4. The stress-strain and strain-displacement relationships are considered linear, adhering to classical elasticity theory.
5. Since the shell structure is thin, transverse shear deformations are assumed to be negligible but not zero. The normal to the mid-surface before deformation remains straight after deformation but not necessarily perpendicular to the mid-surface. A shear correction factor of unity is used to account for minor shear effects.
6. Perfect bonding between the individual plies is assumed, implying no delamination or relative sliding occurs between layers under loading.

Combining Equations (4.14) and (4.50) we get in stress-strain relationship for a laminate,

And $\begin{Bmatrix}\sigma_x\\ \sigma_y\\ \tau_{xy}\end{Bmatrix} = \begin{bmatrix}Q_{xx} & Q_{xy} & Q_{xs}\\ Q_{yx} & Q_{yy} & Q_{ys}\\ Q_{sx} & Q_{sy} & Q_{ss}\end{bmatrix}\begin{Bmatrix}\varepsilon_x\\ \varepsilon_y\\ \gamma_{xy}\end{Bmatrix} = \begin{bmatrix}Q_{xx} & Q_{xy} & Q_{xs}\\ Q_{yx} & Q_{yy} & Q_{ys}\\ Q_{sx} & Q_{sy} & Q_{ss}\end{bmatrix}\left\{\begin{bmatrix}\varepsilon_x^0\\ \varepsilon_y^0\\ \gamma_{xy}^0\end{bmatrix} + z\begin{Bmatrix}k_x\\ k_y\\ k_{xy}\end{Bmatrix}\right\}$

$$\begin{Bmatrix}\sigma_x\\ \sigma_y\\ \tau_{xy}\end{Bmatrix} = \left\{\begin{bmatrix}Q_{xx} & Q_{xy} & Q_{xs}\\ Q_{yx} & Q_{yy} & Q_{ys}\\ Q_{sx} & Q_{sy} & Q_{ss}\end{bmatrix}\begin{bmatrix}\varepsilon_x^0\\ \varepsilon_y^0\\ \gamma_{xy}^0\end{bmatrix} + z\begin{bmatrix}Q_{xx} & Q_{xy} & Q_{xs}\\ Q_{yx} & Q_{yy} & Q_{ys}\\ Q_{sx} & Q_{sy} & Q_{ss}\end{bmatrix}\begin{bmatrix}k_x\\ k_y\\ k_{xy}\end{bmatrix}\right\} \quad (4.53)$$

From Equation (4.52) we get out of plane stress-strain relationship for a laminate,

$$\begin{Bmatrix}\tau_{yz}\\ \tau_{xz}\end{Bmatrix} = \begin{bmatrix}m^2G_{23} - n^2G_{31} & mn(G_{23} - G_{31})\\ mn(G_{23} - G_{31}) & n^2G_{23} + m^2G_{31}\end{bmatrix}\begin{Bmatrix}\gamma_{yz}^0\\ \gamma_{xz}^0\end{Bmatrix} \because k_{yz} = k_{xz} = 0 \quad (4.54)$$

4.8.3 Equilibrium Equations

Equation (4.53) and (4.54) represent in plane and out of plane stress components of the kth lamina. To get the force and moment resultants of a lamina it is required to integrate stress over its thickness (h).

$$\{F\} = \begin{Bmatrix}N_x\\ N_y\\ N_{xy}\\ M_x\\ M_y\\ M_{xy}\\ Q_x\\ Q_y\end{Bmatrix} = \int_{-\frac{h}{2}}^{\frac{h}{2}} \begin{Bmatrix}\sigma_x dz\\ \sigma_y dz\\ \tau_{xy} dz\\ \sigma_x z dz\\ \sigma_y z dz\\ \tau_{xy} z dz\\ k\tau_{xz} dz\\ k\tau_{yz} dz\end{Bmatrix} \quad (4.55)$$

Stress varies discontinuously along the fibers and to get the stress resultants of a laminate it is requires adding the stress resultant for each layer numerically. In that way the normal stress resultants of a laminate are,

$$\begin{Bmatrix}N_x\\ N_y\\ N_{xy}\end{Bmatrix} = \sum_{k=1}^{n}\left\{\begin{bmatrix}Q_{xx} & Q_{xy} & Q_{xs}\\ Q_{yx} & Q_{yy} & Q_{ys}\\ Q_{sx} & Q_{sy} & Q_{ss}\end{bmatrix}\begin{bmatrix}\varepsilon_x^0\\ \varepsilon_y^0\\ \gamma_{xy}^0\end{bmatrix}\int_{z_{k-1}}^{z_k} dz + \begin{bmatrix}Q_{xx} & Q_{xy} & Q_{xs}\\ Q_{yx} & Q_{yy} & Q_{ys}\\ Q_{sx} & Q_{sy} & Q_{ss}\end{bmatrix}\begin{bmatrix}k_x\\ k_y\\ k_{xy}\end{bmatrix}\int_{z_{k-1}}^{z_k} z dz\right\} \quad (4.56)$$

Bending stress resultants are,

$$\begin{Bmatrix} M_x \\ M_y \\ M_{xy} \end{Bmatrix} = \sum_{k=1}^{n} \left\{ \begin{bmatrix} Q_{xx} & Q_{xy} & Q_{xs} \\ Q_{yx} & Q_{yy} & Q_{ys} \\ Q_{sx} & Q_{sy} & Q_{ss} \end{bmatrix} \begin{bmatrix} \varepsilon_x^0 \\ \varepsilon_y^0 \\ \gamma_{xy}^0 \end{bmatrix} \int_{z_{k-1}}^{z_k} z dz \right.$$

$$\left. + \begin{bmatrix} Q_{xx} & Q_{xy} & Q_{xs} \\ Q_{yx} & Q_{yy} & Q_{ys} \\ Q_{sx} & Q_{sy} & Q_{ss} \end{bmatrix} \begin{bmatrix} k_x \\ k_y \\ k_{xy} \end{bmatrix} \int_{z_{k-1}}^{z_k} z^2 dz \right\} \quad (4.57)$$

Transverse shear resultants are,

$$\begin{Bmatrix} Q_x \\ Q_y \end{Bmatrix} = \sum_{k=1}^{n} k \begin{bmatrix} m^2 G_{23} - n^2 G_{31} & mn(G_{23} - G_{31}) \\ mn(G_{23} - G_{31}) & n^2 G_{23} + m^2 G_{31} \end{bmatrix} \begin{Bmatrix} \gamma_{yz}^0 \\ \gamma_{xz}^0 \end{Bmatrix} \int_{z_{k-1}}^{z_k} dz \quad (4.58)$$

Where σ_x and σ_y are the normal stresses along X and Y directions, respectively and τ_{xy}, τ_{xz} . and τ_{yz} are shear stresses in XY, XZ and YZ planes, respectively. The thickness of a laminate is denoted by h. Here ' k ' is the shear correction factor to consider the transverse shear stress and for the present case it is considered '1' as the thickness is very small. In the present case upward deflection, tensile inplane forces, hogging moments and inplane shears tending to rotate the shell element anti-clockwise are taken positive.

$$\begin{Bmatrix} N_x \\ N_y \\ N_{xy} \\ M_x \\ M_y \\ M_{xy} \\ Q_x \\ Q_y \end{Bmatrix} = \begin{bmatrix} A_{11} & A_{12} & A_{16} & B_{11} & B_{12} & B_{16} & 0 & 0 \\ A_{12} & A_{22} & A_{26} & B_{12} & B_{22} & B_{26} & 0 & 0 \\ A_{16} & A_{26} & A_{66} & B_{16} & B_{26} & B_{66} & 0 & 0 \\ B_{11} & B_{12} & B_{16} & D_{11} & D_{12} & D_{16} & 0 & 0 \\ B_{12} & B_{22} & B_{26} & D_{12} & D_{22} & D_{26} & 0 & 0 \\ B_{16} & B_{26} & B_{66} & D_{16} & D_{26} & D_{66} & 0 & 0 \\ 0 & 0 & 0 & 0 & 0 & 0 & S_{11} & S_{12} \\ 0 & 0 & 0 & 0 & 0 & 0 & S_{12} & S_{22} \end{bmatrix} \begin{Bmatrix} \varepsilon_x^0 \\ \varepsilon_y^0 \\ \gamma_{xy}^0 \\ k_x \\ k_y \\ k_{xy} \\ \gamma_{xz}^0 \\ \gamma_{yz}^0 \end{Bmatrix} \quad (4.59)$$

Or, $\{F\} = [D]\{\varepsilon\}$ (4.60)

$\{F\} = [D](\{\varepsilon\}^L + \{\varepsilon\}^{NL})$

$$\{F\} = [E]\left([B_L] + \frac{1}{2}[B_{NL}]\right)\{\delta_i\} \quad (4.61)$$

[D] laminate constitutive relationship matrix and is adopted from Chakravorty et al. (1995).

Where, $A_{ij} = \sum_{k=1}^{n} \left(Q_{ij}\right)_k (z_k - z_{k-1})$

$$B_{ij} = \frac{1}{2} \sum_{k=1}^{n} \left(Q_{ij}\right)_k (z_k^2 - z_{k-1}^2)$$

$$D_{ij} = \frac{1}{3}\sum_{k=1}^{n} \left(Q_{ij}\right)_k (z_k^3 - z_{k-1}^3);$$

$$S_{ij} = \sum_{k=1}^{n} \left(G_{ij}\right)_k (z_k - z_{k-1})$$

In the above equations z_k and z_{k-1} are the distances measured from the mid-plane of a laminate to the bottom of the k[th] and (k - 1)[th] laminate, respectively. $\left(Q_{ij}\right)^k$ is the in plane elastic constant matrix for the k[th] lamina in global co-ordinate system and (G_{ij}) is the out-off plane elastic constant matrix for the k[th] lamina in global co-ordinate system. The 8×8 matrix in Equation (4.59) is termed as the laminate stiffness matrix $[D]$.

4.8.3.1 Force-deflection relationship

The following equation represents the force – deflection relationship of composite shell.

$$\{F\}^{/} = [E]\left([B_L] + \frac{1}{2}[B_{NL}]\right)\{\delta_i\} \tag{4.61}$$

where $\{\delta_i\} = \{u_i \quad v_i \quad w_i \quad \alpha_i \quad \beta_i\}^T$ and i = 1 to 8.

The stress resultants $\{F\}^{/}$ and matrix $[E]$ are given in Bakshi and Chakravorty (2014).

For stiffener along $x^{/}$ – axis,

$$\left\{F_{sx/}\right\}^{/} = \left[E_{sx/}\right]\left([B_L]^{sx} + \frac{1}{2}[B_{NL}]^{sx}\right)\left\{\delta_{sxj}\right\} \tag{4.62}$$

where $\left\{F_{sx/}\right\}^{/} = \begin{Bmatrix} N_{sx}^{/} \\ M_{sx}^{/} \\ T_{sx}^{/} \\ Q_{sx}^{/} \end{Bmatrix} = \int_{-\frac{d_{sx}}{2}}^{+\frac{d_{sx}}{2}} \int_{-\frac{b_{sx}}{2}}^{+\frac{b_{sx}}{2}} \begin{Bmatrix} \sigma_{sx}^{/} \\ \sigma_{sx}^{/} z \\ \left(\tau_{sxy}^{/} z - \tau_{sxz}^{/} y\right) \\ k_s \tau_{sxz}^{/} \end{Bmatrix} dydz$

In this context, b_{sx} and d_{sx} represent the width and depth of the stiffener oriented along the $x^{/}$-direction, respectively. The term $\sigma_{sx}^{/}$ denotes the longitudinal normal stress developed within the x-direction stiffener. Similarly, $\tau_{sxy}^{/}$and $\tau_{sxz}^{/}$refer to the shear stresses acting on the stiffener in the x–y and x–z planes, respectively. To account for the non-uniform distribution of shear stress across the cross-section of the stiffener, a shear correction factor k_s is introduced. In this study, a commonly used value of $k_s = \left(\frac{5}{6}\right)$ is adopted, which is standard for rectangular cross-sections.

For stiffener along $y^{/}$ –axis:

$$\left\{F_{sy/}\right\}^{/} = \left[E_{sy/}\right]\left([B_L]^{sy} + \frac{1}{2}[B_{NL}]^{sy}\right)\left\{\delta_{syj}\right\} \tag{4.63}$$

where $\{F_{sy/}\}^{/} = \begin{Bmatrix} N_{sy}^{/} \\ M_{sy}^{/} \\ T_{sy}^{/} \\ Q_{sy}^{/} \end{Bmatrix} = \int_{-\frac{d_{sy}}{2}}^{+\frac{d_{sy}}{2}} \int_{-\frac{b_{sy}}{2}}^{+\frac{b_{sy}}{2}} \begin{Bmatrix} \sigma_{sy}^{/} \\ \sigma_{sy}^{/} z \\ (\tau_{syx}^{/} z - \tau_{syz}^{/} y) \\ k_s \tau_{syz}^{/} \end{Bmatrix} dydz$

In the case of the stiffener aligned along the $y^{/}$-direction, b_{sy} and d_{sy} represent its width and depth, respectively. The term $\sigma_{sy}^{/}$ indicates the longitudinal normal stress acting within the $y^{/}$-direction stiffener. Additionally, the shear stresses acting on this stiffener are denoted by $\tau_{syx}^{/}$ and $\tau_{syz}^{/}$corresponding to shear in the *y–x* and *y–z* planes, respectively. To more accurately represent the non-uniform shear distribution across the cross-section of the stiffener, a shear correction factor k_s is used. In this analysis, a standard value of $k_s = \left(\frac{5}{6}\right)$ is assumed, which is widely accepted for rectangular cross-sections in composite and structural analysis. $[E_{sx/}]$ and $[E_{sy/}]$ are given in Bakshi (2021*a*). The compatibility between shell to stiffener elements follow the steps given in Bakshi (2021*a*).

4.9 Generalized Inertia Matrix:

The generalized inertia matrix, defined per unit area of the shell structure, accounts for both translational and rotational inertia effects. Translational inertia is related to the mass of the shell and represents its resistance to linear acceleration, whereas rotational inertia corresponds to the shell's opposition to angular acceleration, influenced by its moment of inertia. These inertial resistances are quantitatively expressed through the following formulations.

Mass per unit area is denoted by *m* and is given by

$m = \rho h$

Where ρ is mass density of shell,

Moment of inertia per unit are is denoted by *I* and is given by

$I = \frac{\rho h^3}{12}$

Incorporating both the translatory and rotary inertia terms, the generalized inertia matrix $[m]$ takes the following form,

$$[m] = \begin{bmatrix} \rho h & 0 & 0 & 0 & 0 \\ 0 & \rho h & 0 & 0 & 0 \\ 0 & 0 & \rho h & 0 & 0 \\ 0 & 0 & 0 & \frac{\rho h^3}{12} & 0 \\ 0 & 0 & 0 & 0 & \frac{\rho h^3}{12} \end{bmatrix} \quad (4.64)$$

Inertia matrix for *x*-stiffener:

$$[m_x] = \sum_{i=1}^{3} \begin{bmatrix} \rho . b_{sx}\, d_{sx} & 0 & 0 & 0 \\ 0 & \rho . b_{sx}\, d_{sx} & 0 & 0 \\ 0 & 0 & \frac{\rho . b_{sx}\, {d_{sx}}^2}{12} & 0 \\ 0 & 0 & 0 & \frac{\rho\left(b_{sx}\, {d_{sx}}^3 + d_{sx}\, {w_{sx}}^3\right)}{12} \end{bmatrix} \quad (4.65)$$

Inertia matrix for *y*-stiffener:

$$[m_y] = \sum_{i=1}^{3} \begin{bmatrix} \rho . b_{sy}\, d_{sy} & 0 & 0 & 0 \\ 0 & \rho . b_{sy}\, d_{sy} & 0 & 0 \\ 0 & 0 & \frac{\rho . b_{sy}\, {d_{sy}}^2}{12} & 0 \\ 0 & 0 & 0 & \frac{\rho\left(b_{sy}\, {d_{sy}}^3 + d_{sy}\, {b_{sy}}^3\right)}{12} \end{bmatrix} \quad (4.66)$$

4.10 General Dynamic Problem:

Hamilton's principle applied to the dynamic analysis of elastic bodies states that "among all admissible displacements which satisfy the specific boundary conditions, the actual solution makes the functional $\int (\mathrm{T} + \mathrm{W})\mathrm{dt}$ stationary, where T and W are the kinetic energy and work done by conservative and non-conservative forces. The stationary value is actually a minimum".

In the case of a dynamic problem without damping, the conservative forces are the elastic forces developed within the deformed body and the non-conservative forces are the external forcing functions.

The work done U_1 by conservative forces in shell element is given by,

$$\mathrm{U}_1 = \frac{1}{2}\int_v \{\sigma\}\{\varepsilon\}^T\, dv \quad (4.67)$$

Where $\{\varepsilon\}$ can be obtained through 4.20

Using 4.60 we get, $U_1 = \frac{1}{2}\int \int_A \{\varepsilon\}^T [D]\{\varepsilon\}\, dA$ (4.68)

The above is an area integral because for thin shells explicit integration has been performed through the thickness and thus the generalized force and moment resultants can directly be related to the strain components through the laminate stiffness matrix as in Equation (4.51). Substituting the relevant strain-displacement relations (4.13) for the shell in Equation (4.60)

we get, $U_1 = \frac{1}{2}\int \{\delta_i\}^T [B]^T [D][B]\{\delta_i\} dxdy$ (4.69)

$$\frac{\partial U_1}{\partial\{\delta\}} = \int_A \left[\overline{B}\right]^T [E]\left([B_L] + \frac{1}{2}[B_{NL}]\right)\{\delta_i\}\, dA$$

The kinetic energy U_2 of vibration of an element is expressed as an area integral and given by

$$U_2 = \frac{1}{2}\int \int_A \{\dot{\delta}\}^T [m]\left[\dot{\delta}\right] dA \quad (4.70)$$

Where the dot (.) represents derivative with respect to time. Substitution of the relations of the generalized displacement vector of the shell with the elemental nodal degrees of freedom (4.8) we get from 4.70,

$$U_2 = \frac{1}{2}\int \int_A \left\{\dot{\delta}_i\right\}^T [N_i]^T [m][N_i]\left\{\dot{\delta}_i\right\} dxdy \quad (4.71)$$

$$\frac{d}{dt}\left\{\frac{\partial U_2}{\partial\{\dot{\delta}\}}\right\} = \sum_{i=1}^{8} \int_A [N_i]^T [m][N_i]\left\{\ddot{\delta}_i\right\} dA \quad (4.72)$$

The work done U_3 by surface tractions in an element is given by

$$U_3 = -\int \int_A \{\delta\}^T [q] dA \quad (4.73)$$

$$\{q\} = [q_x \quad q_y \quad q_z \quad \mu_x \quad \mu_y]^T$$

in which q_x, q_y and q_z are the uniformly distributed loads per unit area along X, Y and Z axes, respectively, and μ_x and μ_y are the moments per unit area along X and Y axes, respectively. In case of shells subjected to transverse loads only q_x q_y μ_x and μ_y vanish and q_z remains, which is represented by the scalar notation 'q' hereafter.

From Equations (4.8) and (4.61), it is obtained that

$$U_3 = -\int \int_A \{\delta_i\}^T [N_i]^T [q] dxdy \quad (4.74)$$

Hamilton's principle may be used to derive Lagrange's equation of motion given by,

$$\frac{d}{dt}\left\{\frac{\partial U_2}{\partial\{\dot{\delta}\}}\right\} - \left\{\frac{\partial U_2}{\partial\{\delta\}}\right\} + \left\{\frac{\partial}{\partial\{\delta\}}(U_1 + U_3)\right\} = 0 \quad (4.75)$$

Since the kinetic energy U_2 depends on velocity alone, the second term of Equation (4.75) does not exist and the equation can be written as,

$$\frac{d}{dt}\left\{\frac{\partial U_2}{\partial\{\dot{\delta}\}}\right\}+\left\{\frac{\partial U_1}{\partial\{\delta\}}\right\}=-\left\{\frac{\partial U_3}{\partial\{\delta\}}\right\} \tag{4.76}$$

Substituting Equations (4.69), (4.71) and (4.74) in Equation (4.76) one gets,

$$\left\{\int\int_A [N_i]^T[m][N_i]dxdy\right\}\{\ddot{\delta}_i\}+\left\{\int\int_A [B]^T[D][B]dxdy\right\}\{\delta_i\}=$$

$$\int\int_A\{\delta_i\}^T[N_i]^T[q]dxdy \tag{4.77}$$

Equation (4.76) can be rewritten in the following form,

$$\sum_{i=1}^{8}\int_A [N_i]^T[m][N_i]\{\ddot{\delta}_i\}\,dA+\int_A\left[\overline{B}\right]^T[E]\left([B_L]+\frac{1}{2}[B_{NL}]\right)\{\delta_i\}\,dA$$

$$=\sum_{i=1}^{8}\int_A\{\delta_i\}^T[N_i]^T[q]dA \tag{4.78}$$

The coefficient of the acceleration vector $\{\ddot{\delta}_i\}$ of Equation (4.65) represents the consistent e element mass matrix$[M_e]$ and that of the displacement vector $\{\delta_i\}$ represents the element stiffness matrix $[K_e]$ and the term on the right hand side represents the consistent element nodal load vector $\{Q_e\}$.

Thus, Equations (4.77) result in

$$[M_e]\{\ddot{\delta}_i\}+[K_e]\{\delta_i\}=\{Q_e\} \tag{4.79}$$

$$[M_e]=\int\int_A [N_i]^T[m][N_i]dxdy \tag{4.80}$$

$$[K_e]=\int\int_A [B]^T[D][B]dxdy \tag{4.81}$$

$$\{Q_e\}=\int\int_A [N_i]^T\{q\}dxdy \tag{4.82}$$

Equation (4.76) can be rewritten as the following by combining Equations (4.25) and (4.26),

$$\sum_{i=1}^{8}\int_A [N_i]^T[m][N_i]\{\ddot{\delta}_i\}\,dA+\int_A\left[\overline{B}\right]^T[E]\left([B_L]+\frac{1}{2}[B_{NL}]\right)\{\delta_i\}\,dA=0$$

Equation (4.79) takes the following form for shell element,

$$[M_{sh}]\ \{\ddot{\delta}_\iota\}\ +[K_s]\{\delta_i\}\ =0$$

where, mass of panel is, $[M_{sh}] = \sum_{i=1}^{8} \int_A [N_i]^T [m][N_i] dA$

and stiffness of panel is, $[K_s] = \int_A \left[\overline{B}\right]^T [E] \left([B_L] + \frac{1}{2}[B_{NL}]\right) dA$

The stiffness ($[K_x]$ and $[K_y]$) and mass ($[M_{sx}]$ and $[M_{sy}]$) matrices for stiffeners can be obtained similarly. The matrices are given below,

***x* – stiffener:**

$$[M_{sx}] = \sum_{j=1}^{3} \int_A \left[N_{\xi j}\right]^T [m_x] \left[N_{\xi j}\right] dA$$

$$[K_x] = \int_A [\bar{B}]_x^T [E_{sx}] \left([B_L]^{sx} + \frac{1}{2}[B_{NL}]^{sx}\right) dA$$

***y* – stiffener:**

$$\left[M_{sy}\right] = \sum_{j=1}^{3} \int_A \left[N_{\eta j}\right]^T \left[m_y\right] \left[N_{\eta j}\right] dA$$

$$\left[K_y\right] = \int_A [\bar{B}]_y^T \left[E_{sy}\right] \left(\left[B_{sy}\right]^L + \frac{1}{2}\left[B_{sy}\right]^{NL}\right) dA$$

$[m_x]$ and $\left[m_y\right]$ are reported in Bakshi (2021*b*).

The stiffness and mass ($[K_e]$ and $[M_e]$) of stiffened elliptic paraboloidal panel is given below,

$[K_e] = [K_s] + [K_x] + \left[K_y\right]$ and $[M_e] = [M_{sh}] + [M_{sx}] + \left[M_{sy}\right]$

The stiffness matrix, $[K_e]$ is unsymmetric and modified following Nanda and Bandyopadhyay (2007). The modified stiffness matrix, $[K_{se}]$, is given below,

$$[K_{se}] = [K_L] + \frac{1}{2}[N_1] + \frac{1}{3}[N_2]$$

where,

$$[K_L] = \int_A ([B_L]^T [E][B_L]) dA$$

$$+ \int_A \{([B_L]^{sx})^T [E_{sx}][B_L]^{sx}\} dA$$

$$+ \int_A \left\{([B_L]^{sy})^T \left[E_{sy}\right][B_L]^{sy}\right\} dA$$

$$[N_1] = \int_A ([B_L]^T[E][B_{NL}] + [B_{NL}]^T[E][B_L] + [G]^T[S_L][G])dA$$

$$+ \int_A \begin{Bmatrix} ([B_L]^{sx})^T[E_{sx}][B_{NL}]^{sx} + ([B_{NL}]^{sx})^T[E_{sy}][B_L]^{sx} \\ +[G_{sx}]^T[S_{Lx}][G_{sx}] \end{Bmatrix} dA$$

$$+ \int_A \begin{Bmatrix} ([B_L]^{sy})^T[E_{sx}][B_{NL}]^{sy} + ([B_{NL}]^{sy})^T[E_{sy}][B_L]^{sy} \\ +[G_{sy}]^T[S_{Ly}][G_{sy}] \end{Bmatrix} dA$$

$$[N_2] = \int_A ([B_{NL}]^T[E][B_{NL}] + [G]^T[S_{NL}][G])dA$$

$$+ \int_A \{([B_{NL}]^{sx})^T[E_{sx}][B_{NL}]^{sx} + [G_{sx}]^T[S_{NLx}][G_{sx}]\}dA$$

$$+ \int_A \left\{([B_{NL}]^{sy})^T[E_{sy}][B_{NL}]^{sy} + [G_{sy}]^T[S_{NLy}][G_{sy}]\right\} dA$$

Transforming the equations (4.80, 4.81, 4.82) to local natural coordinates of ξ, η of the element, the element matrices can be expressed as

$$[K_e] = \int_{-1}^{+1}\int_{-1}^{+1} [B]^T[D][B]|J|d\xi d\eta \tag{4.83}$$

$$[M_e] = \int_{-1}^{+1}\int_{-1}^{+1} [N_i]^T[m][N_i]|J|d\xi d\eta \tag{4.84}$$

$$\{Q_e\} = \int_{-1}^{+1}\int_{-1}^{+1} [N_i]^T\{q\}|J|d\xi d\eta \tag{4.85}$$

The stiffness terms for the shell panel are given below,

The matrix $[G]$ is given in Bakshi and Chakravorty (2014).

$$[S_L] = \begin{bmatrix} N_x & N_{xy} \\ N_{xy} & N_y \end{bmatrix}^L \text{ and } [S_{NL}] = \begin{bmatrix} N_x & N_{xy} \\ N_{xy} & N_y \end{bmatrix}^{NL}$$

$$N_x = \sum_{m=1}^{n} \int_{z_{m-1}}^{z_m} \sigma_x \, dz \quad , \quad N_y = \sum_{m=1}^{n} \int_{z_{m-1}}^{z_m} \sigma_y \, dz \quad \text{and} \quad N_{xy} = \sum_{m=1}^{n} \int_{z_{m-1}}^{z_m} \sigma_{xy} \, dz$$

The stiffness terms for the x - stiffener are given below,

$$[G_{sx}] = \sum_{j=1}^{3} \begin{bmatrix} -\frac{N_{\xi j}}{R_{xx}} & \frac{\partial N_{\xi j}}{\partial x} & 0 & 0 \\ 0 & 0 & 0 & 0 \\ 0 & 0 & 0 & 0 \\ 0 & 0 & 0 & 0 \end{bmatrix} \quad , \quad [S_{Lx}] = [N_{sx}]^L \quad \text{and} \quad [S_{NLx}] = [N_{sx}]^{NL}$$

The stiffness terms for the y - stiffener are given below,

$$[G_{sy}] = \sum_{i=1}^{3} \begin{bmatrix} -\frac{N_{\eta j}}{R_{yy}} & \frac{\partial N_{\eta j}}{\partial y} & 0 & 0 \\ 0 & 0 & 0 & 0 \\ 0 & 0 & 0 & 0 \\ 0 & 0 & 0 & 0 \end{bmatrix} \quad , \quad [S_{Ly}] = [N_{sy}]^{L} \quad \text{and} \quad [S_{NLy}] = [N_{sy}]^{NL}$$

2×2 Gauss quadrature rule evaluates all terms of the matrices ($[K_{se}]$ and $[M_e]$). The global stiffness and mass are denoted as $[K_g]$ and $[M_g]$. An assembly of matrices over all elements is carried out for global ones.

$$[K_g] = \sum_{e=1}^{n} [K_{se}] \qquad \text{and} \qquad [M_g] = \sum_{e=1}^{n} [M_e] \qquad \text{where } n = \text{number of elements.}$$

The free vibration equation of stiffened panel is the following:

$[M_g]\{\ddot{\delta}_k\}_g + [K_g]\{\delta_k\}_g = 0$, where k = number of nodes. (4.87)

$\{\ddot{\delta}_k\}_g$ and $\{\delta_k\}_g$ represent global acceleration and displacement vectors. Equation (4.87) can be written as the following as given by Nanda and Bandyopadhyay (2007).

$$([K_g] - \omega^2[M_g])\{\delta_k\}_g = 0 \quad (4.88)$$

Equation (4.88) is solved iteratively using the steps suggested by Nanda and Bandyopadhyay (2007).

To accurately compute the element stiffness matrix ($[K_e]$)and mass matrix ($[M_e]$) ,numerical integration is carried out using Gaussian quadrature. Specifically, a 2×2 reduced integration scheme is adopted to mitigate the issue of shear locking, which can lead to over-stiffening of thin shell elements. This approach ensures efficient and precise evaluation of integrals within each finite element. The use of two-point Gaussian quadrature provides an optimal balance between computational cost and accuracy in capturing the behaviour of laminated composite hyperbolic and elliptical paraboloidal shells with cutouts under free vibration.

In the present analysis of laminated composite hyperbolic and elliptical paraboloidal shells with cutouts under free vibration, the element stiffness and mass matrices are directly defined in the global coordinate system (X-Y-Z). This approach eliminates the need for explicit coordinate transformation matrices. The simplification is justified by the geometric characteristics of the shell: since the elements are modelled as rectangular, their local axes naturally align with the global X and Y directions. Moreover, due to the shallow curvature of the shell surface, the local Z'-axis is

nearly aligned with the global Z-axis, leading to minimal angular deviation. Once computed in this manner, the element matrices and corresponding load vectors are assembled into the overall system by ensuring compatibility with the degrees of freedom at all nodal points. As a result, the global stiffness matrix $[K_g]$, global mass matrix $[M_g]$,and global load vector $[Q_g]$ for the entire shell structure, including stiffeners, are systematically formed.

$$[K_g] = \sum_{e=1}^{n} [K_{se}], [M_g] = \sum_{e=1}^{n} [M_e] \text{ and } [Q_g] = \sum_{i=1}^{n} [Q_e] \quad (4.89)$$

In the present analysis of laminated composite hyperbolic and elliptical paraboloidal shells with cutouts, a dedicated subroutine is employed to assemble global stiffness and mass matrices. These matrices are efficiently organized using the 'skyline' storage scheme, as suggested by Bathe (2002), which significantly reduces memory usage by storing only the relevant non-zero entries in a one-dimensional array. The same subroutine also constructs the global nodal load vector, ensuring correct alignment with the nodal degrees of freedom. Consequently, the dynamic equilibrium equation of motion for the shell structure in its global form is simplified and expressed as:

$$[M_g]\{\ddot{\delta}_k\}_g + [K_g]\{\delta_k\}_g = [Q_g] \quad (4.90)$$

The free vibration equation of stiffened panel is the following:

$$[M_g]\{\ddot{\delta}_k\}_g + [K_g]\{\delta_k\}_g = 0, \text{ where } k = \text{number of nodes.} \quad (4.87)$$

$\{\ddot{\delta}_k\}_g$ and $\{\delta_k\}_g$ represent global acceleration and displacement vectors. Equation (4.87) can be written as the following as given by Nanda and Bandyopadhyay (2007).

$$([K_g] - \omega^2[M_g])\{\delta_k\}_g = 0 \quad (4.88)$$

Equation (4.88) is solved iteratively using the steps suggested by Nanda and Bandyopadhyay (2007).

4.11 Imposition of Boundary Conditions and Solution Procedure:

In the context of the finite element analysis of laminated composite hyperbolic and elliptical paraboloidal shells with cutouts, the application of boundary conditions refers to the specification of the presence or restriction of generalized displacements namely, translational components u, v, w and rotational components α and β at various nodal locations within the discretized model. These constraints are crucial for accurately simulating real-world support

conditions and ensuring the stability of the solution. The imposition of zero-displacement boundary conditions is numerically implemented by eliminating the corresponding rows and columns from the global stiffness and mass matrices, as well as from the global load vector.

The overall dynamic analysis framework includes static, free vibration, and forced vibration cases as specific scenarios. The methodologies for solving these problems differ slightly, and a detailed explanation of the solution techniques employed for each case is provided in the subsequent subsections.

4.12 Formulating Free Vibration Problem:

If the load vector of Equation (4.90) is dropped, the equation of free vibration is obtained as

$$[M_g]\{\ddot{\delta}_k\}_g + [K_g]\{\delta_k\}_g = 0 \quad (4.91)$$

In this Equation (4.91) the displacement $\{\delta\}$ is a function of space and time. To solve the free vibration problem separation of space and time co-ordinates is done by the following substitution

$$\{d(x,y,z,t)\} = ae^{iwt}\{\phi(x,y)\}$$

Or, $$\{\delta\} = ae^{iwt}\{\phi\} \quad (4.92)$$

Therefore, $$\{\ddot{\delta}\} = -a\omega^2 e^{iwt}\{\phi\} \quad (4.93)$$

Combining Equations (4.92) and (4.93) in equation (4.91), we get,

$$ae^{iwt}(-\omega^2[M]\{\phi\} + [K]\{\phi\}) = 0$$

As $ae^{iwt} = 0$ as Equation (4.92) is an assumed solution, therefore,

$$\omega^2[M]\{\phi\} = [K]\{\phi\} \quad (4.94)$$

where ω and $\{\phi\}$ represent the natural frequencies the corresponding eigenvectors of the generalized eigen-value problem. The problem is solved by the subspace iteration algorithm.

Chapter 5

Vibration Characteristics of Elliptical Paraboloidal Shell with Cutout

5.1 General:

Using the mathematical formulation presented in the previous chapter, a number of numerical problems of laminated shells are analyzed and results are presented in tabular and graphical forms.

For elliptical paraboloidal shell $R_{xx}/R_{yy}>0$

5.2 Numerical Problems on Elliptical Paraboloidal Panels

Verification issues are resolved to ensure that the suggested nonlinear finite element method is accurate. The specifics of verification issues are reported in the "Benchmark Problems" section. Additional issues pertaining to the free vibration of skewed elliptic paraboloids with composite stiffeners are resolved in the "Parametric Studies" section.

5.2.1 Benchmark problems

The proposed code calculates the non-dimensional frequencies of spherical panels with finite element mesh divisions of 2×2, 4×4, 6×6, and 8×8.

Table 5.1: Nondimensional fundamental frequencies [$\varpi = \omega a^2(\rho/E_{22}h^2)^{0.5}$] of simply supported composite spherical shell

Lamination	$0^0/90^0$	$0^0/90^0/0^0$	$0^0/90^0/90^0/0^0$
Reddy (1984)	9.687	15.183	15.184
Present code with 2×2 mesh	4.895	8.292	8.225
4×4 mesh	7.723	12.207	12.221
6×6 mesh	9.698	15.176	15.185
8×8 mesh	9.685	15.181	15.184

$E_{11}=25\times10^3$ KN/cm^2, $E_{22}=10^3$KN/cm^2, $G_{12}=G_{13}=500$KN/cm^2, $G_{23}=200$KN/cm^2, $\nu_{12}=0.25$, $a/b=1$, $h/a=0.01$, $R/a=10^{30}$

The findings are shown in Table 5.1, which shows that convergence is reached for 8×8 meshes because further refinement of that mesh does not enhance the results by more than 1%. Additionally, the results exhibit excellent agreement with the closed form ones provided by Reddy

(1984), confirming that the suggested code appropriately formulates the composite doubly curved panel. Elastic constants for the material and panel dimensions are also reported in the table.

Table 5.2: Nondimensional frequency of 0°/90°/0°/90° composite skew elliptic paraboloid.

R_{xx}/R_{yy}	Modes	Chaubey et al. (2018)			Present formulation		
		$\phi = 15^0$	$\phi = 30^0$	$\phi = 45^0$	$\phi = 15^0$	$\phi = 30^0$	$\phi = 45^0$
1.0	1	21.20	25.72	35.38	20.42	23.75	34.52
	2	43.07	47.13	58.06	41.88	45.78	57.45
	3	47.57	60.21	85.64	45.69	58.69	84.49
	4	60.64	69.83	90.49	58.42	68.43	89.42

$a/b = 1.0$, $a/h = 100$, $a'/a = 0.0$, $E_{11}/E_{22} = 25$, $G_{23} = 0.2E_{22}$, $G_{12} = G_{13} = 0.5E_{22}$, $\nu_{12} = 0.25$, $\rho = 1.0$.

With a constant step of 15^0, the linear frequencies of composite elliptic paraboloids are solved for the first four modes of vibration and skew angles ranging from 15^0 to 45^0. Results from Chaubey et al. (2018) and the suggested code for solid shell panels ($a'/a = 0.0$) are contrasted in Table 5.2. Since the current findings closely match those provided by Chaubey et al. (2018), the comparison validates the accuracy of the suggested algorithm for skewed elliptic paraboloidal panels. The material constants and dimensions of the composite skewed elliptic paraboloids are shown in Table 5.2 along with the results.

Table 5.3: Nonlinear fundamental frequencies of simply supported $[0^0/0^0/\pm30^0]_2$ spherical shell.

Source	$R/a = 5$	$R/a = 10$	$R/a = 100$	$R/a = 1000$
Naidu and Sinha (2022)	47.800	39.800	14.800	13.600
Present FEM	47.507	39.209	14.021	12.968

$E_{11} = 130\times10^3$ MPa, $E_{22} = 9.5\times10^3$ MPa, $G_{12} = G_{13} = 6.0\times10^3$ MPa, $G_{23} = 3.0\times10^3$ MPa, $a/b = 1$, $h/a = 0.01$, $\nu_{12} = 0.3$, $\rho = 1.6 \times 10^{-6}$ kg/mm^3, amplitude ratio $(w_{max}/h) = 0.2$.

The suggested code solves the nonlinear fundamental frequencies of spherical panels, and the results are shown in Table 5.3. In the table, current findings are contrasted with those provided by Naidu and Sinha (2007) for simply supported $[0^0/0^0/\pm30^0]_2$ composite panels subjected to different temperatures (T) and moisture concentrations (C). Together with the table, the current answers are found for the material properties at $T = 300^0$K and $C = 0\%$. The comparison shows that the current results are quite close to the published ones (Naidu and Sinha 2007), confirming that the suggested nonlinear coding for doubly curved elliptic paraboloids is correct.

Table 5.4: Frequencies (rad/sec) of biaxially stiffened $90^0/0^0/0^0/90^0$ spherical shell.

Modes of vibration	Number of stiffeners	Goswami and Mukhopadhyay (1995)	Present FEM (8×8)
1	1×1	21.549	21.508
	2×2	25.130	25.089
	3×3	40.334	40.134
2	1×1	23.740	23.701
	2×2	39.624	39.584
	3×3	62.389	62.158
3	1×1	24.252	24.211
	2×2	42.826	42.786
	3×3	63.944	63.844

E_{11}=40×10^{3}KN/cm^2, E_{22} = 10^{3}KN/cm^2, G_{12} = G_{13} = 0.6E_{22}, G_{23}= 0.6E_{22}, v_{12}=0.25, a/b=1, h/a=0.01, R/a=100, b_{st}/d_{st} = 0.1, ρ = 8.0 × 10^{-6} N-sec^2/cm^2.

The next step is to solve the first three frequencies of a biaxially stiffened spherical panel with a $90^0/0^0/0^0/90^0$ laminate. The panel features centrally aligned stiffeners that measure 1×1, 2×2, and 3×3. The fibres of the stiffeners are longitudinal. The results are compared with the linear frequencies provided by Goswami and Mukhopadhyay (1995) in Table 5.4. The accuracy of the suggested formulation for stiffeners on spherical panels is confirmed by the excellent agreement between the current and published results. Elastic constants and stiffened panel dimensions are also reported in Table 5.4.

Table 5.5: Natural frequencies (Hz) of orthogonally stiffened cylindrical panel

Modes	Mustafa and Ali (1987)		Goswami and Mukhopadhaya (1995)	Present code
	8 – noded element	Experimental	(9 – noded element)	
1	133	139	143	135.84
2	252	250	248	248.75
3	362	368	376	358.96
4	587	558	566	554.58

a = 304.8 mm, R_{yy} = 609.6 mm, h = 3.175 mm, v = 0.3, $e = e_t$, E = 209 GPa, ρ = 7800 kg/m^3

The suggested formulation is used to solve the frequencies of an isotropic cylindrical panel with biaxial centre stiffeners. To mimic the cylindrical panel, the spherical panel code assigns $R_{xx} = R_{xy}$ = 10^{40}. The results are shown in Table 5.5 along with a comparison to Mustafa and Ali (1987) finite element and experimental predictions. The current outputs and the finite element predictions made by Goswami and Mukhopadhaya (1995) are contrasted in the table. Since the outputs of the

suggested code closely match the experimental and finite elements predictions provided in the literature, the comparisons verify that stiffeners are appropriately formulated. The stiffened panel's size and material qualities are reported in the table as footnotes as well.

5.2.2 Parametric studies

Four distinct composites, consisting of two angle and two cross ply, are used by the authors to address free vibration issues of stiffened elliptic paraboloidal panels under clamped and simple supported boundary conditions (Table 5.6).

Table 5.6: Laminations for elliptical panels.

	Cross-ply	**Angle-ply**
2-layer	$0^0/90^0$	$45^0/-45^0$
3-layer	$0^0/90^0/0^0$	$45^0/-45^0/45^0$

The following are the characteristics of the composites:

Table 5.7: Engineering properties of the elliptical composite panels.

Elastic constants	**Graphite/epoxy**	**Bamboo/epoxy**
E_{11}	142.5 GPa	20.9 GPa
E_{22}	9.790 GPa	30.4 GPa
E_{33}	9.790 GPa	9.950 GPa
G_{12}	4.270 GPa	2.89 GPa
G_{13}	4.270 GPa	8.41 GPa
G_{23}	1.192 GPa	8.41 GPa
v_{12}	0.27	0.275
v_{13}	0.27	0.318
v_{23}	0.25	0.318
ρ	1.0×10^{-6} N-sec^2/cm^2	1830 kg/m^3

The elliptic paraboloidal panels have the following measurements:

Table 5.8: Dimensions of the elliptical paraboloidal panels.

Elastic constants	Graphite/epoxy
a/b	1
h/a	0.01
w_{max}/h	0.3
ϕ	0^0
R_{yy}/R_{xx}	1
a'/a	0.1

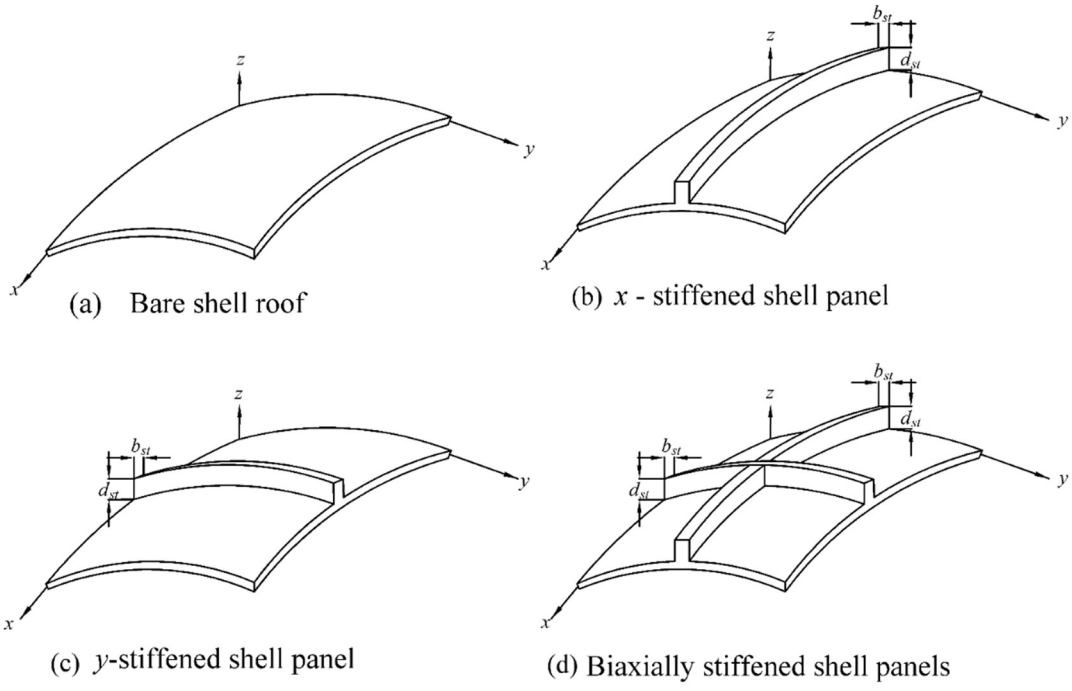

Figure 5.1: Elliptic paraboloidal panel with central stiffeners.

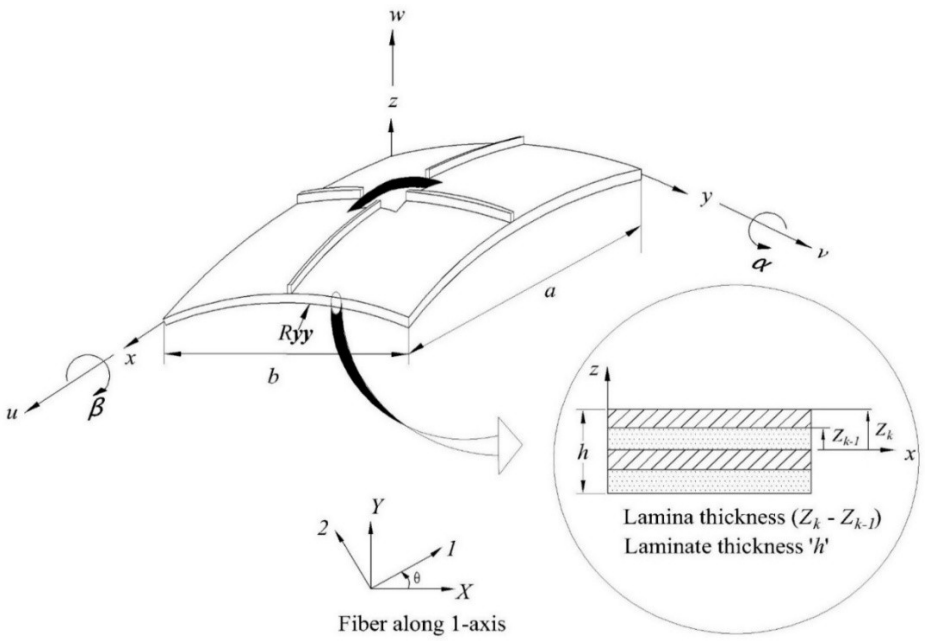

Figure 5.2: Centrally stiffened elliptical paraboloidal shell with cutout.

Fibres run along the length in single-layer in composite stiffeners. The fundamental frequencies of panels that are *x*–stiffened, *y*–stiffened and biaxially stiffened are examined. Figure 5.1 shows the stiffeners are located at top, concentric and bottom of the panels. The results show that for both simply supported and clamped boundary conditions, the (45^0/-45^0/ 45^0) composite performed the best. The performance of multi-stiffened skewed panels is also examined for (45^0/-45^0/ 45^0) composite. The performance of simply supported and multi-stiffened clamped panels is examined for different stiffener eccentricities at (e= e_t, 0, e= e_b), stiffener thickness to panel depth (d_{st}/h) ratios, and radii of curvatures (R_{yy}/R_{xx}) ratios. The mode shapes for the first four modes of vibration are also included in the performance evaluation of 9×9 multi-stiffened panels.

5.3 Results and Discussion

5.3.1 Relative performances of stiffened panels with cutout for graphite epoxy

Table 5.9: Nondimensional fundamental frequencies of simply supported and clamped elliptical paraboloid shell with cutout and graphite epoxy composite.

Lamination	a'/a	Simply supported			Clamped		
		n_x=1, n_y=0	n_x =0, n_y =1	n_x =1, n_y=1	n_x=1, n_y=0	n_x =0, n_y =1	n_x =1, n_y=1
$0^0/90^0$	0	163.3306^L	163.3319^L	163.3513^L	203.4151^L	203.4124^L	203.4967^L
		163.8990^N	164.1092^N	164.2888^N	205.1244^N	205.1371^N	205.4437^N
	0.1	158.6001^L	158.6521^L	159.5733^L	184.6605^L	185.0022^L	189.3972^L
		159.4497^N	159.6768^N	160.7438^N	188.0440^N	188.4018^N	192.5392^N
	0.2	138.5677^L	149.5655^L	149.7352^L	145.2381^L	166.0779^L	166.4245^L
		144.1065^N	151.7770^N	152.0060^N	154.8474^N	169.6585^N	170.9387^N
	0.3	124.2787^L	136.5225^L	140.6041^L	127.6938^L	150.9654^L	153.7301^L
		129.6392^N	139.9326^N	142.8686^N	134.3238^N	154.5261^N	156.7270^N
	0.4	102.0962^L	107.9995^L	125.0016^L	103.6632^L	132.7530^L	133.6986^L
		107.8218^N	114.1951^N	128.6326^N	109.3713^N	136.7567^N	138.1429^N
	0.5	84.3999^L	74.0672^L	88.2807^L	86.0031^L	93.6519^L	94.7149^L
		84.9483^N	78.3831^N	93.1943^N	89.2165^N	99.0180^N	99.8364^N
$0^0/90^0/0^0$	0	164.3190^L	164.3194^L	164.3406^L	208.3692^L	208.3632^L	208.4079^L
		164.2428^N	165.0110^N	165.2944^N	208.7890^N	209.4578^N	209.7920^N
	0.1	160.2876^L	160.2923^L	160.9442^L	192.3870^L	192.7820^L	195.7949^L
		161.0240^N	161.0362^N	161.0658^N	195.2445^N	194.7752^N	197.1504^N
	0.2	145.4616^L	152.7860^L	152.8653^L	157.8000^L	174.9693^L	175.1356^L
		148.9836^N	153.6015^N	153.9083^N	165.2275^N	177.4014^N	178.0569^N
	0.3	132.7344^L	144.5087^L	146.0427^L	140.1130^L	161.8261^L	164.3150^L
		137.8314^N	146.5550^N	148.0808^N	147.1126^N	164.6817^N	167.1017^N
	0.4	113.6728^L	134.6806^L	135.3554^L	117.8151^L	149.5648^L	149.8269^L
		119.3242^N	135.0577^N	137.3497^N	123.9487^N	151.6217^N	151.8634^N
	0.5	99.6153^L	94.3997^L	112.4795^L	104.5700^L	123.5376^L	123.9672^L
		101.8903^N	97.3742^N	114.6096^N	106.8181^N	126.0078^N	126.4702^N
$45^0/-45^0$	0	198.1115^L	194.5805^L	225.5891^L	205.7786^L	207.6477^L	248.5643^L
		200.8004^N	195.2789^N	225.9981^N	209.8561^N	211.0754^N	251.2267^N
	0.1	194.1727^L	189.7285^L	222.9446^L	203.3653^L	204.9159^L	238.2803^L
		198.3212^N	193.5215^N	226.7125^N	207.1042^N	209.0620^N	236.6910^N
	0.2	184.9091^L	179.0267^L	200.1787^L	198.1451^L	199.5219^L	213.1892^L
		190.4022^N	185.4089^N	202.3599^N	201.9827^N	203.3962^N	216.4610^N
	0.3	152.9435^L	148.2708^L	175.9548^L	164.3940^L	166.8621^L	191.8386^L
		156.3338^N	154.2898^N	182.3503^N	169.5354^N	175.2027^N	198.4833^N
	0.4	142.6435^L	115.1932^L	153.0846^L	146.0512^L	131.8210^L	169.5761^L
		149.0250^N	120.7035^N	157.2932^N	152.3720^N	133.3232^N	174.2938^N
	0.5	87.5374^L	74.6712^L	108.6947^L	99.8636^L	95.9293^L	119.9482^L
		93.1358^N	78.6112^N	114.0687^N	105.5813^N	101.2451^N	126.2755^N

$45^0/-45^0/45^0$	0	206.6772^L 207.4290^N	199.4868^L 203.0974^N	241.1840^L 237.1218^N	216.2197^L 218.8307^N	218.3125^L 221.2471^N	267.3666^L 265.9233^N
	0.1	201.9063^L 205.9205^N	195.2339^L 199.2102^N	236.8725^L 238.0725^N	214.3151^L 217.3093^N	216.2073^L 219.5458^N	256.2661^L 263.1910^N
	0.2	194.6713^L 194.6719^N	186.5197^L 192.1574^N	212.6965^L 218.1987^N	209.4985^L 211.8763^N	212.2737^L 215.8922^N	225.5535^L 231.4669^N
	0.3	165.3075^L 168.3180^N	156.1807^L 162.2215^N	179.2486^L 187.2989^N	178.2229^L 183.7019^N	175.3573^L 184.4075^N	194.3447^L 203.2210^N
	0.4	155.6518^L 157.1194^N	123.7016^L 129.0378^N	162.9294^L 169.9205^N	161.0188^L 162.4829^N	140.5013^L 148.0508^N	178.5915^L 186.8238^N
	0.5	99.4830^L 103.3465^N	82.2058^L 86.0183^N	119.3612^L 125.8940^N	113.4597^L 117.1977^N	103.4696^L 108.7683^N	131.3953^L 138.9138^N

E_{11} = 142.5 GPa, $G_{12} = G_{13}$ = 4.72 GPa, E_{22} = 9.79 GPa, v_{12} = 0.27, G_{23} = 1.192 GPa,,
a/b=1,a/h=100, R_{yy}/R_{xx} =1

Linear nonlinear frequencies of elliptical paraboloid shell with cutout for Simply supported and Clamped boundary condition where a/b=1, a/h=100, R_{yy}/R_{xx} =1, by varying cutout ratio a'/a, Lamination and stiffener conditions of graphite epoxy is represented in Table 5.9 and their relative behavior is represented in Figures 6.1 and 6.2.

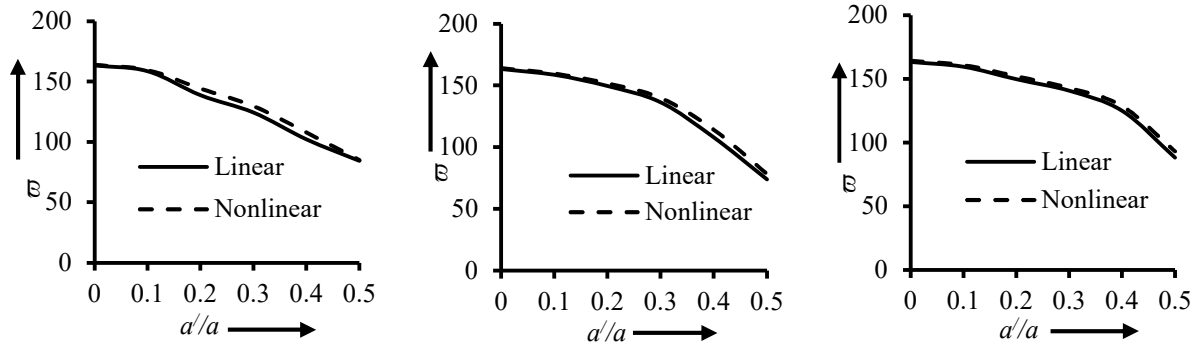

n_x=1, n_y=0
$0^0/90^0$

n_x=0, n_y=1
$0^0/90^0$

n_x=1, n_y=1
$0^0/90^0$

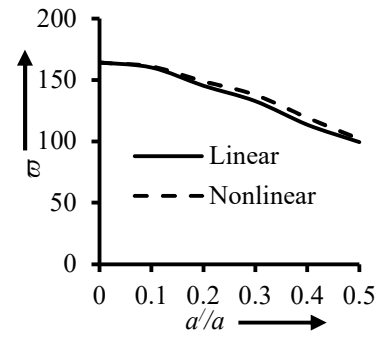

n_x=1, n_y=0
$0^0/90^0/0^0$

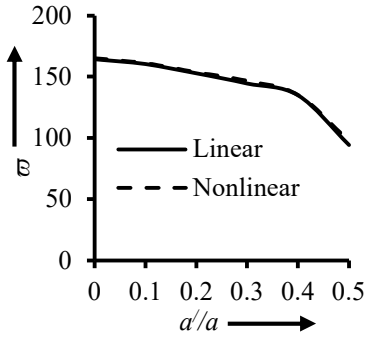

n_x=0, n_y=1
$0^0/90^0/0^0$

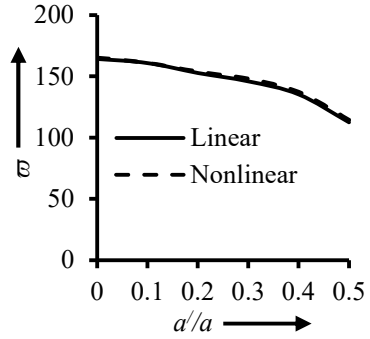

n_x=1, n_y=1
$0^0/90^0/0^0$

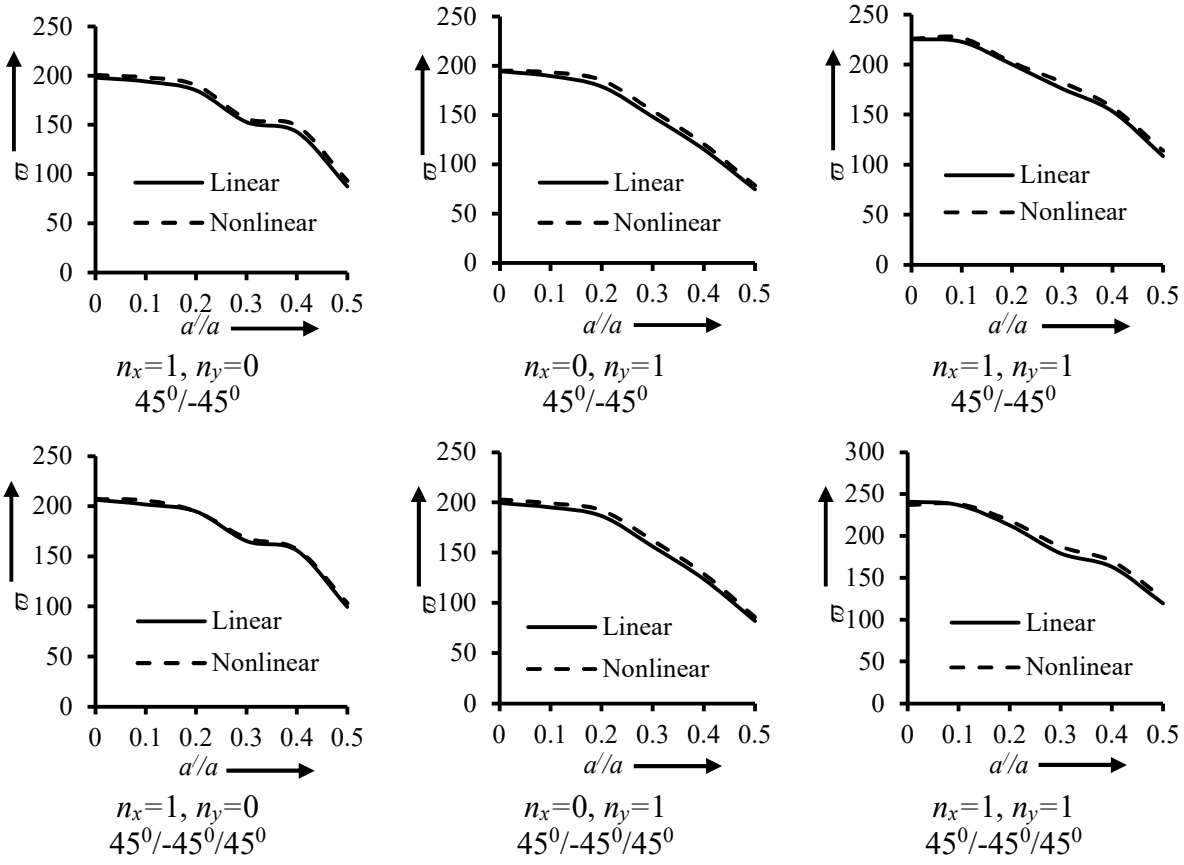

Figure 5.3: Nondimensional fundamental frequencies $\left[\varpi = \omega a^2 \left(\frac{\rho}{E_{22}h^2}\right)^{\frac{1}{2}}\right]$ of elliptical paraboloid with cutout for simply supported boundary condition with graphite epoxy composite.

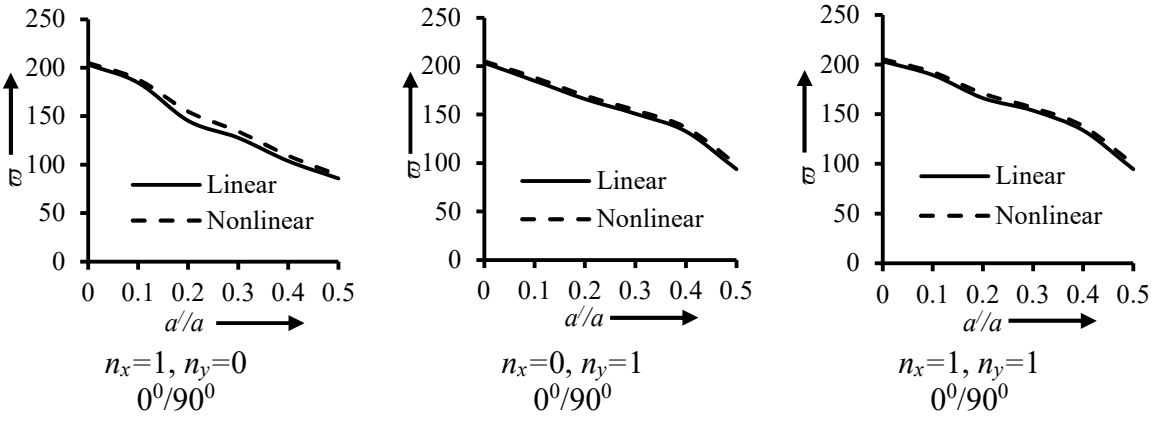

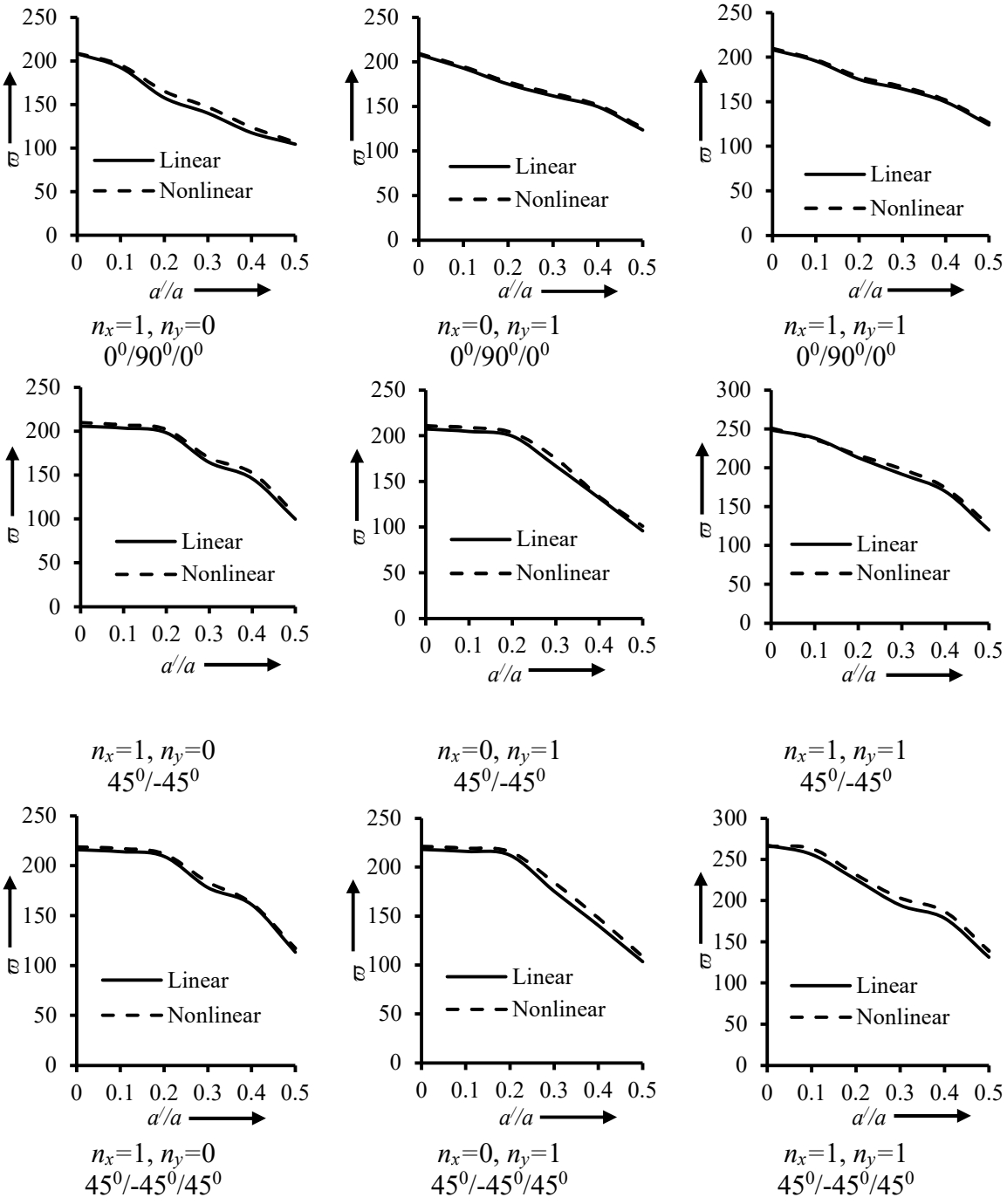

Figure 5.4: Nondimensional fundamental frequencies of elliptical paraboloid with cutout for clamped boundary condition with graphite epoxy composite.

Non-dimensional fundamental frequencies [$\varpi = \omega a^2(\rho/E_{22}h^2)^{0.5}$] of clamped and simply supported elliptic-paraboloidal panels for graphite epoxy are reported in Figure 5.3 and Figure 5.4, respectively, for three distinct central stiffeners (shown in Figure 5.1) and different cutout ratios. Figures show that, for every given lamination and central stiffener, the fundamental frequencies

of elliptic paraboloids constantly fall when the cutout ratio is varied from 0 to 0.5. Panels with cutouts are less stiff than those without (a'/a =0) for any given cutout ratio (a'/a) if a'/a >0. This behaviour is explained by the cutouts' presence, which breaks the shell surface's continuity. For this reason, cutout shells offer lower fundamental frequencies than non-cutout shells. Taking into account all of the laminations and stiffeners examined in Figures 5.3 and 5.4, the greatest frequencies are provided by both clamped and simply supported panels with cutout for a'/a = 0.1.

x – stiffened (n_x = 1, n_y = 0), y – stiffened (n_x = 0, n_y = 1) and biaxially stiffened (n_x = 1, n_y = 1) are the classifications for the elliptic paraboloids. In order to maximise the frequencies within a fixed casting cost, the elliptic paraboloids cutout ratio a'/a =0.1 requires a biaxial stiffener, according to the performances of clamped and simply supported panels for every given lamination. Biaxial stiffened panels improve load distribution and deformation resistance by offering reinforcement in both directions for panels with cutouts. For this reason, of the centrally stiffened panels examined in Figures 5.3 and 5.4, biaxially stiffened panels are the stiffest.

The frequency of cross and angle-ply laminates are also shown in Figures 5.3 and 5.4. The table unequivocally demonstrates that, when the number of layers within panel thickness is constant, angle-ply laminates can optimise the performance of doubly stiffened elliptic paraboloids with cutout. The fundamental frequency of various angle-ply laminates often increases as the number of layers increases. The greatest fundamental frequencies are provided by the $45^0/-45^0/45^0$ laminate for clamped and simply supported panels. The tables also verify that clamped panels have greater frequencies than simply supported ones for any given lamination of doubly stiffened elliptic paraboloids with cutout. Such higher performances are the result of clamped panels maximum support constraints.

5.3.2 Relative performances of stiffened panels with cutout for bamboo/epoxy

Table 5.10: Nondimensional fundamental frequencies of simply supported and clamped elliptical paraboloid shell with cutout and bamboo epoxy composite.

Lamination	*a'/a*	Simply supported			Clamped		
		n_x=1, n_y=0	n_x=0, n_y=1	n_x=1, n_y=1	n_x=1, n_y=0	n_x=0, n_y=1	n_x=1, n_y=1
$0^0/90^0$	0	137.8014	137.9151	137.3086	148.6355	147.9431	149.4473
	0.1	129.0079	129.2640	131.6795	134.2046	134.3363	137.5204
	0.2	108.5228	116.7230	117.4733	109.7031	119.3916	120.1284
	0.3	94.8263	95.6955	106.3063	95.9974	105.2454	109.4772
	0.4	82.5237	75.0196	93.9025	83.5544	90.6095	96.2854
	0.5	62.9761	51.7460	68.5808	68.9157	72.0613	73.9475
$0^0/90^0/0^0$	0	136.1183	136.5473	137.0889	147.3903	148.0965	148.6695
	0.1	129.1720	129.2484	131.6351	134.7264	134.6086	137.2243
	0.2	109.4933	117.1481	117.8231	110.8023	120.0355	120.6830
	0.3	96.9333	98.9726	107.6316	97.5409	107.2586	110.7624
	0.4	84.1844	78.2184	95.9323	85.3795	94.5298	98.4990
	0.5	67.1035	53.9371	71.9659	73.2097	76.2882	77.7049
$45^0/-45^0$	0	146.8408	146.6597	157.6223	149.3930	151.0678	159.7155
	0.1	139.7192	139.6359	150.7152	143.3683	144.1920	149.7716
	0.2	120.9249	123.9262	130.7427	121.3316	129.7803	132.5173
	0.3	101.3366	96.7154	114.1273	105.8512	107.2381	118.2572
	0.4	93.4427	75.9643	99.8893	94.6262	90.4430	103.8382
	0.5	62.8219	51.8400	72.8964	71.8548	74.1909	79.6979
$45^0/-45^0/45^0$	0	146.3221	146.6132	157.6803	150.0523	150.8085	160.1271
	0.1	140.1536	140.0199	154.0437	143.8322	144.4857	149.7847
	0.2	122.1057	124.6110	131.6152	121.2631	130.5008	132.4987
	0.3	102.2274	97.3612	113.4339	106.9857	107.8401	117.8811
	0.4	94.2661	76.5207	101.0049	94.7787	90.9564	104.9725
	0.5	63.5028	52.2800	73.7564	72.3265	74.6319	80.5797

E_{11} = 20.9 GPa, E_{22} = 30.4GPa, E_{33} = 9.950GPa, G_{12} = 2.89 GPa, G_{13} =8.41 GPa, G_{23} = 8.41 GPa, v_{12} =0.275, v_{13} =0.318, v_{23} =0.318, ρ=1830 kg/m^3, *a/b*=1, *a/h*=100, R_{yy}/R_{xx} =1

Nonlinear frequencies of elliptical paraboloid shell with cutout for Simply supported and Clamped boundary condition by varying cutout ratio *a'/a*, Lamination and stiffener conditions for BMRP epoxy is represented in Table 5.10 and their relative behavior is represented in Figures 5.5 and 5.6.

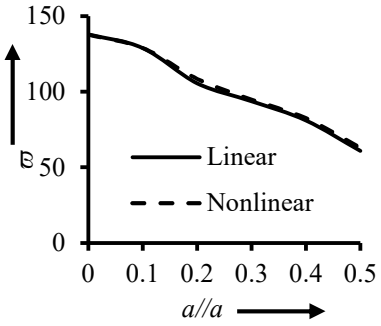

n_x=1, n_y=0

$0^0/90^0$

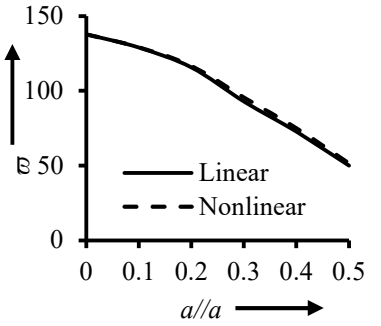

n_x=0, n_y=1

$0^0/90^0$

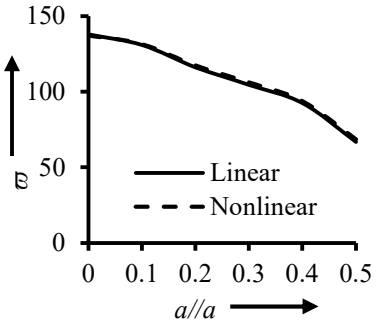

n_x=1, n_y=1

$0^0/90^0$

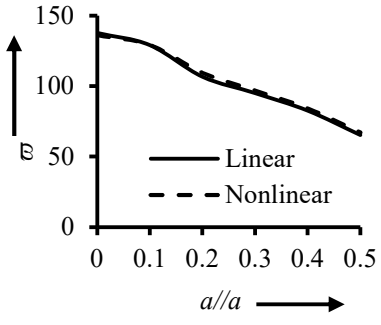

n_x=1, n_y=0

$0^0/90^0/0^0$

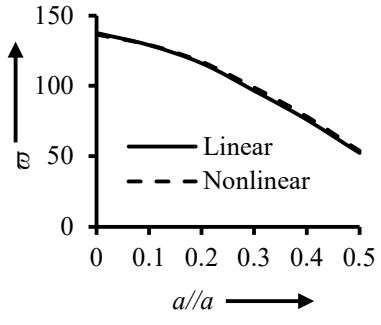

n_x=0, n_y=1

$0^0/90^0/0^0$

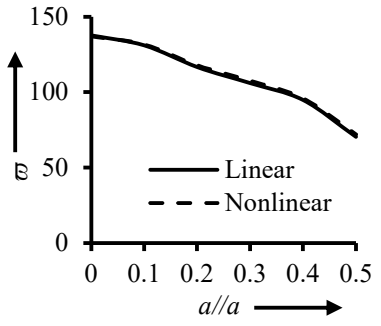

n_x=1, n_y=1

$0^0/90^0/0^0$

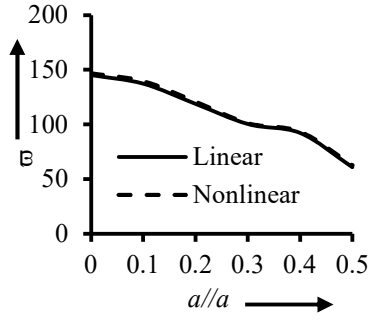

n_x=1, n_y=0

$45^0/-45^0$

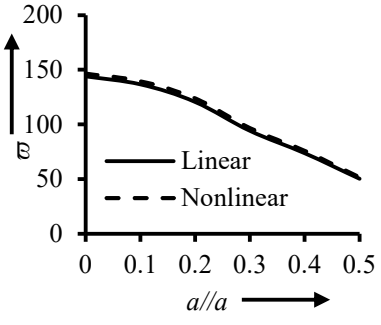

n_x=0, n_y=1

$45^0/-45^0$

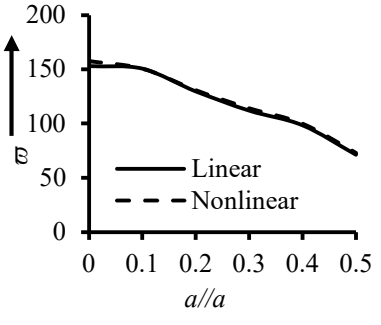

n_x=1, n_y=1

$45^0/-45^0$

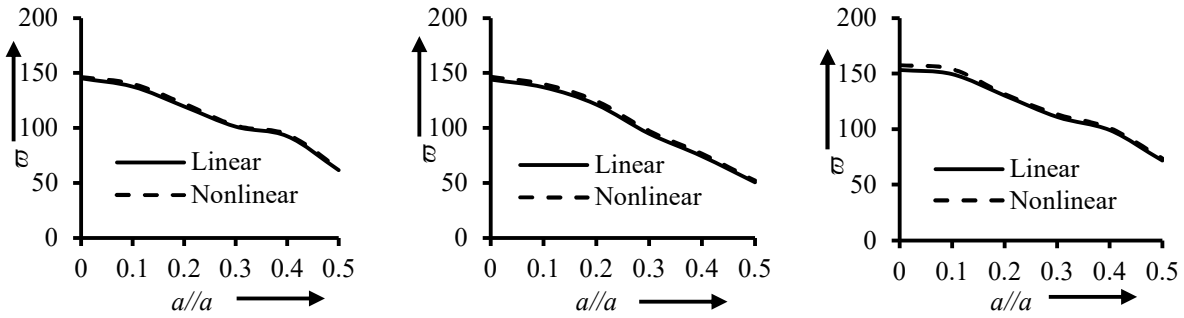

n_x=1, n_y=0 n_x=0, n_y=1 n_x=1, n_y=1

$45^0/-45^0/45^0$ $45^0/-45^0/45^0$ $45^0/-45^0/45^0$

Figure 5.5: Nondimensional fundamental frequencies of elliptical paraboloid with cutout for simply supported boundary condition with bamboo epoxy composite.

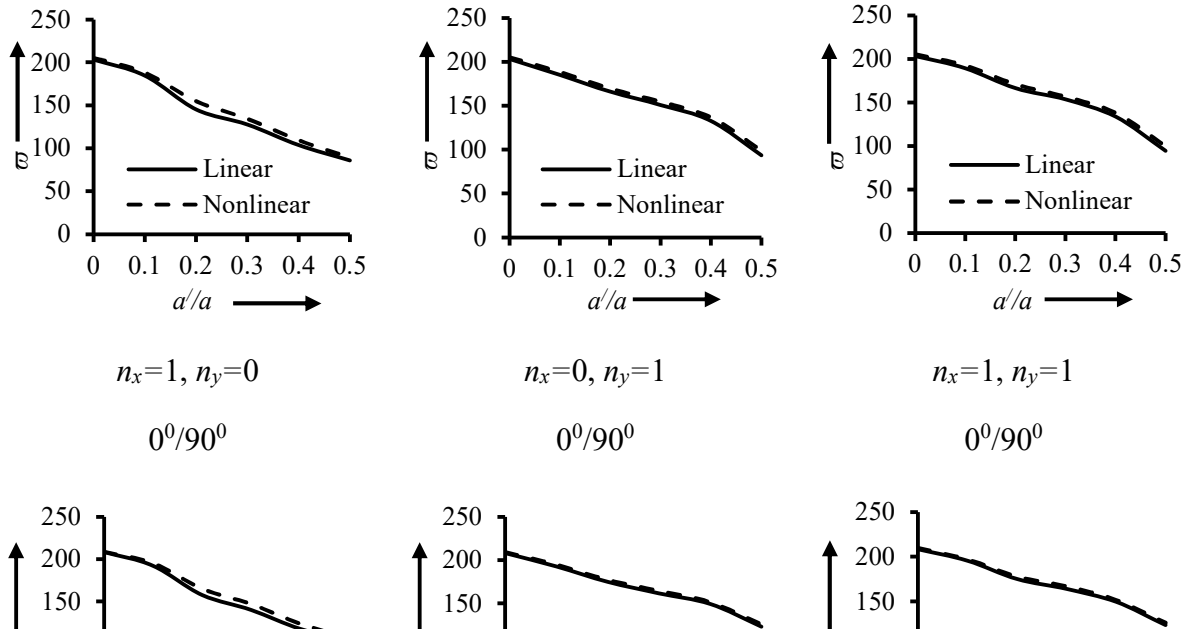

n_x=1, n_y=0 n_x=0, n_y=1 n_x=1, n_y=1

$0^0/90^0$ $0^0/90^0$ $0^0/90^0$

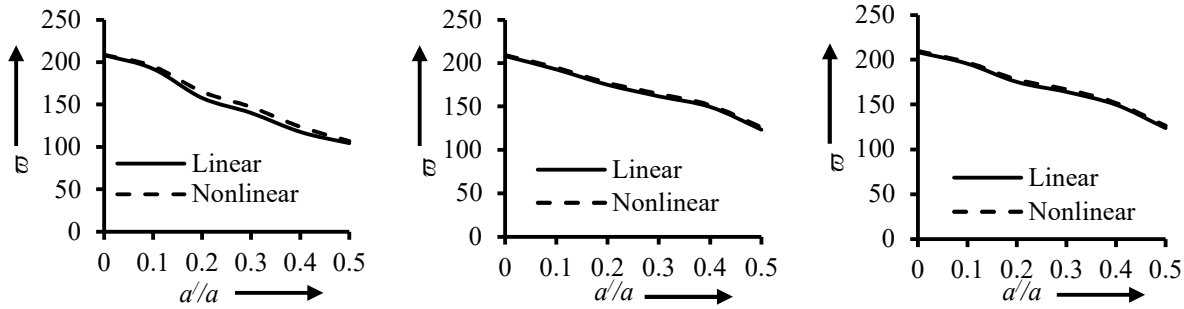

n_x=1, n_y=0 n_x=0, n_y=1 n_x=1, n_y=1

$0^0/90^0/0^0$ $0^0/90^0/0^0$ $0^0/90^0/0^0$

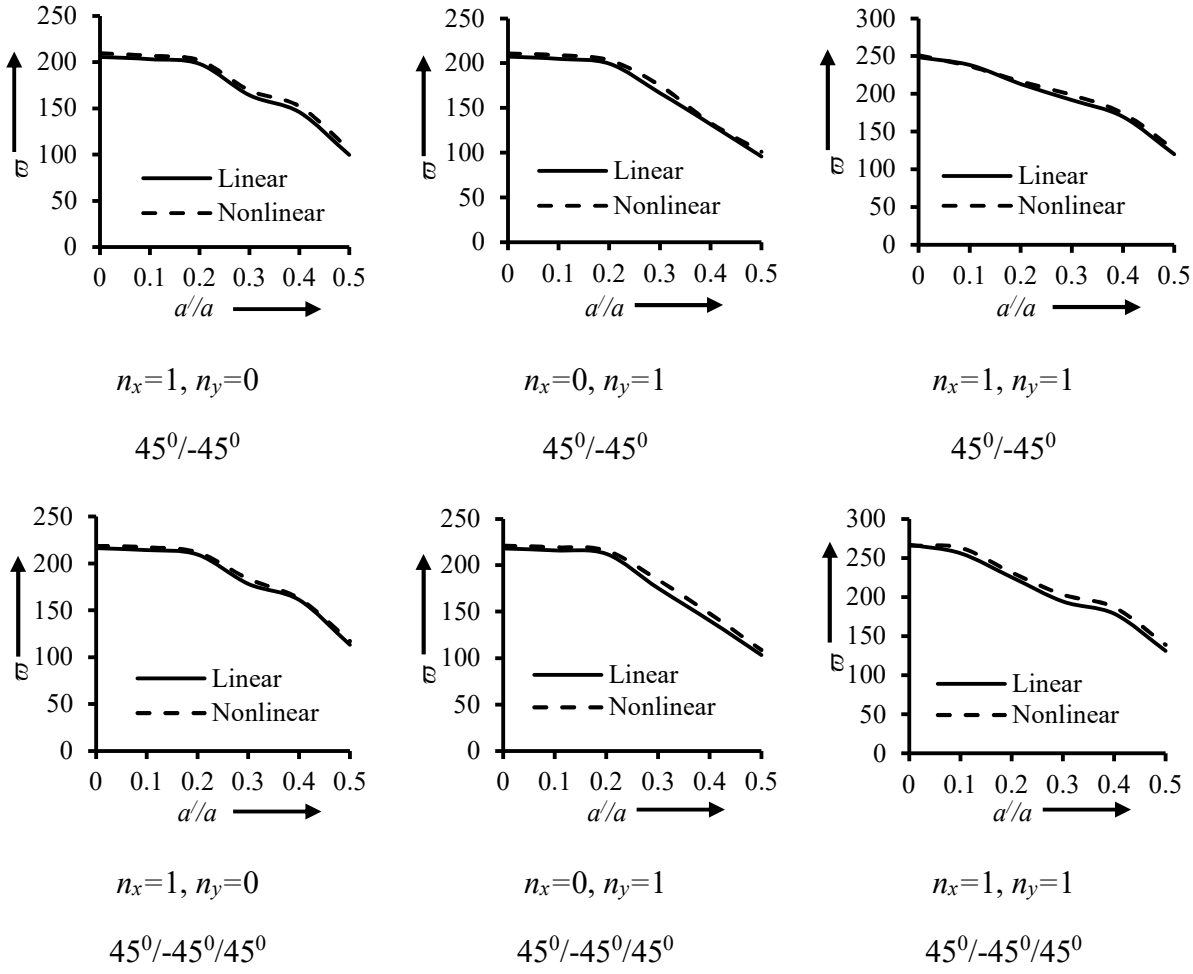

Figure 5.6: Nondimensional fundamental frequencies of elliptical paraboloid with cutout for clamped supported boundary condition with bamboo epoxy composite.

The free vibration behavior of laminated composite shells is significantly influenced by material properties, stiffening configurations, and the presence of cutouts. In this study, we compare the non-dimensional fundamental frequencies of graphite-epoxy and bamboo mat reinforced polymer (BMRP)-epoxy laminated composite elliptical paraboloidal shells with central cutouts, as depicted in Figures 5.3 , 5.4 (graphite-epoxy) and Figures 5.5, 5.6 (BMRP-epoxy).

An increase in the cutout ratio (a'/a) from 0 to 0.5 results in a continuous decrease in the fundamental frequencies for both graphite-epoxy and BMRP-epoxy shells, irrespective of the lamination scheme and stiffening configuration. This trend is attributed to the disruption of the shell's structural continuity due to the presence of cutouts, leading to reduced stiffness and, consequently, lower natural frequencies. Notably, for a cutout ratio of a'/a= 0.1, both clamped and

simply supported panels exhibit maximum frequencies across all studied laminations and stiffeners, suggesting an optimal balance between structural integrity and functional requirements.

The study considers three stiffening configurations: x – stiffened ($n_x = 1$, $n_y = 0$), y – stiffened ($n_x = 0$, $n_y = 1$), and biaxially stiffened ($n_x = 1$, $n_y = 1$). For a given cutout ratio, biaxially stiffened panels demonstrate superior stiffness and higher fundamental frequencies compared to uniaxially stiffened counterparts. This enhancement is due to the improved load distribution and resistance to deformation provided by reinforcement in both principal directions. Therefore, incorporating biaxial stiffening is recommended for maximizing the vibrational performance of laminated composite shells with cutouts.

The analysis includes both cross-ply and angle-ply laminations. Among angle-ply laminates, configurations with increased layering, such as $[45^0/-45^0/45^0]$, exhibit higher fundamental frequencies. This increase is linked to the enhanced stiffness resulting from the specific fiber orientations and stacking sequences. Furthermore, clamped boundary conditions consistently yield higher frequencies than simply supported ones, highlighting the role of boundary constraints in dynamic performance.

While both graphite-epoxy and BMRP-epoxy shells display similar trends concerning cutout ratios, stiffening, and lamination effects, BMRP-epoxy panels consistently exhibit lower fundamental frequencies. This discrepancy is primarily due to the lower stiffness and density properties of BMRP compared to graphite-epoxy, underscoring the importance of material selection in the design of high-performance composite structures. For applications requiring higher natural frequencies and enhanced dynamic performance, the use of graphite-epoxy materials with biaxial stiffening and optimized angle-ply laminations is recommended. However, BMRP-epoxy composites may still be suitable for applications where lower stiffness is acceptable, offering benefits such as sustainability and cost-effectiveness.

5.3.3 Relative performances of stiffened panels with cutout of varying eccentricity for graphite epoxy

Table 5.11: Nondimensional fundamental frequencies of biaxially stiffened simply supported and clamped elliptical paraboloids with varying locations of cutouts along.

Boundary Condition	e_y	e_x= -0.2	e_x = -0.1	e_x =0	e_x =0.1	e_x = 0.2
Clamped	-0.2	**265.2720**^{L}	258.5235^{L}	257.0705^{L}	259.8309^{L}	261.4121^{L}
		262.7695^{N}	256.9669^{N}	253.2994^{N}	256.5696^{N}	260.7835^{N}
	-0.1	257.6637^{L}	255.8428^{L}	258.0719^{L}	259.6991^{L}	255.9634^{L}
		261.8213^{N}	256.3495^{N}	254.4852^{N}	258.2627^{N}	258.5603^{N}
	0	256.4892^{L}	258.0454^{L}	256.2661^{L}	254.1785^{L}	260.1031^{L}
		252.4668^{N}	256.9315^{N}	**263.1910**^{N}	253.4566^{N}	261.5628^{N}
	0.1	259.9633^{L}	260.0221^{L}	254.2310^{L}	256.3838^{L}	258.0632^{L}
		262.5572^{N}	261.6185^{N}	253.5077^{N}	249.6740^{N}	256.9577^{N}
	0.2	260.1918^{L}	255.9959^{L}	259.6730^{L}	257.9724^{L}	255.9797^{L}
		259.7484^{N}	258.0036^{N}	258.4020^{N}	258.4905^{N}	256.3930^{N}
Simply Supported	-0.2	**239.7225**^{L}	233.2236^{L}	234.3485^{L}	233.9528^{L}	237.5321^{L}
		239.5082^{N}	231.6494^{N}	235.8761^{N}	232.6781^{N}	237.4868^{N}
	-0.1	236.1418^{L}	233.2166^{L}	237.3198^{L}	236.7139^{L}	238.7309^{L}
		235.9723^{N}	231.3706^{N}	240.5841^{N}	237.6627^{N}	240.5931^{N}
	0	230.9786^{L}	232.9861^{L}	236.8725^{L}	236.5927^{L}	234.9603^{L}
		238.9112^{N}	240.8052^{N}	238.0720^{N}	241.2770^{N}	235.1375^{N}
	0.1	230.7590^{L}	235.3641^{L}	236.6923^{L}	236.7421^{L}	232.9115^{L}
		229.5224^{N}	**241.3373**^{N}	235.7739^{N}	237.7839^{N}	240.4514^{N}
	0.2	238.9174^{L}	238.8209^{L}	236.5940^{L}	237.3489^{L}	233.2755^{L}
		238.5736^{N}	238.7887^{N}	240.5217^{N}	240.6039^{N}	231.4879^{N}

E_{11} = 142.5 GPa, G_{12} = G_{13} = 4.72 GPa, E_{22} = 9.79 GPa, v_{12} = 0.27, G_{23} = 1.192 GPa, a/b=1, a/h=100, R_{yy}/R_{xx} =1

Table 5.11 reports Nondimensional fundamental frequencies $\left[\varpi = \omega a^2 \left(\frac{\rho}{E_{22}h^2}\right)^{\frac{1}{2}}\right]$ of elliptical paraboloid with cutout of varying eccentricity of cutout along both directions e_x(along x-direction), e_y (along y-direction) with 1×1 stiffener condition for Simply supported and Clamped boundary condition where a/b=1,a/h=100, R_{yy}/R_{xx} =1, a'/a=0.1, $45^0/-45^0/45^0$, for central stiffener e=0, for clamped boundary condition maximum linear frequency is achieved at e_x= -0.2, e_y =-0.2 and

nonlinear frequency is at e_x =0 , e_y =0 and for simply supported boundary condition maximum linear frequency is achieved at e_x= -0.2, e_y =-0.2 and nonlinear frequency is at e_x =-0.1 , e_y =0.1 .

5.3.4 Relative performances of biaxially- stiffened panels with cutout for graphite epoxy

Table 5.12: Nondimensional fundamental frequencies of simply supported and clamped elliptical paraboloid with cutout.

Number Stiffener	Eccentricity	Simply Supported			Clamped		
		R_{yy}/R_{xx}=0.5	R_{yy}/R_{xx} =1.0	R_{yy}/R_{xx} =1.5	R_{yy}/R_{xx} =0.5	R_{yy}/R_{xx} =1.0	R_{yy}/R_{xx} =1.5
1×1	$e=e_t$	252.9641	213.9218	175.7011	281.8280	235.7782	201.1470
	$e=0$	267.6837	241.3373	206.6974	297.5796	263.1910	218.9821
	$e=e_b$	271.8854	242.1650	208.5538	298.9431	251.0183	220.6783
2×2	$e=e_t$	284.6336	230.1051	187.3638	313.3217	243.9574	209.6347
	$e=0$	290.9229	273.4265	229.6207	338.3911	294.6119	263.2270
	$e=e_b$	298.6733	277.3914	234.8448	339.2668	294.9249	264.2906
3×3	$e=e_t$	287.9784	237.7426	192.9780	321.2995	261.2095	227.4581
	$e=0$	313.0110	277.7094	244.2853	339.3862	294.9405	263.6266
	$e=e_b$	297.6265	260.6167	251.8986	340.2367	297.3546	265.7535
4×4	$e=e_t$	323.7504	249.8277	202.4336	352.9661	271.3302	232.9327
	$e=0$	346.0552	361.1814	330.1810	447.4863	389.4701	334.5372
	$e=e_b$	351.6422	363.0906	327.2324	461.7131	387.2491	336.8418
5×5	$e=e_t$	270.5723	229.4390	189.8500	301.6943	260.8968	222.4004
	$e=0$	286.0949	253.4633	215.0829	314.0788	281.8627	239.2537
	$e=e_b$	285.5060	243.5520	219.2599	315.6658	277.0012	242.6721
6×6	$e=e_t$	286.2394	241.2147	202.0485	332.9462	281.7583	242.2700
	$e=0$	312.9724	261.4044	245.7498	348.4815	307.7292	275.5871
	$e=e_b$	312.9617	266.3675	255.0648	349.0894	301.7209	269.8301
7×7	$e=e_t$	305.8986	248.0768	211.5956	380.5072	300.1274	251.8461
	$e=0$	315.8018	322.8004	297.4538	408.8041	340.0897	307.4235
	$e=e_b$	317.9158	328.0511	307.2364	411.8861	345.7876	313.9898
8×8	$e=e_t$	328.8966	262.2710	218.8639	400.7317	305.5547	257.7258
	$e=0$	354.1691	386.3940	357.5252	543.1291	437.9556	388.1877
	$e=e_b$	357.6001	385.3704	355.0542	560.5976	432.4909	376.6789
9×9	$e=e_t$	338.7013	269.5611	222.2325	404.2855	307.0008	258.2822
	$e=0$	358.6689	**394.9990**	367.2582	**596.9700**	459.6277	389.8209
	$e=e_b$	360.7791	390.0253	357.8035	566.8870	432.9549	377.1141

E_{11} = 142.5 GPa, G_{12} = G_{13} = 4.72 GPa, E_{22} = 9.79 GPa, v_{12} = 0.27, G_{23} = 1.192 GPa, a/b=1,a/h=100, R_{yy}/R_{xx} =1

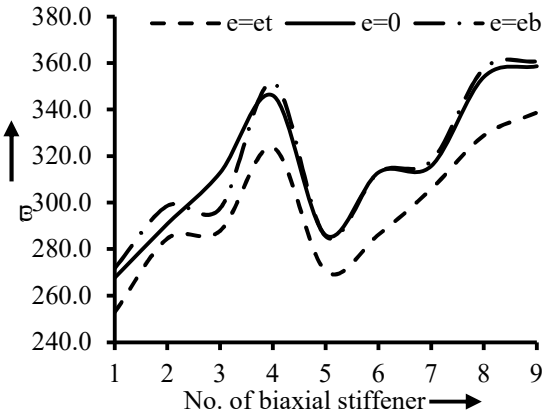

R_{yy}/R_{xx}= 0.5

Simply supported

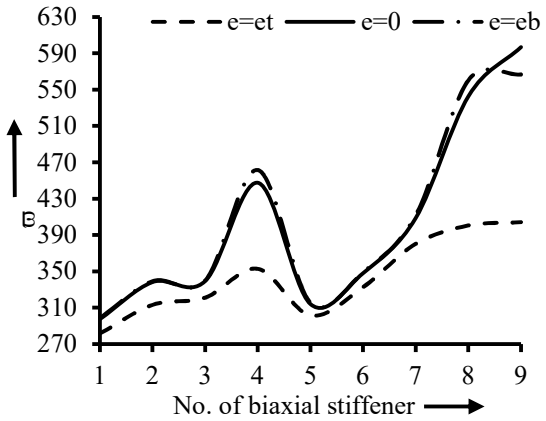

R_{yy}/R_{xx}= 0.5

Clamped

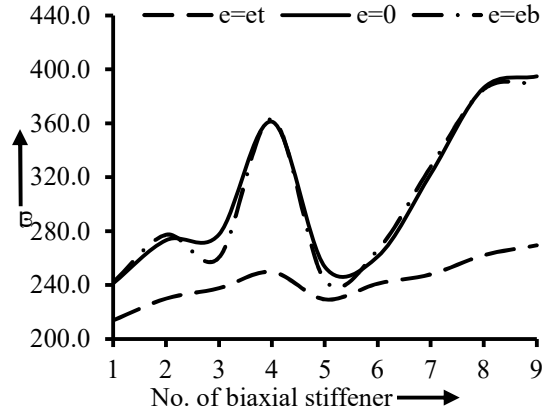

R_{yy}/R_{xx}=1

Simply supported

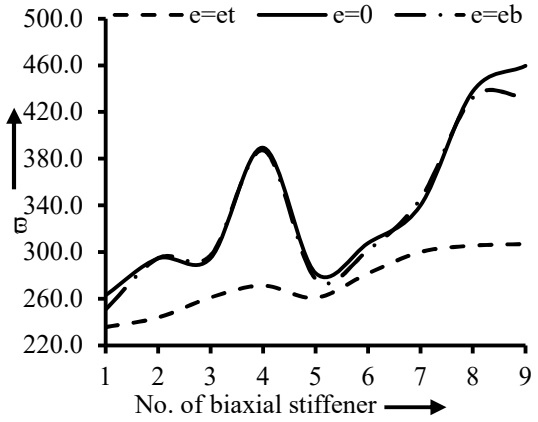

R_{yy}/R_{xx}=1

Clamped

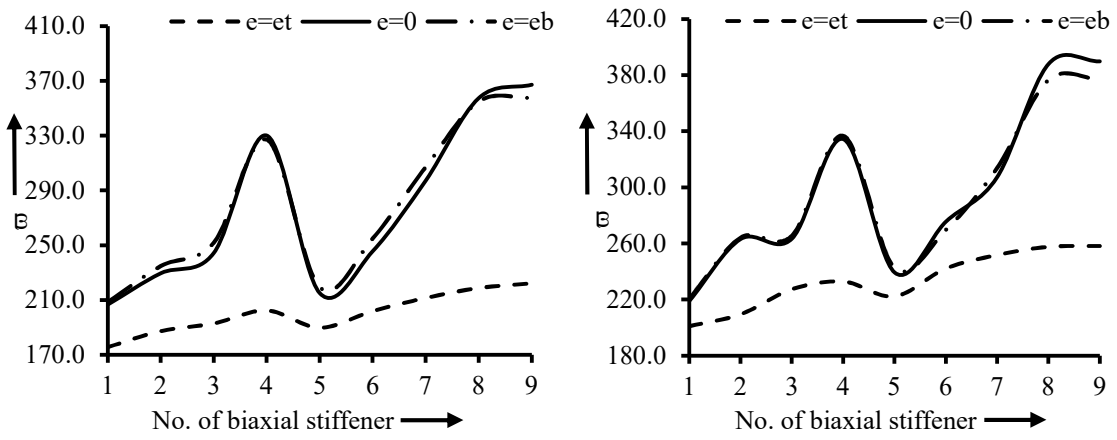

R_{yy}/R_{xx}=1.5

Simply supported

R_{yy}/R_{xx}=1.5

Clamped

Figure 5.7: Nondimensional fundamental frequencies of elliptical paraboloid with cutout for simply supported and clamped boundary conditions.

Figure 5.7 and Table 5.12 show the fundamental frequencies of clamped and simply supported panels that are biaxially stiffened. These frequencies vary depending on the number of biaxial stiffeners and the ratio of radii of curvatures (R_{yy}/R_{xx}), cutout for clamped boundary condition is at e_x =0 , e_y =0 and for simply supported boundary condition is at e_x =-0.1, e_y =0.1, The (R_{yy}/R_{xx}) ratio is varied from 0.5 to 1.5. For each R_{yy}/R_{xx} ratio, the eccentricity of stiffeners at top ($e = e_t$ = -15) at center (e = 0) at bottom ($e = e_b$ = 15).The biaxial stiffener is varied from 1×1 to 9×9.For any given biaxial stiffeners the figures show that the frequencies increasing upto 4×4 after that decrease at 5×5 then increase and maximum at 9×9 due to increase of stiffness, Double-curved panels fundamental frequencies drop when the R_{yy}/R_{xx} ratio rises from 0.5 to 1.5. The frequencies of clamped and simply supported panels are for e=0 and e=e_b maximum for R_{yy}/R_{xx} = 1. Maximum frequency values are achieved for 9×9 biaxial stiffener and e=0

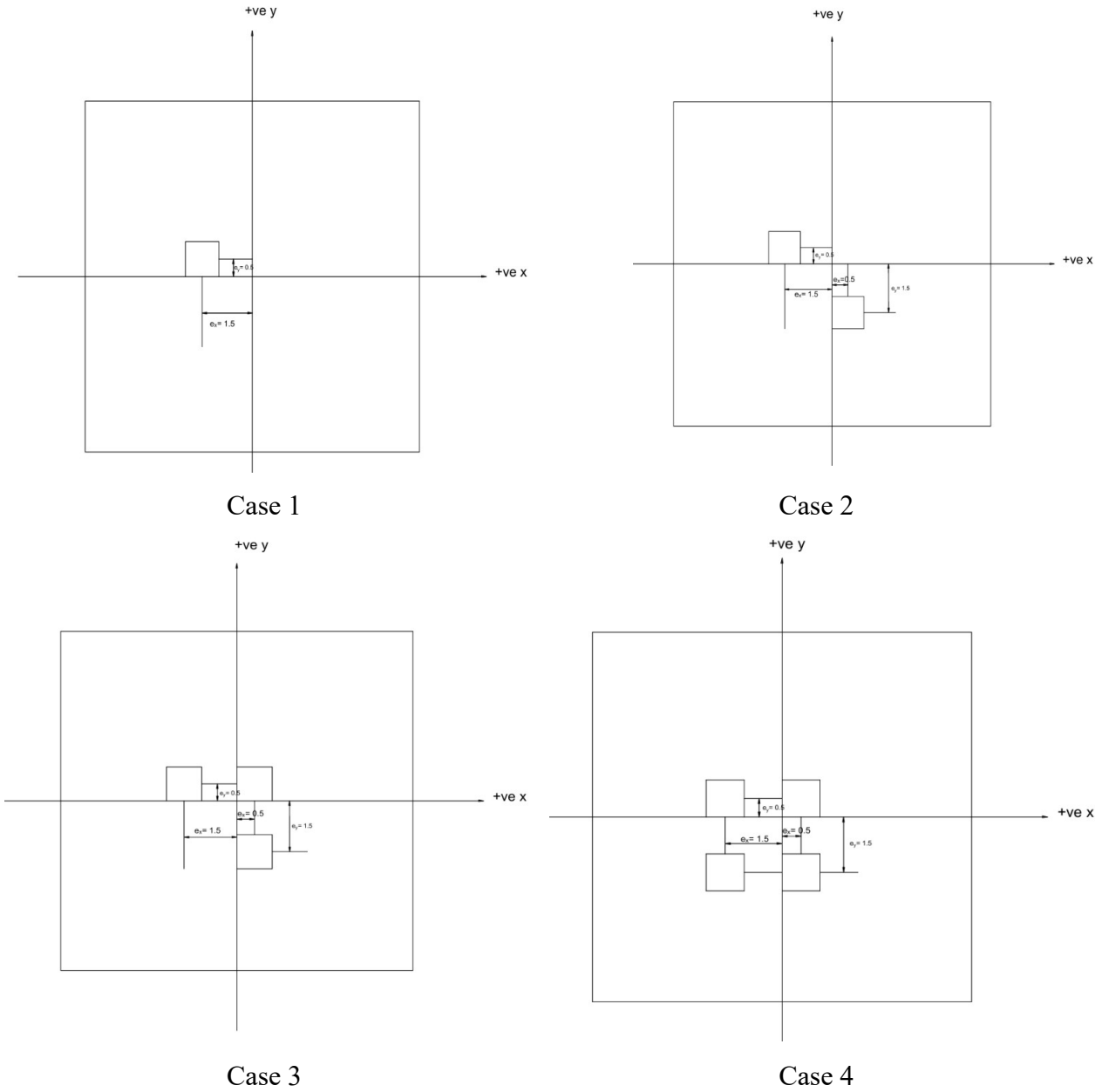

Figure 5.8: Cases of elliptical paraboloidal shell with cutout locations.

5.3.5 Relative performances of biaxially- stiffened panels with cutout for graphite epoxy with varying d_{st}/h ratio

Table 5.13: Nondimensional fundamental frequencies of elliptical paraboloid with cutout for $45^0/-45^0/45^0$, R_{yy}/R_{xx} =1.0, and 9×9 stiffeners.

Cases	d_{st}/h	Simply supported	Clamped
Case 1	1	373.3007	404.6319
	2	394.9990	459.5103
	3	401.1185	487.0964
	4	397.1044	495.6734
	5	390.3764	499.1878
	6	382.6710	500.6702
	7	374.6854	501.0743
	8	366.7674	500.7932
	9	359.0907	500.0126
	10	351.7015	498.8158
Case 2	1	374.0669	404.8095
	2	398.6273	461.6045
	3	401.9447	485.7323
	4	397.9171	494.4434
	5	391.2090	497.9739
	6	383.2805	499.5392
	7	375.2097	500.1720
	8	367.2846	499.9063
	9	359.5348	500.1833
	10	352.0430	498.7616
Case 3	1	374.5121	404.6709
	2	400.0742	452.2245
	3	403.8631	470.2175
	4	399.9926	477.6208
	5	393.1816	481.1192
	6	385.2935	482.9870
	7	377.2045	484.0765
	8	369.0379	484.7239
	9	361.2483	485.0618
	10	353.7054	485.1430
Case 4	1	375.1645	399.7395
	2	401.1830	441.9289
	3	405.3485	456.6812
	4	401.6399	463.3754
	5	394.8636	467.0339
	6	386.9463	469.3515
	7	378.7974	470.9698
	8	370.5559	472.1401
	9	362.6871	472.9638
	10	355.0681	473.4824

E_{11} = 142.5 GPa, G_{12} = G_{13} = 4.72 GPa, E_{22} = 9.79 GPa, v_{12} = 0.27, G_{23} = 1.192 GPa,, a/b=1,a/h=100, R_{yy}/R_{xx} =1

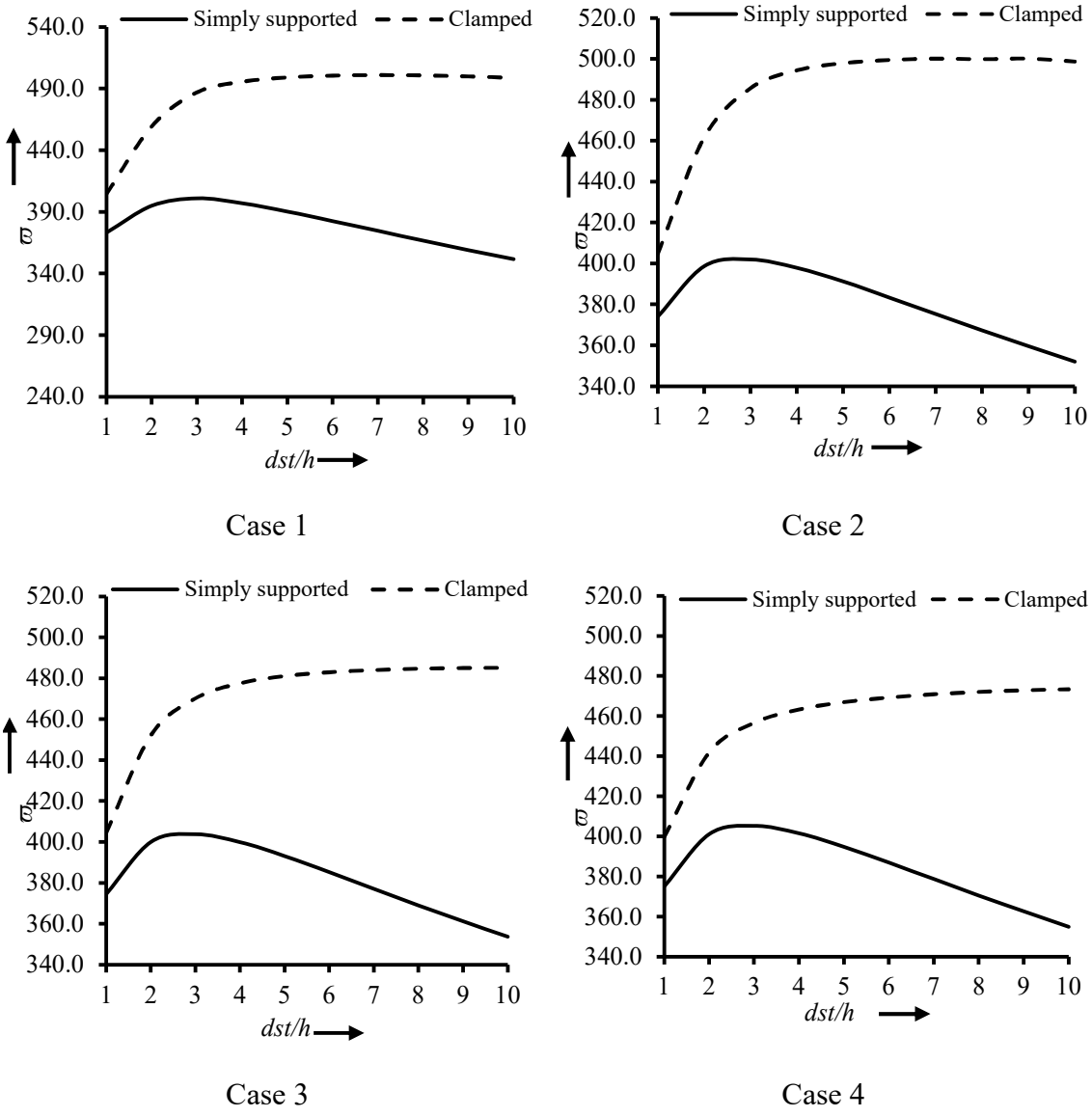

Figure 5.9: Nondimensional fundamental frequencies of elliptical paraboloid with cutout for 45^0/-45^0/45^0, R_{yy}/R_{xx} =1.0, and 9×9 stiffeners.

For different d_{st}/h ratios, the fundamental frequencies of simply supported and biaxially stiffened clamped panels are provided in Table 5.13 and Figure 5.9. As shown in figure 5.2, the panels are assumed to be made from (45^0/-45^0/$45^{0)}$ laminate with cutout size a'/a=0.1, by varying

cutout number at different location as given in Figure 5.8 cases are there. biaxial stiffeners (9×9) with stiffener eccentricity e=0,

The goal of the study is to determine the ideal stiffener depth (d_{st}) that provides the highest skewed panel performance with the fewest headroom constraints. Important engineering criteria from a design perspective are the dead weight of panels and resonant frequencies, which are controlled by the stiffeners depth. The numbers range from 1 to 10 for the d_{st}/h ratio. By comparing the numbers, it is determined that the clamped panels provide higher frequencies than the simply supported ones for all skew angles. The frequencies are observed to rise until d_{st}/h=3. Fundamental frequencies decrease for simply supported boundary conditions with d_{st}/h>3, indicating that the panels are heavier. For clamped boundary conditions, the fundamental frequencies either slightly rise or largely remain constant after d_{st}/h=3, as a result of increased stiffness. The highest frequencies are displayed by clamped panels for d_{st}/h=10 and by simply supported panels for d_{st}/h=3.

5.3.6 Mode shapes of biaxially-stiffened panels with cutout

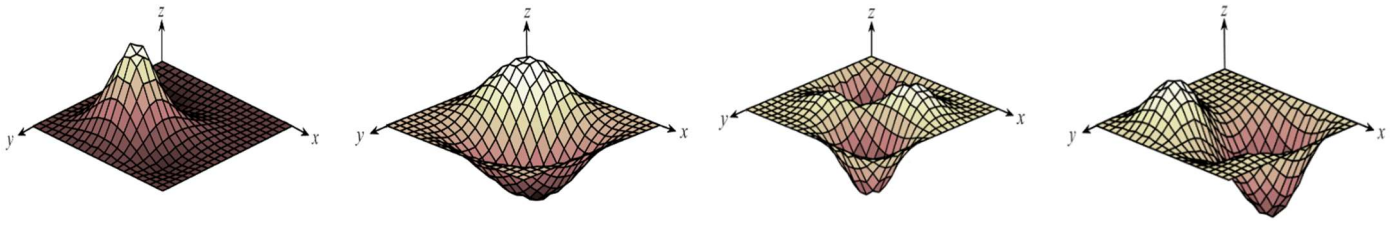

ϖ_1 = 474.5820 ϖ_2 = 479.7230 ϖ_3 = 485.3349 ϖ_4 = 488.7188

Case 1

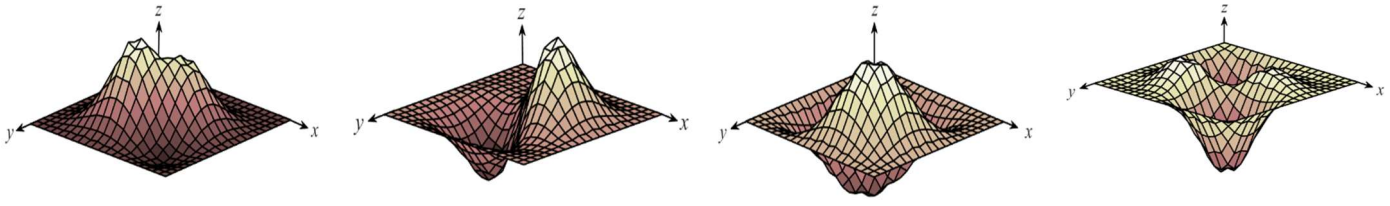

ϖ_1 = 473.4256 ϖ_2 = 476.6637 ϖ_3 = 479.1802 ϖ_4 = 484.9843

Case 2

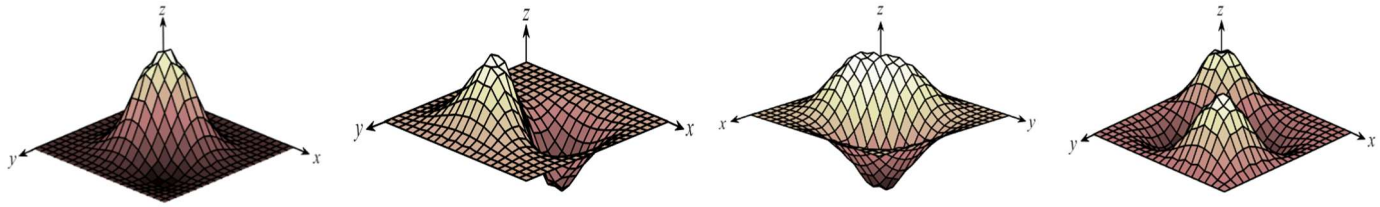

$\varpi_1 = 457.4927$ $\varpi_2 = 473.7119$ $\varpi_3 = 476.9110$ $\varpi_4 = 484.3125$

Case 3

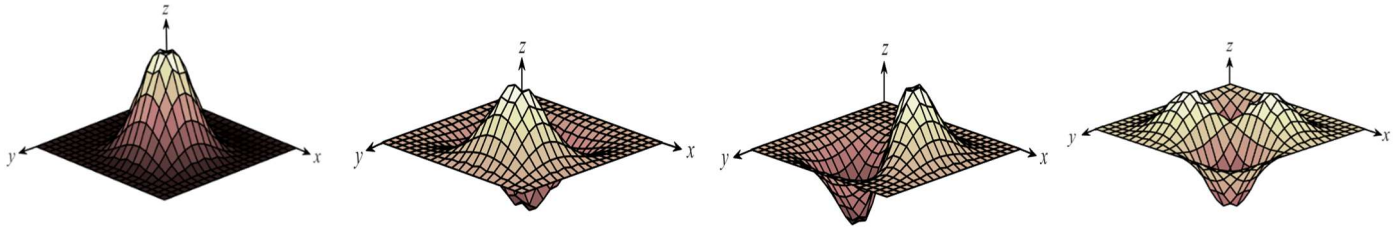

$\varpi_1 = 444.7462$ $\varpi_2 = 469.1030$ $\varpi_3 = 470.7556$ $\varpi_4 = 481.1159$

Case 4

Figure 5.10: Mode shapes of simply supported elliptical paraboloidal shell for varying positions of cutouts.

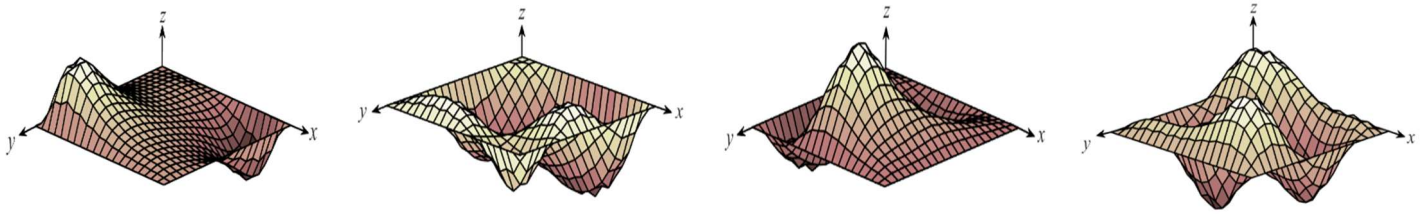

$\varpi_1 = 395.6231$ $\varpi_2 = 423.3823$ $\varpi_3 = 469.1807$ $\varpi_4 = 473.9599$

Case 1

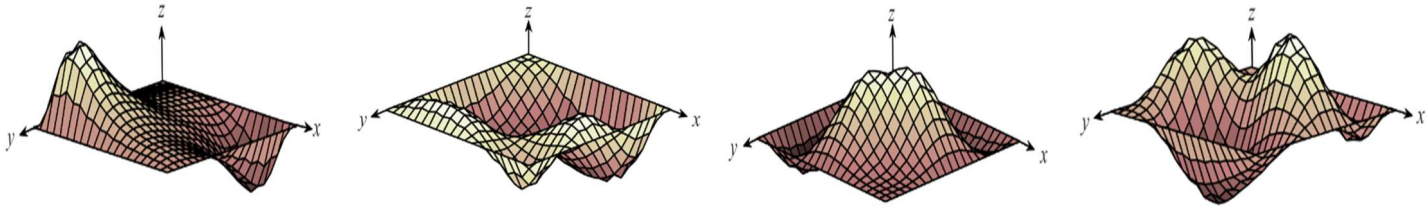

$\varpi_1 = 395.9088$ $\varpi_2 = 424.9037$ $\varpi_3 = 468.1782$ $\varpi_4 = 471.9523$

Case 2

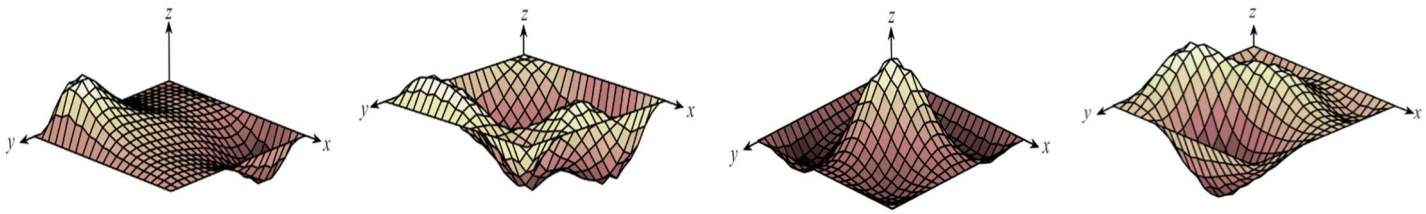

$\varpi_1 = 397.3018$ $\varpi_2 = 425.2261$ $\varpi_3 = 458.2195$ $\varpi_4 = 470.4832$

Case 3

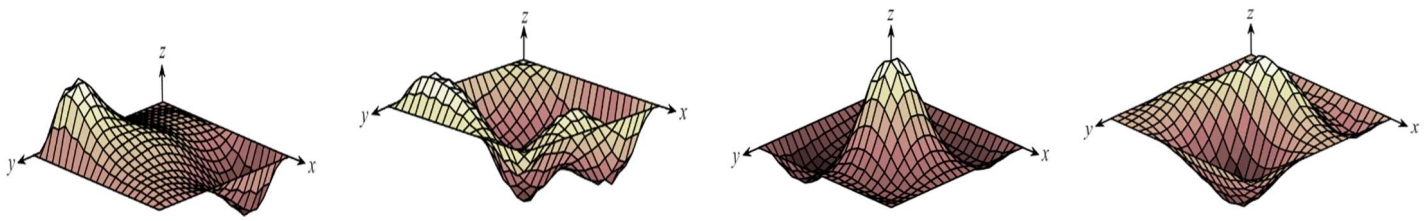

ϖ_1 = 398.1556 ϖ_2 = 423.6899 ϖ_3 = 445.6321 ϖ_4 = 466.8350

Case 4

Figure 5.11: Mode shapes of clamped elliptical paraboloidal shell for varying position of cutouts.

In addition to frequencies, Figures 5.10 and 5.11, respectively, report the mode morphologies of the first four modes of vibration of biaxially-stiffened simply supported and clamped panels. The panel's measurements are a/h = 100 and R_{yy}/R_{xx} = 1.0. As shown in Figure 5.8, the stiffeners 9×9 are employed with a variant of the cutout condition. According to the figures, elliptic paraboloids' fundamental frequencies rise with increasing vibrational modes. The fourth mode of vibration for clamped panels has a frequency that is over sixteen percent greater than the fundamental mode. For the fourth mode of vibration, the fundamental frequency of the simply supported panel is raised by more than 2%. It is crucial to understand that the frequencies for the third and fourth modes of vibration are extremely near to one another, even though both clamped and simply supported panels exhibit noticeable changes in frequency for different modes of vibration.

For various vibrational modes, the mode shapes also varied significantly. Large central crests can be seen in the fundamental mode of simply supported panels. Several crests with comparatively lower peaks are shown in the higher modes. The fundamental mode shape for clamped supported panels shows a crest and a distinct peak, whereas the higher modes display both peaks and crests, which are clearly noticeable. For a thorough free vibration study of stiffened elliptic paraboloids with cutout, practicing engineers must incorporate the first four modes of vibration since Figures 5.10 and 5.11 show that the frequencies and mode shapes of clamped and simply supported exhibit noticeable differences for higher modes of vibration.

5.4 Conclusions

For variable cutout, the nonlinear method presented in this research accurately solves the frequencies of composite stiffened elliptical paraboloidal panels. The fundamental frequencies of clamped and simply supported elliptical paraboloidal panels for cross and angle-ply laminations

and central stiffeners are calculated using the verified code. The stiffer conditions n_x =1, n_y=1, $45^0/-45^0/45^0$ laminate, and R_{yy}/R_{xx}=1 yield the best results for graphite epoxy and BMRP epoxy clamped and simply supported panels with a cutout ratio a'/a = 0.1. For every parametric modification carried out in this research, the clamped panels outperform the merely supported ones; hence, the clamped panels must be used in real applications. Since graphite epoxy and BMRP epoxy behave similarly, BMRP can be used as a substitute material that is both economical and environmentally friendly. Multiple biaxial stiffeners can be used to increase the frequencies of elliptical paraboloidal panels with cutout. Performance is greatly enhanced by increasing the number of biaxial stiffeners up to 4×4 before decreasing and then rising again after 6×6 stiffeners. For the stiffeners, the ideal depth should be d_{st}/h = 3. For R_{yy}/R_{xx} = 1, a/h = 100, and cutout ratio a'/a = 0.1, the frequencies of multi-stiffened composite $45^0/-45^0/45^0$ panels can be maximised. For a thorough free vibration analysis of stiffened composite elliptical paraboloids with variable cutout positions, it is advised that the first four modes of vibration be taken into account.

Chapter 6

Vibration Characteristics of Hyperbolic Paraboloidal Shell with Cutout

6.1 General

Using the mathematical formulation presented in the previous chapter, several numerical problems of laminated shells are analysed and results are presented in tabular and graphical forms.

For hyperbolic paraboloidal shell $R_{xx}/R_{yy}<0$

6.2 Numerical Problems on Hyperbolic Paraboloidal panels

There are two sections to the difficulties this paper solves. The first one focusses on the issues resolved in order to verify that the current strategy is correct. Section 6.2.1 provides the solutions to these issues, which were solved to examine the relative performances of skewed stiffened hyperbolic paraboloidal panels with cutout for different graphite/epoxy laminations.

6.2.1 Benchmark problems

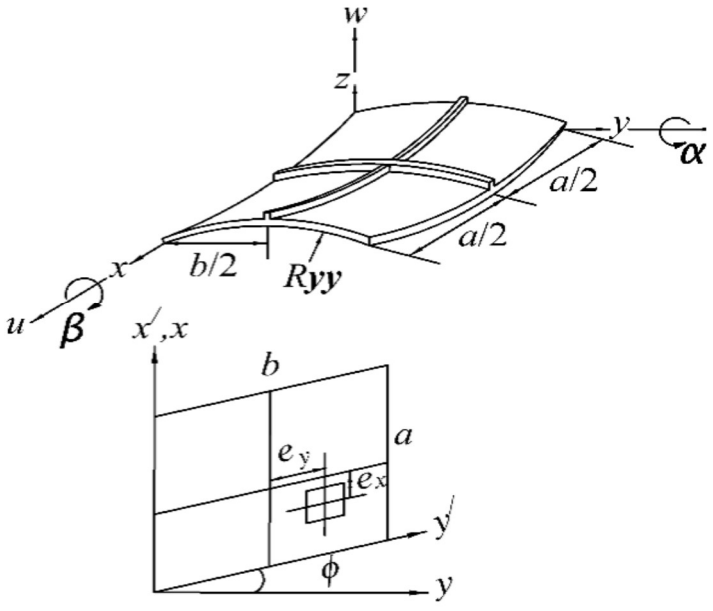

Figure 6.1: Centrally stiffened hyperbolic paraboloidal shell with cutout in plan.

For the first four modes of vibration, angle-ply hyperbolic paraboloidal panels' frequencies are provided. Results for several finite element mesh divisions of clamped and simply supported panels are obtained for each mode. When the fundamental frequencies for any mesh do not increase

by more than 1% with additional mesh refinement, the convergence of the finite element mesh is deemed to have been accomplished. The convergence for both boundary conditions is provided by an 8×8 mesh, as the table demonstrates. The converged results are found to be extremely near to Ye et al. (2013)'s exact solutions. Therefore, it is verified that the current code correctly formulates the composite hyperbolic paraboloid. The table as a footnote gives the panel's dimensions and material qualities.

Table 6.1: Non-dimensional fundamental frequencies of clamped and simply supported hyperbolic paraboloidal panels. ω = frequency in rad/sec, ρ = mass density.

Modes	Lamination = 45^0/-45^0/45^0/-45^0					
	Clamped panel			Simply supported panel		
	Mesh division	Present code	Ye et al. (2013)	Mesh division	Present code	Ye et al. (2013)
1	2×2	38.428	20.539	2×2	36.469	16.795
	4×4	24.628		4×4	20.425	
	6×6	20.947		6×6	17.129	
	8×8	20.728		8×8	16.949	
2	2×2	45.528	25.211	2×2	38.524	21.690
	4×4	29.519		4×4	23.458	
	6×6	25.687		6×6	22.109	
	8×8	25.448		8×8	21.897	
3	2×2	54.897	33.187	2×2	47.825	29.874
	4×4	36.987		4×4	31.459	
	6×6	33.819		6×6	30.448	
	8×8	33.488		8×8	30.171	
4	2×2	61.589	40.836	2×2	50.634	30.044
	4×4	46.268		4×4	34.556	
	6×6	41.604		6×6	30.789	
	8×8	41.198		8×8	30.331	

b/a = 2, h/a = 0.01, R_{xx}/a = 10, E_{11} = 15E_{22}, E_{22} = 2GPa, υ_{12} = 0.25, G_{12} = 0.5E_{22}, ρ = 1500 kg/m^3

For the first two modes of vibration and non-uniform boundary conditions, the frequencies of composite hyperbolic paraboloids are calculated. While the second panel has two adjacent edges clamped and other sides free (C–F–F–C), the first panel is cantilever (C–F–F–F). Table 6.2 provides the findings of $0^0/\theta^0/0^0$ laminates, where 'θ' is taken to be 0^0, 45^0 and 90^0. For both boundary conditions, modes of vibration, and all laminations, the discrepancies between the current results and the precise values provided by Ye et al. (2013) are less than 2%. The accuracy

of the suggested code is shown by the comparative analysis in Table 6.2. The panel's size and material qualities are also reported in the table.

Table 6.2: Non-dimensional fundamental frequencies of CFFF and CFFC hyperbolic paraboloidal panels. ω = frequency in rad/sec, ρ = mass density.

Boundary condition	Lamination	Modes	Present code (8×8)	Ye et al. (2013)	Differences (%)
C–F–F–F	$0^0/0^0/0^0$	1	4.2484	4.2934	1.048
		2	5.8879	5.9786	1.517
	$0^0/45^0/0^0$	1	4.8956	4.9887	1.866
		2	6.5487	6.6391	1.362
	$0^0/90^0/0^0$	1	5.1987	5.2934	1.789
		2	6.6994	6.8331	1.957
C–F–F–C	$0^0/0^0/0^0$	1	17.307	17.596	1.642
		2	17.699	17.974	1.530
	$0^0/45^0/0^0$	1	15.448	15.635	1.196
		2	15.797	16.099	1.876
	$0^0/90^0/0^0$	1	15.247	15.429	1.180
		2	15.478	15.747	1.708

b/a = 1, h/a = 0.01, R_{xx}/a = 5, E_{11} = 138 GPa, E_{22} = 8.96GPa, υ_{12} = 0.3, G_{12} = 7.1GPa, ρ = 1500 kg/m^3

For symmetric and anti-symmetric laminations, Table 6.3 reports the frequencies of clamped and simply supported skewed hyperbolic paraboloids. The skew angles for each boundary conditions are 15^0, 30^0 and 45^0. The current results and those published by Kumar et al. (2013) are compared in the table, and there is a 2% difference between the two. The current frequencies are calculated using eight noded elements, whereas Kumar et al. (2013) used nine noded elements to generate their frequencies. This explains the discrepancies in the results. The dimensions and material parameters of the composite panel are reported in the table's footnote.

Table 6.3: Non-dimensional fundamental frequencies of skewed hypar panels. ω = frequency in rad/sec, ρ = mass density.

Boundary condition	Skew angle	Lamination	Present code (8×8)	Kumar et al. [52]	Differences (%)
Clamped	15^0	$0^0/45^0/0^0/45^0$	129.682	131.605	1.461
		$0^0/45^0/45^0/0^0$	127.856	130.327	1.896
		$0^0/90^0/0^0/90^0$	115.895	116.862	0.827
		$0^0/90^0/90^0/0^0$	116.874	117.185	0.265
	30^0	$0^0/45^0/0^0/45^0$	147.598	150.108	1.672
		$0^0/45^0/45^0/0^0$	142.487	143.892	0.976
		$0^0/90^0/0^0/90^0$	129.745	131.129	1.055
		$0^0/90^0/90^0/0^0$	129.865	130.543	0.519
	45^0	$0^0/45^0/0^0/45^0$	186.698	188.153	0.773
		$0^0/45^0/45^0/0^0$	173.584	174.821	0.708
		$0^0/90^0/0^0/90^0$	159.968	162.510	1.564
		$0^0/90^0/90^0/0^0$	158.587	159.428	0.528
Simply supported	15^0	$0^0/45^0/0^0/45^0$	41.2956	41.9635	1.592
		$0^0/45^0/45^0/0^0$	39.9589	40.6650	1.736
		$0^0/90^0/0^0/90^0$	46.4746	46.9078	0.924
		$0^0/90^0/90^0/0^0$	42.2745	43.0824	1.875
	30^0	$0^0/45^0/0^0/45^0$	43.5874	44.1727	1.325
		$0^0/45^0/45^0/0^0$	41.0587	41.3150	0.620
		$0^0/90^0/0^0/90^0$	52.2874	53.0184	1.379
		$0^0/90^0/90^0/0^0$	44.4874	45.1971	1.570
	45^0	$0^0/45^0/0^0/45^0$	52.8874	53.5860	1.304
		$0^0/45^0/45^0/0^0$	47.6987	48.0470	0.725
		$0^0/90^0/0^0/90^0$	66.8746	67.3628	0.725
		$0^0/90^0/90^0/0^0$	53.2874	54.2594	1.791

$a/b = 1$, $h/a = 0.01$, $c/a = 0.2$, $E_{11}/E_{22} = 25$, $G_{12} = G_{13} = 0.5E_{22}$, $G_{23} = 0.2E_{22}$, $\upsilon_{12} = 0.25$

Table 6.4 reports non-dimensional fundamental frequencies for symmetric and anti-symmetric stackings of cross and angle-ply laminations of stiffened hyperbolic paraboloidal panels with straight edge boundaries (hypar shells). Along the x – axis ($n_x = 1$, $n_y = 0$), y – axis ($n_x = 0$, $n_y = 1$) and both axes ($n_x = 1$, $n_y = 1$), the stiffeners are orientated. The table contrasts the current findings with those of Sahoo and Chakravorty's (2006) finite element analysis. The discrepancies between the current results and those reported by Sahoo and Chakravorty (2006) attest to the fact that the

current code accurately formulates the stiffened panels. The stiffened panel's size and material qualities are reported in the table as footnotes as well.

Table 6.4: Non-dimensional fundamental frequencies of simply supported skewed stiffened hypar panels. ω = frequency in rad/sec, ρ = mass density.

Stiffeners	Lamination	Present code (8×8)	Sahoo and Chakravorty (2006)	Differences (%)
$n_x = 1$, $n_y = 0$	$0^0/90^0$	5.9973	6.1093	1.833
	$0^0/90^0/0^0$	8.6474	8.7334	0.985
	$45^0/-45^0$	5.8846	5.9968	1.871
	$45^0/-45^0/45^0$	8.7046	8.7687	0.731
$n_x = 0$, $n_y = 1$	$0^0/90^0$	5.9874	6.0659	1.294
	$0^0/90^0/0^0$	6.3574	6.473	1.786
	$45^0/-45^0$	5.8843	5.9779	1.566
	$45^0/-45^0/45^0$	8.6875	8.8066	1.352
$n_x = 1$, $n_y = 1$	$0^0/90^0$	7.5123	7.6083	1.262
	$0^0/90^0/0^0$	8.5753	8.741	1.896
	$45^0/-45^0$	7.5287	7.624	1.250
	$45^0/-45^0/45^0$	10.079	10.172	0.914

$a/b = 1$, $h/a = 0.01$, $c/a = 0.2$, $E_{11}/E_{22} = 25$, $G_{12} = G_{13} = 0.5E_{22}$, $G_{23} = 0.2E_{22}$, $\upsilon_{12} = 0.25$

Table 6.5 presents the findings of the solution of the nonlinear fundamental frequencies of simply supported hyperbolic paraboloidal panels for $[0^0/0^0/30^0/-30^0]_2$ lamination. Various variations of the radius of curvature to span ratios (R/a ratio) are used to determine the frequencies. The table compares the current findings with those found by Naidu and Sinha (2007) for each R/a ratio. Less than 2% separates the current results from those reported by Naidu and Sinha (2007), confirming the accuracy of the current nonlinear code. The dimensions and material parameters of the composite panel are reported in the table's footnote.

Table 6.5: Nonlinear fundamental frequencies [$\varpi = \omega a^2(\rho/E_{22}h^2)^{0.5}$] of simply supported $[0^0/0^0/30^0/-30^0]_2$ hyperbolic paraboloid shell.

Source	$R/a = 5$	$R/a = 10$	$R/a = 100$	$R/a = 1000$
Naidu and Sinha (2007)	49.909	30.379	13.554	13.508
Present FEM (8×8)	48.927	29.949	13.381	13.468
Differences (%)	1.968	1.415	1.276	0.2960

E_{11}=130 GPa, E_{22} = 9.5 GPa, G_{12}=G_{13} =6.0 GPa, G_{23}=3.0 GPa, a/b=1, h/a=0.01, υ_{12}=0.3, ρ = 1600 kg/m^3, amplitude ratio (w_{max}/h) = 0.2.

An isotropic centrally stiffened square plate's frequencies for the first four vibrational modes are calculated in the final problem. In order to represent the plate, the current code gives the radii of curvatures high values (10^{70}). To simulate the isotropic material, equal values of the elastic and shear moduli are assigned. Results for the clamped border condition are provided. Additionally, the table contrasts the current findings with the experimental and theoretical conclusions provided by Olson and Hazell (1977). Triangular components were used to arrive at the theoretical conclusions presented in Olson and Hazell (1977). The findings of the suggested code differ from the finite element results of Olson and Hazell (1977) by less than 2 percent. However, when compared to the experimental values, the discrepancies are slightly greater (less than 5%). The suggested code formulated the plate as fully clamped, which explains the discrepancies between the current results and experimental data. It is challenging to maintain comparable constraints around the plate edges throughout the experiment. For this reason, the current results show a stiffer plate than the one Olson and Hazell (1977) produced from the experiment.

Table 6.6: Fundamental frequencies (Hz) of centrally stiffened clamped square plate.

Modes	Olson and Hazell (1977)		Present FEM	Differences (%)	
	Theoretical	Experimental	(10×10)	Theoretical	Experimental
1	718.1	689	718.32	0.031	4.082
2	751.4	725	762.46	1.451	4.913
3	997.4	961	1011.5	1.394	4.993
4	1007.1	986	1026.6	1.899	3.955

$a = b = 203.2$ mm, $h = 1.3716$ mm, $b_{st} = 6.35$ mm, $d_{st} = 12.7$ mm, $e = e_b$, $E = 6.87 \times 10^7$ KN/m^2, $v = 0.3$, $\rho = 2823$ kg/m^3

6.2.2 Parametric Studies

Table 6.7: Laminations for skewed hypar panels.

	Cross-ply	**Angle-ply**
2-layer	$0^0/90^0$	$45^0/-45^0$
3-layer	$0^0/90^0/0^0$	$45^0/-45^0/45^0$
4-layer	$0^0/90^0/90^0/0^0$	$45^0/-45^0/45^0/-45^0$
	$0^0/90^0/0^0/90^0$	$45^0/-45^0/-45^0/45^0$

Table 6.8: Engineering properties of the hypar composites.

Elastic constants	Graphite/epoxy
E_{11}	142.5GPa
E_{22}	9.790GPa
E_{33}	9.790GPa
G_{12}	4.270GPa
G_{13}	4.270GPa
G_{23}	1.192GPa
v_{12}	0.27
v_{13}	0.27
v_{23}	0.25
ρ	1.0×10^{-6} N-sec^2/cm^2

The hyperbolic paraboloidal panel measurements are as follows:

Table 6.9: Dimensions of the hypar shell with Cutout.

constants	Graphite/epoxy
a/b	1
h/a	0.01
R'_{xx}/a	0.75
R'_{yy}/b	0.75
w_{max}/h	0.3
ϕ	$\geq 0^0$
R_{xx}/R_{yy}	$\cos\phi$

With cutout for CSCS and SCSC boundary conditions, the authors solve free vibration problems of skewed stiffened hyperbolic paraboloidal panels with cutout. They use eight distinct composites, consisting of four symmetric orders ($0^0/90^0/0^0$, $0^0/90^0/90^0/0^0$, $45^0/-45^0/45^0$ and $45^0/-45^0-45^0/45^0$) and four antisymmetric ($0^0/90^0$, $0^0/90^0/0^0/90^0$, $45^0/-45^0$ and $45^0/-45^0/45^0/-45^0$). $(0^0/90^0)_s$ and $(45^0/-45^0)_s$ are the designations for the symmetric ones, $0^0/90^0/90^0/0^0$ and $45^0/-45^0/-45^0/45^0$, respectively. They are called $(0^0/90^0)_2$ and $(45^0/-45^0)_2$ for the antisymmetric ones, $0^0/90^0/0^0/90^0$ and $45^0/-45^0/45^0/-45^0$ with cutout ratio (a'/a) = 0.125,0.25, 0.1,0.2,0.3,0.4.

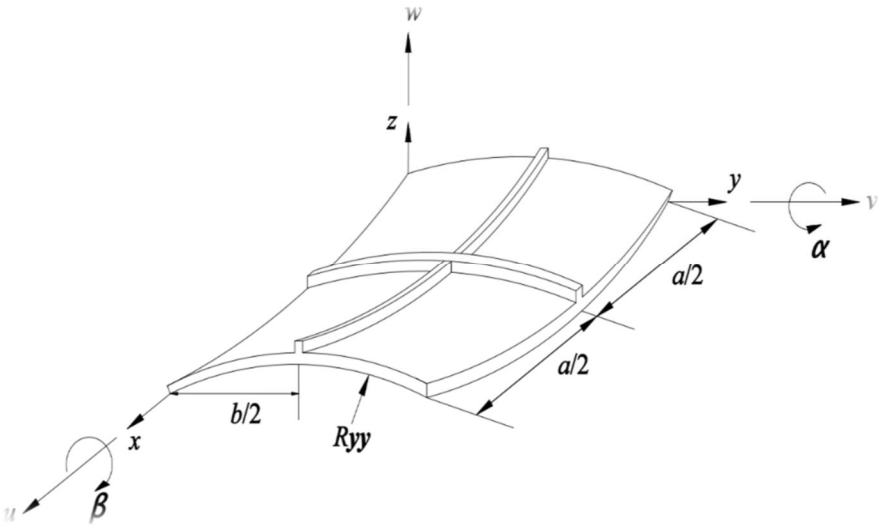

Figure 6.2: Hyperbolic paraboloidal panel with central stiffeners.

Fibres run the length of the one-layer composite stiffeners. The fundamental frequencies of panels that are *x, y*, and biaxially stiffened are examined. Figure 6.2 shows the panels that have been strengthened. The panels' top, bottom, and concentric are where the stiffeners are situated. The results show that the optimal composite for CSCS and SCSC boundary conditions was (45^0/-45^0/45^0/-45^0) and (45^0/-45^0/-45^0/45^0), respectively. Additionally, the performance of multi-stiffened panels is examined for (45^0/-45^0/45^0/-45^0) composite.

6.3 Results and Discussion:

6.3.1 Relative performances of panels with cutout for graphite epoxy

Table 6.10: Non-dimensional fundamental frequencies of CSCS and SCSC laminated composite hyperbolic-paraboloidal shell with varying (a_1/a) ratio and lamination.

Boundary Condition	Lamination (Degree)	$a_1/a = 0$	$a_1/a = 0.1$	$a_1/a = 0.2$	$a_1/a = 0.3$	$a_1/a = 0.4$
CSCS	$0^0/90^0$	95.8200	95.5167	95.0130	95.6411	95.2826
	$0^0/90^0/0^0$	95.3766	95.1784	94.7916	95.2078	95.1274
	$0^0/90^0/0^0/90^0$	104.0589	103.6663	103.02013	102.36051	102.1842
	$0^0/90^0/90^0/0^0$	99.6798	99.1657	98.5101	98.4690	98.2912
	$45^0/-45^0$	124.5739	124.2227	124.91842	123.68108	121.0611
	$45^0/-45^0/45^0$	127.7208	127.2834	126.49793	125.3705	121.5908
	$45^0/-45^0/45^0/-45^0$	133.5854	**132.9931**	132.62736	131.2987	130.4509
	$45^0/-45^0/-45^0/45^0$	130.9077	129.3883	124.91935	129.19133	126.8110
SCSC	$0^0/90^0$	96.6967	96.2877	96.0837	95.1116	91.3338
	$0^0/90^0/0^0$	111.8437	111.2160	110.3443	108.18347	105.5787
	$0^0/90^0/0^0/90^0$	104.7888	104.4208	103.92751	102.17967	99.5393
	$0^0/90^0/90^0/0^0$	109.7310	109.3134	108.59094	106.89287	104.3620
	$45^0/-45^0$	122.7802	122.6405	122.35539	118.47158	116.2267
	$45^0/-45^0/45^0$	129.1136	128.5466	127.60491	124.36835	120.6809
	$45^0/-45^0/45^0/-45^0$	131.0265	130.5278	129.56046	126.10089	123.9622
	$45^0/-45^0/-45^0/45^0$	131.2767	**130.8781**	129.95994	126.43033	123.5657

E_{11} = 142.5 GPa, $G_{12} = G_{13}$ = 4.72 GPa, E_{22} = 9.79 GPa, ν_{12} = 0.27, G_{23} = 1.192 GPa, R_{xx}/R_{yy} = -1, a/b = 1, h/a=0.01, $b_{st} = h$, d_{st}/b_{st} = 2

From Table 6.10 for CSCS boundary condition the maximum non dimensional frequency is obtained for angle ply ($45^0/-45^0/45^0/-45^0$) and a_1/a =0.1. Similarly, for SCSC boundary condition the maximum non dimensional frequency is obtained for angle ply ($45^0/-45^0/-45^0/45^0$) and a_1/a =0.1. stiffness of panel is reducing when we increase cutout ratio, in Table 6.10 non-dimensional frequencies reducing when we are increasing a_1/a ratio. CSCS boundary conditions give higher results that the SCSC.

6.3.2 Relative performances of multi- stiffened panels with cutout

Table 6.11: Non-dimensional fundamental frequencies of CSCS and SCSC laminated composite hyperbolic-paraboloidal shell $45^0/-45^0/-45^0/45^0$ and a_1/a =0.1.

Boundary Condition	***e***	n_x=0,n_y=0	n_x=2,n_y=0	n_x=0,n_y=2	n_x=2,n_y=2	n_x=4,n_y=0	n_x=0,n_y=4	n_x=4,n_y=4
CSCS	e_b	129.3883	140.6968	146.6600	150.1308	180.2215	180.5822	181.8329
	0	129.3883	140.0809	146.5290	151.4960	179.4336	179.4442	**188.1683**
	e_t	129.3883	137.4377	147.9578	142.5005	164.2478	184.6215	156.2960
SCSC	e_b	130.8781	143.8580	137.4315	146.1590	178.1372	185.1140	181.5386
	0	130.8781	143.5278	137.0720	147.9283	177.1209	184.6308	**187.5418**
	e_t	130.8781	140.1864	137.3884	131.2480	159.7769	186.6443	154.8548

E_{11} = 142.5 GPa, G_{12} = G_{13} = 4.72 GPa, E_{22} = 9.79 GPa, v_{12} = 0.27, G_{23} = 1.192 GPa, R_{xx}/R_{yy} = -1, a/b = 1, h/a=0.01, b_{st} = h, d_{st}/b_{st} = 2, a_1/a =0.1

In Table 6.11 for CSCS and SCSC boundary conditions with increase in number of stiffeners non dimensional frequencies increasing and the maximum non dimensional frequency is obtained at eccentricity e=0 and stiffener position (n_x=4, n_y=4).

6.3.3 Relative performances of multi- stiffened panels with cutout variation

Table 6.12: Non-dimensional fundamental frequencies of simple supported composite hyperbolic-paraboloidal shell.

Lamination (Degree)	ϕ	a_1/a = 0.0			a_1/a = 0.125			a_1/a = 0.25		
		n_x=1, n_y=0	n_x=0, n_y=1	n_x=1, n_y=1	n_x=1, n_y=0	n_x=0, n_y=1	n_x=1, n_y=1	n_x=1, n_y=0	n_x=0, n_y=1	n_x=1, n_y=1
0/90	0	36.454	36.481	36.392	36.282	36.292	36.235	36.131	36.044	36.220
	5	37.640	37.731	37.902	37.469	**38.006**	37.563	37.326	37.373	37.879
	10	41.244	41.969	42.417	41.081	41.815	41.784	40.963	41.647	**42.623**
	15	46.653	48.136	48.858	46.482	47.988	47.817	46.309	47.748	47.640
	20	53.095	55.287	54.944	52.878	**56.399**	54.718	**53.706**	54.726	54.456
	25	60.042	64.467	63.887	59.730	64.060	61.914	**60.666**	63.395	59.164
	30	67.206	72.238	71.510	66.746	71.667	69.149	66.117	70.711	66.552
	35	76.442	78.210	78.941	75.583	77.701	76.548	72.915	77.814	**79.696**
0/90/0	0	46.900	46.799	46.496	46.744	46.643	41.659	46.574	46.436	41.505
	5	47.627	48.143	47.612	**47.669**	47.657	42.899	47.331	47.474	42.597
	10	50.090	51.292	50.155	**50.416**	50.454	46.264	49.780	50.243	46.172
	15	54.004	55.712	54.377	53.843	55.500	51.054	**54.284**	55.185	50.818
	20	58.988	60.142	59.529	**59.878**	**61.052**	56.713	**59.382**	**60.811**	57.160
	25	66.379	66.208	66.857	64.467	65.888	62.962	65.157	**66.757**	63.642
	30	73.250	72.960	73.778	72.634	72.411	69.709	69.882	**73.145**	70.574
	35	80.808	82.372	81.202	77.685	81.304	**81.797**	76.348	79.988	77.957
0/90/0/90	0	44.733	44.750	44.500	44.581	44.591	44.377	44.426	44.393	44.227
	5	45.782	45.784	45.764	45.641	**46.060**	45.485	45.519	45.616	45.314
	10	48.867	49.370	49.595	48.730	49.232	49.070	48.590	49.071	49.101
	15	53.643	54.836	55.310	53.490	54.690	54.422	53.289	54.463	54.242
	20	59.553	62.732	62.144	59.348	62.457	60.813	**59.954**	62.052	60.544
	25	66.171	70.417	69.533	**67.247**	70.014	69.068	65.368	69.207	65.211
	30	75.025	78.214	77.146	74.495	77.423	76.486	72.043	76.495	**77.516**
	35	80.789	86.174	84.898	80.072	85.303	82.384	78.884	83.816	83.408
0/90/90/0	0	46.996	46.931	46.655	46.839	46.770	46.522	46.676	46.569	46.370
	5	47.936	47.868	47.855	47.791	**47.924**	47.549	47.651	47.753	47.258
	10	50.869	51.149	51.388	50.729	**51.620**	50.849	50.568	**51.409**	50.758
	15	55.416	57.125	55.893	55.262	56.929	55.748	**55.648**	56.633	52.374
	20	61.076	63.735	61.824	60.859	63.477	61.609	**61.438**	63.020	58.723
	25	67.477	70.792	69.859	**68.533**	70.367	69.360	**67.782**	69.673	**70.149**
	30	76.285	78.286	77.193	73.985	77.403	74.938	73.072	75.061	75.859
	35	82.085	86.217	84.881	81.173	85.216	82.151	79.926	82.158	83.190

E_{11} = 142.5 GPa, $G_{12} = G_{13}$ = 4.72 GPa, E_{22} = 9.79 GPa, v_{12} = 0.27, G_{23} = 1.192 GPa, R_{xx}/R_{yy} = -1, a/b = 1, h/a=0.01, $b_{st} = h$, d_{st}/b_{st} = 2

Table 6.12 presents the variation in non-dimensional fundamental frequencies for different configurations of concentric cutout sizes (a_1/a), skew angles (ϕ), and lamination schemes in laminated composite panels. The findings are particularly significant for real-world applications where the presence of cutouts is often unavoidable due to functional requirements such as ventilation, lighting, or access. For a fixed skew angle, the data indicates that several shell panels with cutouts outperform their solid counterparts in terms of fundamental frequency. These superior configurations are emphasized in bold in Table 6.12. Specifically, for panels with $a_1/a = 0.125$, 12 configurations show higher frequencies than the corresponding solid panels. For $a_1/a = 0.25$, 16 such favourable instances are recorded. This improvement in frequency, despite the introduction of cutouts, can be attributed to the dual effect of cutouts reducing both mass and stiffness. While reduced stiffness tends to lower natural frequencies, the concurrent reduction in mass can counteract this and lead to an overall increase. Therefore, under certain conditions, panels with small cutouts can exhibit enhanced vibrational characteristics. Among all combinations, the highest fundamental frequencies are observed for panels with a cutout ratio of $a_1/a = 0.125$, a lamination scheme of [0°/90°/90°/0°], and a skew angle of 35°. This combination appears to provide an optimal balance between structural continuity and weight reduction. From a practical standpoint, the study suggests that maintaining the cutout size within $a_1/a \leq 0.125$ is beneficial when aiming to preserve or enhance dynamic performance. These results hold particular relevance for civil engineers, as optimizing cutout dimensions can significantly influence the cost, weight, and resonance characteristics of shell structures. In terms of stiffening configuration, Table 6.12 shows that panels reinforced in the y-direction n_x=0, n_y=1 generally yield the highest fundamental frequencies across various skew angles. Although a few instances exist where biaxially stiffened panels n_x=1, n_y=1 perform slightly better, the difference is marginal (within 5%). Hence, for cost-effective and efficient structural design, particularly in skewed hyperbolic paraboloidal panels with $a_1/a = 0.125$ and the [0°/90°/90°/0°] laminate, y-direction stiffeners are recommended.

6.3.4 Relative performances of singly- stiffened panels with cutout by varying eccentricity

Table 6.13: Non-dimensional fundamental frequency of panels for a_1/a = 0.125, 0°/90°/90°/0° composite, ϕ = 35° and n_x=0, n_y=1 stiffeners.

e_y/b	e_x/a			
	0	0.125	0.25	0.375
0	85.2161	85.1590	85.7983	86.0291
0.125	85.1158	85.5344	87.0286	86.7262
0.25	85.3962	85.9091	86.5237	84.2571
0.375	79.1711	80.1075	80.9895	84.0038

E_{11} = 142.5 GPa, G_{12} = G_{13} = 4.72 GPa, E_{22} = 9.79 GPa, v_{12} = 0.27, G_{23} = 1.192 GPa, R_{xx}/R_{yy} = -1, a/b = 1, h/a=0.01, b_{st} = h, d_{st}/b_{st} = 2

Table 6.13 presents the variation in non-dimensional fundamental frequencies corresponding to different eccentricities of a fixed-size cutout (a_1/a = 0.125). In this analysis, the position of the cutout is shifted along both the $x^{/}$-axis (e_x) and $y^{/}$-axis (e_y). to examine the influence of eccentricity on the vibrational behavior of hyperbolic paraboloidal panels. The study is carried out for panels composed of 0°/90°/90°/0° laminated composites, stiffened in the y-direction n_x=0, n_y=1, with a skew angle of 35°. Among all configurations examined, the optimal performance is observed when the eccentricity ratios are e_x/a = 0.25 and e_y/b = 0.375. This specific arrangement results in the highest fundamental frequency, indicating a significant improvement over panels with centrally located (concentric) cutouts. These findings highlight the importance of cutout positioning in tuning the dynamic response of shell structures, offering potential design strategies for achieving better vibration performance in lightweight composite systems.

6.4 Conclusions

Among the various configurations studied, hyperbolic paraboloidal panels constructed with a 0°/90°/90°/0° laminated composite demonstrate the most favorable vibration characteristics. These dynamic performances are further enhanced when the panels are reinforced with unidirectional stiffeners aligned along the y-axis n_x=0, n_y=1 and oriented at a skew angle of 35° relative to the same axis. In real-world applications, cutouts are often incorporated in shell structures for ventilation, weight reduction, and tuning of the natural frequencies. Based on the present analysis, a cutout size of a_1/a = 0.125 proves to be optimal, as it offers a balanced trade-off minimizing the loss in stiffness while improving the fundamental frequency relative to fully solid shells. Additionally, positioning the cutout eccentrically at e_x/a = 0.25 and e_y/b = 0.375 yields the most efficient vibrational response. These insights offer valuable guidance for the structural design of lightweight, efficient, and dynamically stable composite shell systems.

Chapter 7

FUTURE SCOPE

The literature reviewed in Chapter 2 indicates that the analysis of laminated composite skewed and stiffened elliptical and hyperbolic paraboloidal panels is an active area of research, with ongoing contributions from various scholars. However, gaps still remain that offer potential for future exploration. The present study, as outlined in Chapter 3, provides a foundation for further research that can be extended to different boundary conditions where the edges are restrained in varied ways. Additionally, the current geometrically linear and nonlinear approaches can be applied to other shell configurations such as conoidal shells, which are structurally and architecturally significant. Future investigations may also focus on buckling behavior, impact response, progressive failure under static loads, hygrothermal effects, and dynamic instability. Since practical shell structures often feature cutouts for functional purposes like ventilation, lighting, cable routing, or resonant frequency control, this research can be extended to evaluate skewed panels with such cutouts across other geometries. Moreover, optimization studies can be undertaken to improve the performance-to-weight ratio and structural efficiency. It is important to note that the future directions mentioned here are indicative and not exhaustive, and ongoing advancements in materials and computational tools may further broaden the scope of this research.

Chapter 8

REFERENCES

[1] Ahmadi, H., Bayat, A., and Duc, N.D. 2021, "Nonlinear Forced Vibrations Analysis of Imperfect Stiffened FG Doubly Curved Shallow Shell in Thermal Environment Using Multiple Scales Method," Compos. Struct., 256: 113090. https://doi.org/10.1016/j.compstruct.2020.113090.

[2] Amabili, M. 2005, "Non-Linear Vibrations of Doubly Curved Shallow Shells," Int. J. Non-Linear Mech., 40(5): 683–710. https://doi.org/10.1016/j.ijnonlinmec.2004.08.007.

[3] Ansari, E., Hemmatnezhad, M., and Taherkhani, A. 2023, "Free Vibration Analysis of Grid-Stiffened Composite Truncated Spherical Shells," Thin-Walled Struct., 182: 110237. https://doi.org/10.1016/j.tws.2022.110237.

[4] Ashour, A.S. 2009, "The Free Vibration of Symmetrically Angle-Ply Laminated Fully Clamped Skew Plates," J. Sound Vib., 323: 444–450. https://doi.org/10.1016/j.jsv.2008.12.027.

[5] Bakshi, K., and Chakravorty, D. 2014, "Geometrically Linear and Nonlinear First-Ply Failure Loads of Composite Cylindrical Shells," J. Eng. Mech., 140: 04014094. https://doi.org/10.1061/(ASCE)EM.1943-7889.0000808.

[6] Bakshi, K. 2021*a*, "Numerical Study on Nonlinear Bending Performance of Transversely Loaded Composite Singly Curved Stiffened Surfaces," J. Strain Anal. Eng. Des., 56: 430–442. https://doi.org/10.1177/0309324720977415.

[7] Bakshi, K. 2021*b*, "A Numerical Study on Nonlinear Vibrations of Laminated Composite Singly Curved Stiffened Shells," Compos. Struct., 278: 114718. https://doi.org/10.1016/j.compstruct.2021.114718.

[8] Bich, D.H., Dung, D.V., and Nam, V.H. 2013, "Nonlinear Dynamic Analysis of Eccentrically Stiffened Imperfect Functionally Graded Doubly Curved Thin Shallow Shells," Compos. Struct., 96: 384–395. https://doi.org/10.1016/j.compstruct.2012.10.009.

[9] Bich, D.H., Duc, N.D., and Quan, T.Q. 2014, "Nonlinear Vibration of Imperfect Eccentrically Stiffened Functionally Graded Double Curved Shallow Shells Resting on Elastic Foundation Using the First Order Shear Deformation Theory," Int. J. Mech. Sci., 80: 16–28.https://doi.org/10.1016/j.ijmecsci.2013.12.009.

[10] Buragohmt, D.N., and Patodi, S.C. 1978, "Large Displacement Analysis of Skew Plates by Lumped Triangular Element Formulation," Comput. Struct., 9: 183–189. https://doi.org/10.1016/0045-7949(78)90137-2

[11] Chakravorty, D., Bandyopadhyay, J.N., and Sinha, P.K. 1995, "Free Vibration Analysis of Point-Supported Laminated Composite Doubly Curved Shells—A Finite Element Approach," Comput. Struct., 54(2): 191–198. https://doi.org/10.1016/0045-7949(94)00329-2.

[12] Chaubey, A.K., Kumar, A., and Mishra, S.S. 2018, "Dynamic Analysis of Laminated Composite Rhombic Elliptic Paraboloid Due to Mass Variation," J. Aerosp. Eng., 31(5): 1943–5525. https://doi.org/10.1061/(asce)as.1943-5525.0000881.

[13] Chaudhuri, P. B., Mitra, A., & Sahoo, S. (2018). Free vibration analysis of antisymmetric angle ply laminated composite stiffened hypar shell with cut out. Mater. Today: Proceedings, *5*(2), 5563-5572. https://doi.org/10.1016/j.matpr.2017.12.147

[14] Chaudhuri, P. B., Mitra, A., & Sahoo, S. (2022). Design of experiments analysis of fundamental frequency of laminated composite hypar shells with cut-out. Mater. Today: Proceedings, 66, 2332-2337. https://doi.org/10.1016/j.matpr.2022.06.327

[15] Daripa, R., and Singha, M.K. 2009, "Influence of Corner Stresses on the Stability Characteristics of Composite Skew Plates," Int. J. Non-Linear Mech., 44: 138–146. https://doi.org/10.1016/j.ijnonlinmec.2008.10.003.

[16] Duc, N.D. 2013, "Nonlinear Dynamic Response of Imperfect Eccentrically Stiffened FGM Double Curved Shallow Shells on Elastic Foundation," Compos. Struct., 99: 88–96. https://doi.org/10.1016/j.compstruct.2012.11.017.

[17] Fazilati, J., & Ovesy, H. R. (2013). Parametric instability of laminated longitudinally stiffened curved panels with cutout using higher order FSM. Compos. struct., *95*, 691-696. https://doi.org/10.1016/j.compstruct.2012.08.034

[18] Fazzolari, F.A. 2014, "A Refined Dynamic Stiffness Element for Free Vibration Analysis of Cross-Ply Laminated Composite Cylindrical and Spherical Shallow Shells," Compos. B Eng., 62: 143–158. https://doi.org/10.1016/j.compositesb.2014.02.021.

[19] Goswami, S., and Mukhopadhyay, M. 1995, "Geometrically Non-Linear Transient Dynamic Response of Laminated Composite Stiffened Shells," J. Reinf. Plast. Compos., 14(6): 618–640. https://doi.org/10.1177/073168449501400604.

[20] Goswami, S., and Mukhopadhyay, M. 1995, "Finite Element Free Vibration Analysis of Laminated Composite Stiffened Shell," J. Compos. Mater., 29(18): 2388–2422. https://doi.org/10.1177/002199839502901802.

[21] Hirwani, C.K., Mishra, P.K., and Panda, S.K. 2021, "Nonlinear Steady-State Responses of Weakly Bonded Composite Shell Structure Under Hygro-Thermo-Mechanical Loading," Compos. Struct., 265: 113768. https://doi.org/10.1016/j.compstruct.2021.113768.

[22] Hota, S. S., & Chakravorty, D. (2007). Free vibration of stiffened conoidal shell roofs with cutouts. JVC, 13(3), 221-240.https://doi.org/10.1177/1077546307072353

[23] Kallannavar, V., Kumaran, B., and Kattimani, S.C. 2020, "Effect of Temperature and Moisture on Free Vibration Characteristics of Skew Laminated Hybrid Composite and Sandwich Plates," Thin Walled Struct., 157: 107113. https://doi.org/10.1016/j.tws.2020.107113.

[24] Karimiasl, M., Ebrahimi, F., and Vinyas, M. 2019, "Nonlinear Vibration Analysis of Multiscale Doubly Curved Piezoelectric Composite Shell in Hygrothermal Environment," J. Intell. Mater. Syst. Struct., 30(10): 1594–1609. https://doi.org/10.1177/1045389X19835956.

[25] Karpov, V. V. (2018). Models of the shells having ribs, reinforcement plates and cutouts. Int. J. Solids Struct., 146, 117-135.https://doi.org/10.1016/j.ijsolstr.2018.03.024

[26] Kiani, Y., and Żur, K.K. 2022, "Free Vibrations of Graphene Platelet Reinforced Composite Skew Plates Resting on Point Supports," Thin-Walled Struct., 176: 109363. https://doi.org/10.1016/j.tws.2022.109363.

[27] Lee, S.Y. 2010, "Finite Element Dynamic Stability Analysis of Laminated Composite Skew Plates Containing Cutouts Based on HSDT," Compos. Sci. Technol., 70(8): 1249–1257. https://doi.org/10.1016/j.compscitech.2010.03.013.

[28] Liao, C.L., and Lee, Z.Y. 1993, "Elastic Stability of Skew Laminated Composite Plates Subjected to Biaxial Follower Forces," Int. J. Numer. Methods Eng., 36: 1825–1847. https://doi.org/10.1002/nme.1620361104.

[29] Lv, H., Chen, B., Shi, S., & Wen, Z. (2024). Minimum mass optimization of curved grid-honeycomb sandwich panels with cutouts under buckling constraints. In Struct. (Vol. 63, p. 106359). Elsevier. https://doi.org/10.1016/j.istruc.2024.106359

[30] Mahapatra, T.R., and Panda, S.K. 2016, "Nonlinear Free Vibration Analysis of Laminated Composite Spherical Shell Panel Under Elevated Hygrothermal Environment: A Micromechanical Approach," Aerosp. Sci. Technol., 49: 276–288. https://doi.org/10.1016/j.ast.2015.12.018.

[31] Malekzadeh, P., and Karami, G. 2006, "Differential Quadrature Nonlinear Analysis of Skew Composite Plates Based on Higher-Order Shear Deformation Theory," Eng. Struct., 28(9): 1307–1318. https://doi.org/10.1016/j.engstruct.2005.12.013.

[32] Mustafa, B.A.J., and Ali, R. 1987, "Prediction of natural frequency of vibration of stiffened cylindrical shells and orthogonally stiffened curved panels," J Sound Vib., 113 (2): 317–327. https://doi.org/10.1016/S0022-460X(87)80218-3.

[33] Naghsh, A., and Azhari, M. 2015, "Non-Linear Free Vibration Analysis of Point Supported Laminated Composite Skew Plates," Int. J. Non-Linear Mech., 76: 64–76. https://doi.org/10.1016/j.ijnonlinmec.2015.05.008.

[34] Naidu, N.V.S., and Sinha, P.K. 2007, "Nonlinear Free Vibration Analysis of Laminated Composite Shells in Hygrothermal Environments," Compos. Struct., 77(4): 475–483. https://doi.org/10.1016/j.compstruct.2005.08.002.

[35] Nanda, N., Sahu, S.K., and Bandyopadhyay, J.N. 2010, "Effect of Delamination on the Nonlinear Transient Response of Composite Shells in Hygrothermal Environments," Int. J. Struct. Integr., 1(3): 259–279. https://doi.org/10.1108/17579861011092382.

[36] Nanda, N. 2010, "Non-Linear Free and Forced Vibrations of Piezoelectric Laminated Shells in Thermal Environments," IES J. Part A: Civ. Struct. Eng., 3(3): 147–160. https://doi.org/10.1080/19373260.2010.490329.

[37] Nanda, N., and Pradyumna, S. 2011, "Nonlinear Dynamic Response of Laminated Shells with Imperfections in Hygrothermal Environments," J. Compos. Mater., 45(20): 2103–2112. https://doi.org/10.1177/0021998311401061.

[38] Nanda, N., and Bandyopadhyay, J.N. 2007, "Nonlinear Free Vibration Analysis of Laminated Composite Cylindrical Shells with Cutouts," J. Reinf. Plast. Compos., 26: 1413–1427. https://doi.org/10.1177/0731684407079776.

[39] Naveen, K.H.S., Kattimani, S., and Thoi, T.N. 2021, "Influence of Porosity Distribution on Nonlinear Free Vibration and Transient Responses of Porous Functionally Graded Skew Plates," Def. Technol., 17: 1918–1935. https://doi.org/10.1016/j.dt.2021.02.003.

[40] Noh, M.H., and Lee, S.Y. 2014, "Dynamic Instability of Delaminated Composite Skew Plates Subjected to Combined Static and Dynamic Loads Based on HSDT," Compos. B Eng., 58: 113–121. https://doi.org/10.1016/j.compositesb.2013.10.073.

[41] Patel, S.N. 2014, "Nonlinear Bending Analysis of Laminated Composite Stiffened Plates," Steel Compos. Struct., 17: 867–890, https://doi.org/10.12989/scs.2014.17.6.867.

[42] Prusty, B.G., and Satsangi, S.K. 2001, "Finite Element Transient Dynamic Analysis of Laminated Stiffened Shells," J. Sound Vib., 248(2): 215–233. https://doi.org/10.1006/jsvi.2001.3678.

[43] Prusty, B.G. 2008, "Free Vibration and Buckling Response of Hat-Stiffened Composite Panels Under General Loading," Int. J. Mech. Sci., 50(8): 1326–1333. https://doi.org/10.1016/j.ijmecsci.2008.03.003.

[44] Przekop, A., Azzouz, M.S., Guo, X., Mei, C., and Azrar, L. 2004, "Finite Element Multiple-Mode Approach to Nonlinear Free Vibrations of Shallow Shells," AIAA J., 42(11): 2373–2381. https://doi.org/10.2514/1.483.

[45] Rao, E., and Fu, T. 2024, "Vibro-Acoustic Response Analysis of Stiffened Sandwich PFGM Doubly-Curved Shells with Full Poisson's Ratio Cellular Cores," Eng. Anal. Bound Elem., 165: 105808. https://doi.org/10.1016/j.enganabound.2024.105808.

[46] Reddy, J.N. 2004, *An Introduction to Nonlinear Finite-Element Analysis*, Oxford University Press, New York.

[47] Reddy, J.N. 1984, "Exact Solutions of Moderately Thick Laminated Shells," J. Eng. Mech., 110(5): 794–809. https://doi.org/10.1061/(ASCE)0733-9399(1984)110:5(794).

[48] Sahoo, S. (2014). Laminated composite stiffened shallow spherical panels with cutouts under free vibration–A finite element approach. Int. J. Eng. Sci. Technol., 17(4), 247-259. https://doi.org/10.1016/j.jestch.2014.07.002

[49] Sathyamoorthy, M. 1995, "Nonlinear Vibrations of Moderately Thick Orthotropic Shallow Spherical Shells," Comput. Struct., 57(1): 59–65. https://doi.org/10.1016/0045-7949(94)00585-Q.

[50] Sayyad, A.S., and Ghugal, Y.M. 2019, "Static and Free Vibration Analysis of Laminated Composite and Sandwich Spherical Shells Using a Generalized Higher-Order Shell Theory," Compos. Struct., 219: 129–146. https://doi.org/10.1016/j.compstruct.2019.03.054.

[51] Sengar, V., Nynaru, M., Watts, G., Kumar, R., and Singh, S. 2023, "Postbuckled Vibration Behaviour of Skew Sandwich Plates with Metal Foam Core Under Arbitrary Edge Compressive Loads Using Isogeometric Approach," Thin-Walled Struct., 184: 110524. https://doi.org/10.1016/j.tws.2023.110524.

[52] Singh, V.K., and Panda, S.K. 2014, "Nonlinear Free Vibration Analysis of Single/Doubly Curved Composite Shallow Shell Panels," Thin-Walled Struct., 85: 341–349. https://doi.org/10.1016/j.tws.2014.09.003.

[53] Singha, M.K., and Ganapathi, M. 2004, "Large Amplitude Free Flexural Vibrations of Laminated Composite Skew Plates," Int. J. Non-Linear Mech., 39: 1709–1720. https://doi.org/10.1016/j.ijnonlinmec.2004.04.003.

[54] Singha, M.K., and Daripa, R. 2007, "Nonlinear Vibration of Symmetrically Laminated Composite Skew Plates by Finite Element Method," Int. J. Non-Linear Mech., 42(9): 1144–1152. https://doi.org/10.1016/j.ijnonlinmec.2007.08.001.

[55] Singha, M.K., Ramachandra, L.S., and Bandyopadhyay, J.N. 2006, "Vibration Behavior of Thermally Stressed Composite Skew Plate," J. Sound Vib., 296: 1093–1102. https://doi.org/10.1016/j.jsv.2006.01.070.

[56] Tomar, S.S., and Talha, M. 2019, "Large Amplitude Vibration Analysis of Functionally Graded Laminated Skew Plates in Thermal Environment," Mech. Adv. Mater. Struct., 26(5): 451–464. https://doi.org/10.1080/15376494.2017.1400619.

[57] Upadhyay, A.K., and Shukla, K.K. 2013, "Geometrically Nonlinear Static and Dynamic Analysis of Functionally Graded Skew Plates," Commun. Nonlinear Sci. Numer. Simul., 18(8): 2252–2279. https://doi.org/10.1016/j.cnsns.2012.12.034.

[58] Upadhyay, A.K., and Shukla, K.K. 2012, "Large Deformation Flexural Behavior of Laminated Composite Skew Plates: An Analytical Approach," Compos. Struct., 94: 3722–3735. https://doi.org/10.1016/j.compstruct.2012.06.015.

[59] Wang, S. 1997, "Free Vibration Analysis of Skew Fibre-Reinforced Composite Laminates Based on First-Order Shear Deformation Plate Theory," Comput. Struct., 63(3): 525–538. https://doi.org/10.1016/S0045-7949(96)00357-4.

[60] Zhang, L.W., and Xiao, L.N. 2017, "Mechanical Behavior of Laminated CNT-Reinforced Composite Skew Plates Subjected to Dynamic Loading," Compos. B Eng., 122: 219–230. https://doi.org/10.1016/j.compositesb.2017.03.041.